ADVANCED ENERGY MATERIALS
www.advenergymat.de

Electrolyte Design and Optimization for Alkali Metal-Sulfur Batteries

*Min-Hao Pai and Arumugam Manthiram**

Alkali metal-sulfur batteries, including lithium-sulfur (Li-S), sodium-sulfur (Na-S), and potassium-sulfur (K-S) systems, have garnered significant attention as promising electrochemical energy storage (EES) technologies. Among them, Li-S batteries stand out as strong contenders for next-generation energy storage, owing to their high energy density and the cost-effectiveness of sulfur-based cathodes. However, with the rapid technological advances and the escalating energy demand, lithium resources are becoming increasingly scarce, making it imperative to explore alternative metal anodes to replace lithium. Therefore, Na-S and K-S batteries, serving as counterparts to Li-S systems, are emerging as formidable contenders for next-generation energy storage technologies due to the abundant and cost-effective nature of sodium and potassium. Although Na-S and K-S batteries possess considerable potential in the energy sector, their development is still in its infancy, with performance constrained by the nascent state of electrolyte design and optimization. This review article provides a comprehensive overview of recent advancements and developments in liquid electrolytes for alkali metal-sulfur batteries. Additionally, it identifies key challenges and proposes future research directions aimed at enhancing electrolyte stability, optimizing interfacial compatibility, and improving the overall performance of alkali metal-sulfur batteries.

1. Introduction

Over the recent decades, rechargeable lithium-ion batteries (LIBs) have dominated the electrochemical energy storage (EES) market due to their high energy density and dependable cycling performance.[1,2] They enjoy widespread use in diverse applications, including laptops, communication devices, consumer electronics, and electric vehicles. However, conventional lithium-ion batteries fall short of meeting the energy storage demands required for grid-scale applications. Key challenges encompass the limited availability of scarce metals, high production costs, and inherent energy density limitations of cathodes (≈200 Wh kg^{-1}). Addressing these challenges is essential for advancing the battery technologies that exhibit low material cost, enhanced safety, extended cycle life, and high energy density.[3–7]

Compared to the expensive lithium-ion batteries, lithium-sulfur (Li-S) batteries have emerged as a promising alternative due to their high theoretical energy density and cost-effective sulfur cathodes.[8–18] While the discharge capacity of currently employed LIB cathodes is limited to 250 mAh g^{-1}, sulfur has a high theoretical capacity of 1672 mAh g^{-1} with a two-electron redox process.[19–31] However, the growing demand for lithium and its scarce reserves (0.0017 wt%) continue to pose ongoing challenges for large-scale applications, such as grid storage.[32–34] Therefore, alternative metal-sulfur batteries based on more abundant alkali metals, such as sodium and potassium, have garnered increasing attention for large-scale energy storage, where cost per kilowatt-hour outweighs power density considerations. Sodium-sulfur (Na-S) and potassium-sulfur (K-S) batteries, in particular, offer cost-effective, environmentally friendly solutions, with theoretical specific energy densities reaching up to 1274 and 1023 Wh kg^{-1}, respectively.[35–43] Their reliance on earth-abundant elements and high energy potential renders them promising candidates for grid-scale storage.

However, the development of metal-sulfur batteries, particularly Na-S and K-S systems, remains in their infancy. These batteries encounter several critical challenges that hinder practical implementation, including substantial volumetric expansion of active materials during cycling, severe polysulfide shuttle effects, dendritic growth of alkali metals, and instability of the solid–electrolyte interphase (SEI).[40,44–60] Numerous strategies have been proposed to enhance the performance of metal-sulfur batteries, including cathode structure optimization, separator modification, and the introduction of advanced metal catalysts.[61–89] Among them, electrolyte plays a particularly vital role, much like blood in human body, as it governs ion transport between the two electrodes.[90] Beyond facilitating ionic conduction

M.-H. Pai, A. Manthiram
Materials Science and Engineering Program & Walker Department of Mechanical Engineering
The University of Texas at Austin
Austin, TX 78712, USA
E-mail: rmanth@mail.utexas.edu

The ORCID identification number(s) for the author(s) of this article can be found under https://doi.org/10.1002/aenm.202502691

DOI: 10.1002/aenm.202502691

during cycling, the electrolyte also critically influences the stability of the solid-liquid interface.[91–103] Consequently, electrolyte selection is a key determinant of overall battery performance. An appropriately engineered electrolyte can significantly improve cycle life, rate capability, and safety.

Given the pivotal role of electrolytes in facilitating ion transport, stabilizing electrode interfaces, and dictating overall electrochemical performance, a comprehensive assessment in this area is both timely and necessary. Recently, several reviews have offered a comprehensive overview of alkali metal-sulfur batteries, covering cathode architectures, anode materials, binders, and electrolyte systems.[32,35,39] However, these reviews generally treat the electrolyte component as part of a broader system-level discussion, providing limited detail on the underlying chemical interactions, solvation behavior, and interfacial design principles. In contrast, this review provides a focused and systematic examination of liquid electrolyte systems in Li/Na/K-S batteries. It offers a comparative discussion on the role of electrolytes in each system. Particular attention is given to polysulfide chemistry, SEI and cathode-electrolyte interphase (CEI) stability, and solvation structures. Through this approach, the review aims to address the lack of detailed and electrolyte-focused analysis in the existing literature. It further proposes design principles and future directions tailored to alkali metal-sulfur systems, thereby contributing to a rational development of next-generation sulfur batteries.

The article provides, for the first time, a comprehensive review of electrolytes for alkali metal-sulfur batteries. First, we discuss the fundamental mechanisms of alkali metal-sulfur batteries, the advantages, challenges, key differences and importance of electrolyte engineering for achieving high-performance alkali metal-sulfur batteries. Next, we explore the design principles for electrolytes in alkali metal-sulfur batteries. Subsequently, we review the recent advances in electrolyte systems for alkali metal-sulfur batteries, including conventional liquid electrolytes, low-concentration carbonate-based electrolytes, low-concentration ether-based electrolytes, high-concentration and localized high-concentration electrolytes, and functional electrolyte additives. Finally, we conclude with an overview of the current state and future perspectives of electrolytes for alkali metal-sulfur batteries. Ultimately, overcoming the persistent challenges associated with these systems in terms of electrolyte stability, compatibility, and performance will require sustained research efforts. Continued optimization of electrolyte chemistries is essential for enabling high-performance metal-sulfur batteries that are viable for large-scale energy storage applications. **Figures 1–3** present the developmental timelines of electrolyte architectures for Li-S, Na-S, and K-S batteries, respectively.

In Figure 1, it illustrates the development timeline of Li-S battery electrolytes mainly from 2019 to 2025, highlighting a continuous evolution of electrolyte formulations aimed at enhancing sulfur utilization, stabilizing lithium-metal anode, and suppressing polysulfide shuttling. The timeline begins in 2019 with the introduction of triethyl phosphate (TEP)/1,1,2,2-tetrafluor-oethyl-2,2,3,3-tetrafluoropropyl ether (TTE) concentrated electrolyte designed to improve interfacial compatibility.[104] By 2020, the electrolyte of 1,2-dimethoxyethane (DME)/ 1,3-Dioxolane(DOL) + 3,5-bis(trifluoromethyl)thiophenol (BTB) began incorporating functional additives to promote stable SEI formation and suppress side reactions.[105] In 2021 and 2022, electrolyte systems pairing with weakly solvating solvents, such as lithium bis(fluorosulfonyl)imide (LiFSI) – diethyl ether (DEE) and DME/DOL/di-isopropyl sulfide (DIPS), were further developed to enhance lithium-metal stability and establish sparingly solvated electrolyte environments.[106,107] A key milestone was achieved in 2023 with the development of tetrahydrofuran (THF)/toluene-based electrolytes, which introduced a quasi-solid-state conversion of sulfur redox reactions.[108] Moreover, DME/TTE + lithium tetrafluoroborate ($LiBF_4$) electrolytes were proposed to support Li-S batteries with high-loading cathodes and thin lithium anodes, enabling stable cycling performance under practical conditions in 2024.[109] Most recently, in 2025, the cyclopentyl methyl ether (CPME)/ bis(dimethylthiocarbamyl) sulfide (BDTS) electrolyte system marked a significant advancement by leveraging non-fluorinated cosolvents and novel solvation structures to simultaneously achieve interfacial and chemical stability.[110] Overall, the timeline highlights a clear transition from early-stage electrolyte engineering to a rational design of solvation chemistry and interfacial regulation, paving the way for the development of high-performance Li-S batteries.

As illustrated in Figure 2, the development timeline of Na-S battery electrolytes from 2019 to 2025 reveals a clear progression from high-concentration electrolytes (HCEs) to localized high-concentration electrolytes (LHCEs) and, more recently, to localized saturated electrolytes (LSEs). In 2019, initial research focused on HCE systems, such as trimethyl phosphate (TMP)-based HCEs and PC/FEC with SbI_3, aiming to enhance cycling stability and interfacial compatibility.[36,111] By 2021 and 2022, the introduction of DME-TTE and 2,2,2-trifluoro-N,N-dimethylacetamide (FDMA) and 1,1,2,2-tetrafluoroethyl methyl ether (MTFE) LHCEs marked a shift from HCEs to LHCEs, with the goal of reducing viscosity and cost, while preserving favorable electrochemical performance.[112,113] In 2023, the emergence of LSE (2-methyltetrahydrofuran (MeTHF)-TTE) further enhanced interfacial stability and ionic conductivity.[114] Furthermore, the newly proposed systems in 2024 and 2025, such as DME/toluene LHCE and 1,2-dimethoxypropane (DMP)/TFTFE LHCE, represent emerging trends in Na-S battery research, focusing on optimizing molecular structures and solvent combinations to achieve higher energy efficiency and longer cycle life.[115,116] Overall, this timeline reflects a clear technological progression from HCEs to LHCEs and, more recently, to structure-optimized systems, providing both guidance and key milestones for the continued development of advanced electrolyte designs.

Similarly, Figure 3 outlines the progression of K-S battery electrolyte development from 2019 to 2024, highlighting the transition from conventional HCEs to more advanced LHCE systems. In 2019, tetraethylene glycol dimethyl ether (DEGDME)-based HCEs were initially explored with a focus on enabling reversible K-S electrochemistry.[117] By 2022, potassium bis(trifluoromethanesulfonyl)imide (KFSI)-DME concentrated electrolytes exhibited enhanced electrochemical performance and improved interfacial stability, particularly for potassium-metal anodes.[118] In addition, development progressed in 2023 with the introduction of KFSI-ethylene carbonate (EC) concentrated electrolytes, which enabled more uniform potassium deposition and suppressed side reactions through the tailored

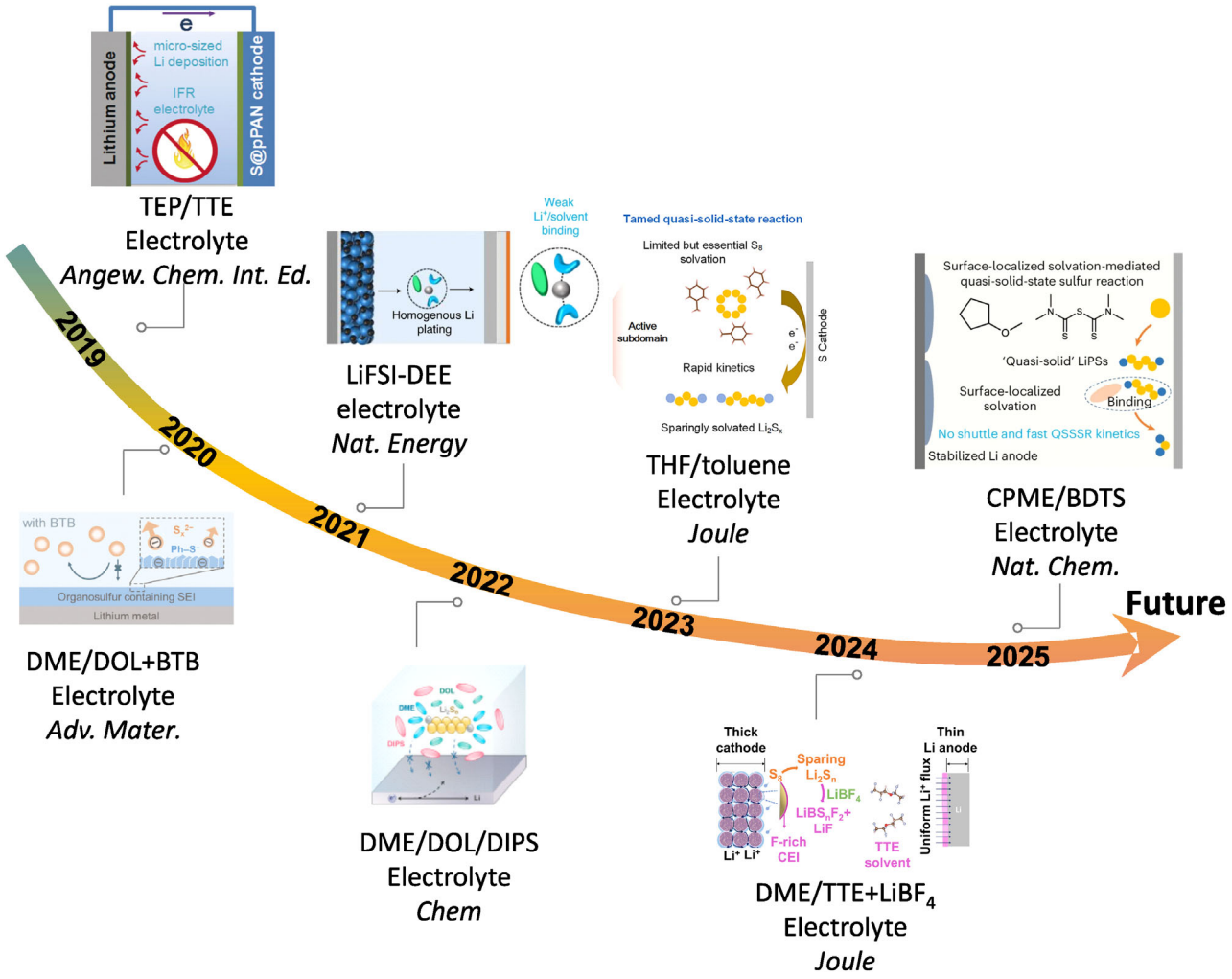

Figure 1. The timeline of the development of Li-S battery electrolytes. Reproduced with permission.[104] Copyright 2019, Wiley-VCH; Reproduced with permission.[105] Copyright 2020, Wiley-VCH; Reproduced with permission.[106] Copyright 2021, Springer Nature; Reproduced with permission.[107] Copyright 2022, Elsevier; Reproduced with permission.[108] Copyright 2023, Elsevier; Reproduced with permission.[109] Copyright 2024, Elsevier; Reproduced with permission.[110] Copyright 2025, Springer Nature.

solvation structure design.[119] The most recent advancement in 2024 is the propylene carbonate (PC)/ 1,1,2,2-tetrafluoroethy-2,2,3,3-tetrafluoropropyl ether (HFE) LHCE system, which represents a significant step forward by incorporating fluorinated ether co-solvents to regulate ion-solvent interactions, thereby stabilizing the electrolyte-anode interface and enabling long-cycle performance.[120] This timeline reflects a steady evolution in K-S battery electrolyte design, from basic concentration strategies to fine-tuned solvation engineering, pointing toward future innovations in high-performance K-S batteries.

2. Fundamental Operating Mechanisms of Alkali Metal-Sulfur Batteries

Li-S, Na-S, and K-S batteries hold great promise for energy storage applications; however, several key challenges must be addressed before their practical deployment. While these systems share common advantages, including high theoretical energy densities and low-cost sulfur cathodes, they also face critical barriers to commercialization. Notably, Na-S and K-S batteries, much like their Li-S counterpart, suffer from severe polysulfide shuttle effect, pronounced volume changes, and interfacial instability, all of which necessitate targeted mitigation strategies (**Figure 4**).

2.1. Reaction Mechanisms of Alkali Metal-Sulfur batteries

Metal-sulfur batteries operate via a series of reversible redox reactions between the alkali-metal anode and the sulfur cathode. Despite variations in ionic size and chemical reactivity among different alkali-metal-anodes, these systems share a fundamental electrochemical mechanism characterized by the stepwise reduction of elemental sulfur during discharge and its reoxidation during charge.

As analogous systems, Li-S and Na-S undergo similar stepwise reduction processes during discharge process, which can be divided into four main stages.

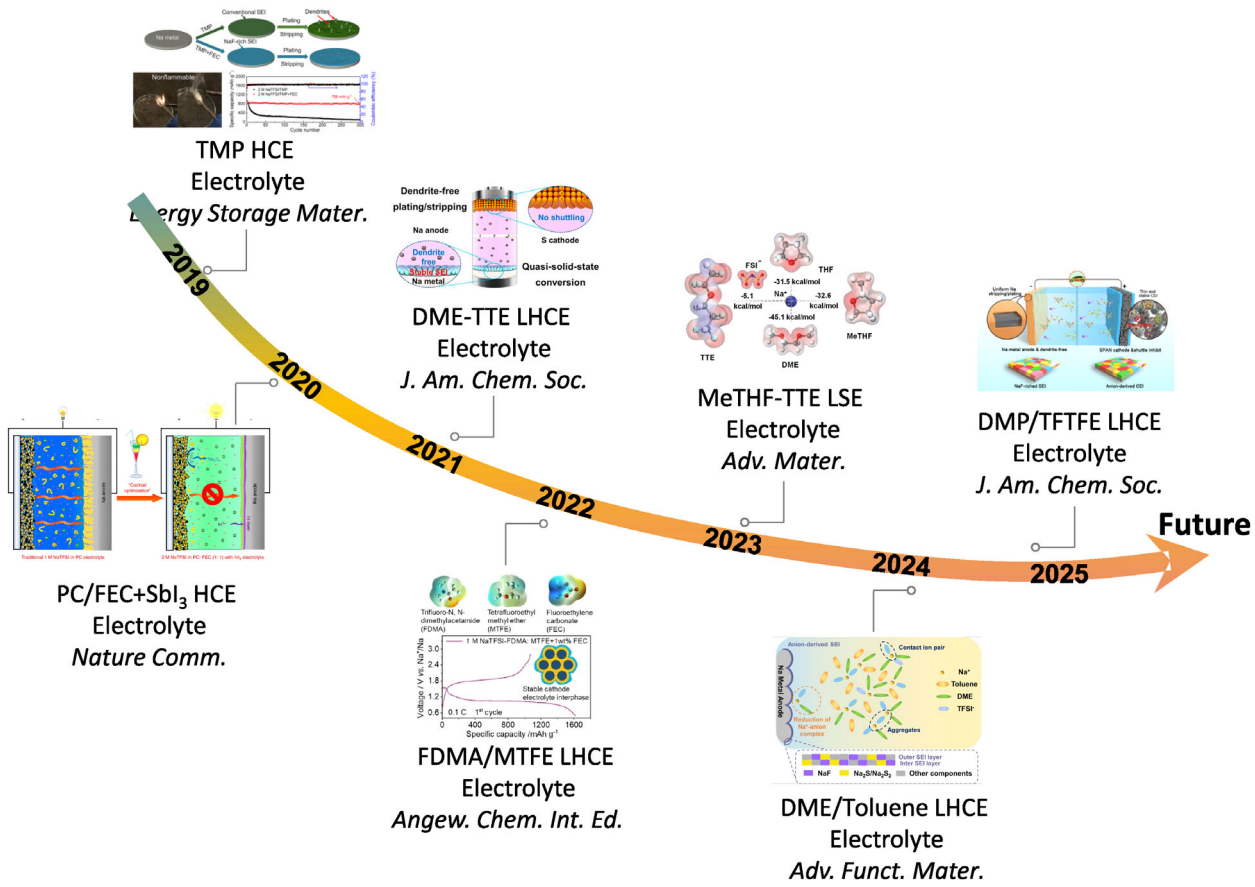

Figure 2. The timeline of the development of Na-S battery electrolytes. Reproduced with permission.[111] Copyright 2019, Elsevier; Reproduced with permission.[36] Copyright 2020, Springer Nature; Reproduced with permission. Copyright 2021, American Chemical Society; Reproduced with permission.[113] Copyright 2022, Wiley-VCH; Reproduced with permission.[114] Copyright 2023, Wiley-VCH; Reproduced with permission.[115] Copyright 2024, Wiley-VCH; Reproduced with permission.[116] Copyright 2025, American Chemical Society.

First stage: Elemental sulfur (S_8) reacts with Li^+ or Na^+ ions to form high-order polysulfides (e.g., Li_2S_8 or Na_2S_8) through a solid-liquid transition. These species are highly soluble in the electrolyte.[44,56,121,122]

Second stage: A liquid-liquid conversion occurs where high-order polysulfides (e.g., Li_2S_8 or Na_2S_8) are reduced to short-chain polysulfides (Li_2S_n or Na_2S_n where $4 \leq n \leq 8$).

Third stage: A liquid-solid transition takes place involving the conversion of soluble Li_2S_4 to insoluble lower-order polysulfides (e.g., Li_2S_n or Na_2S_n where $1 \leq n \leq 3$).

Fourth stage: A solid-solid conversion follows in which the lower-order polysulfides are ultimately reduced to Li_2S or Na_2S. Notably the capacity generated in this stage accounts for approximately two thirds of the theoretical capacity of sulfur.

Similarly, during the charge process, these reactions reverse, regenerating elemental sulfur at the cathode and redepositing lithium/sodium metal at the anode.[123] Notably, the K-S and Na-S systems exhibit processes analogous to those of Li-S, but with less distinct sloping plateaus, lower overall redox voltages, and larger charge–discharge hysteresis. The overall discharge reaction is given below:[35,37,47,124–127]

$$2Li + S_8 \Leftrightarrow Li_2S_8 \quad (1)$$

$$Li_2S_8 + (6n-2)\,Li \Leftrightarrow nLi_2S \quad (2)$$

$$2Na + S_8 \Leftrightarrow Na_2S_8 \quad (3)$$

$$Na_2S_8 + (6n-2)\,Na \Leftrightarrow nNa_2S \quad (4)$$

Intriguingly, the sulfur conversion process in the K-S system has not been as well established as in the Li-S and Na-S systems, primarily due to sluggish reaction kinetics and the distinct thermodynamic behavior of potassium polysulfide species.[128] For instance, K_2S_3 exhibits higher thermodynamic stability than K_2S, as indicated by its more negative Gibbs formation energy ($\Delta G_f^0 = -528$ kJ mol^{-1} at 25 °C) compared to that of K_2S ($\Delta G_f^0 = -410$ kJ mol^{-1}). This suggests that K_2S_3 is thermodynamically more favorable than K_2S, which may hinder the complete reduction to K_2S. In addition, the inherently sluggish kinetics of K^+, attributed to its large ionic radius and low charge density, further suppresses the $K_2S_3 \rightarrow K_2S$ conversion.[33,128] As a result, the overall sulfur reduction pathway in K–S batteries may deviate from the well-defined processes in the Li–S and Na–S systems, and reaction kinetics becomes a critical factor governing the reversibility and capacity output of K–S cells.

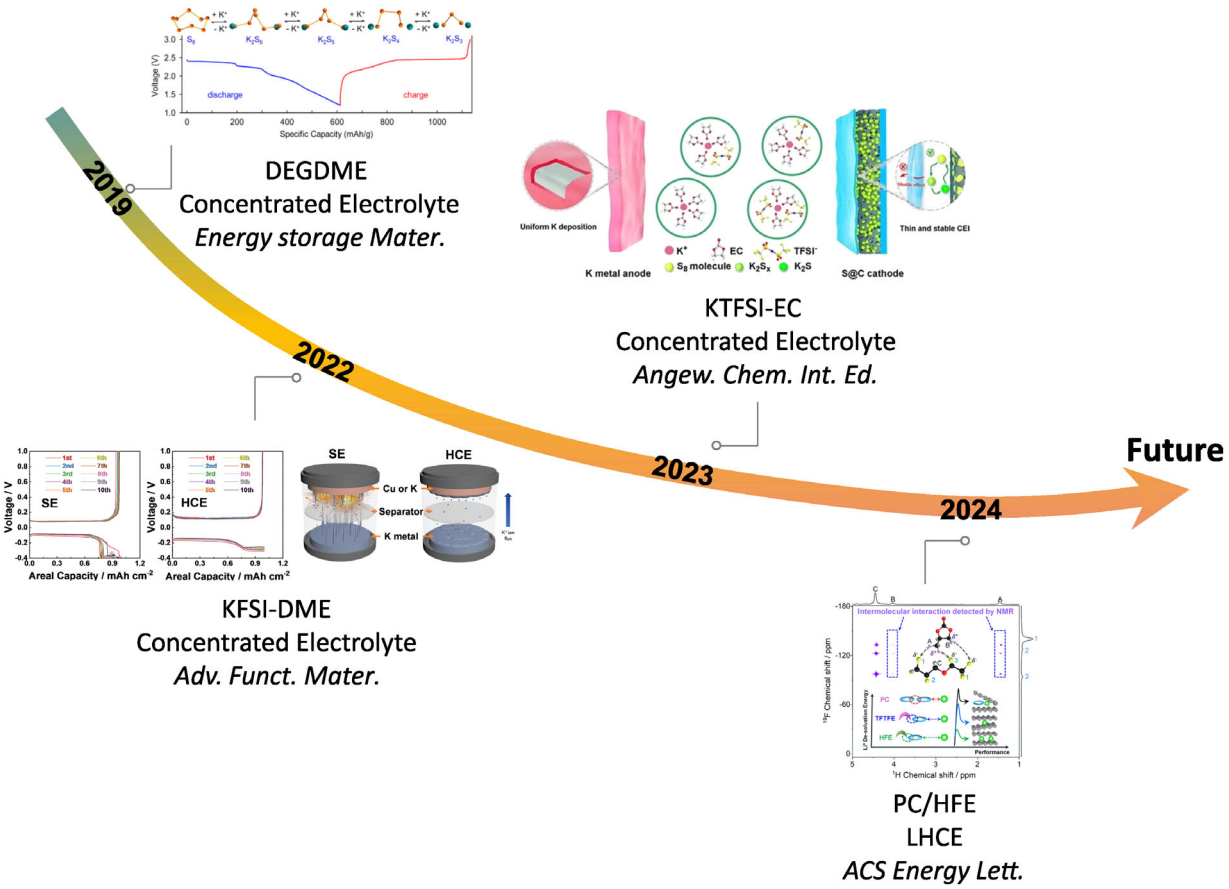

Figure 3. The timeline of the development of K-S battery electrolytes. Reproduced with permission.[117] Copyright 2019, Elsevier; Reproduced with permission.[118] Copyright 2022, Wiley-VCH; Reproduced with permission.[119] Copyright 2023, Wiley-VCH; Reproduced with permission.[120] Copyright 2024, American Chemical Society.

Owing to their distinct multi-step redox mechanisms, Li/Na/K-S batteries encounter several inherent challenges, including the polysulfide shuttle effect, active material loss, self-discharge, and limited cycling stability. Generally, the dissolution of polysulfides within the electrolyte facilitates their migration between electrodes, triggering parasitic reactions and leading to rapid capacity fade. Furthermore, the solid-liquid-solid phase transitions of sulfur and polysulfides induce substantial volume changes in the cathode, causing mechanical stress and structural degradation during prolonged cycling.[129–132] These phenomena involve complex electrochemical dynamics, where soluble intermediates continuously shuttle across the cell, exacerbating performance decay.[129] Such issues are further intensified in Na-S and K-S systems due to the larger ionic radii of Na^+ and K^+, which alter the solvation structures and influence polysulfide behaviors.[37] Additionally, the formation of unstable SEI and the uncontrolled growth of alkali metal dendrites severely compromise anode stability. Therefore, addressing these limitations requires a fundamental understanding of sulfur conversion mechanisms. In particular, rational design of advanced electrolytes plays a pivotal role in mitigating the polysulfide shuttle effect, regulating polysulfide solubility, stabilizing electrode–electrolyte interfaces, and buffering volume changes, thereby facilitating long-term operation of alkali metal-sulfur batteries.

2.2. Advantages of Alkali Metal-Sulfur Batteries

Distinguished by their cost-efficiency, remarkable theoretical capacities, and promising energy density metrics, Li-S, Na-S, and K-S batteries represent a transformative class of electrochemical systems poised to redefine the landscape of next-generation energy storage.

2.2.1. Resource Abundance

One of the most compelling advantages of alkali metal-sulfur batteries is the abundance and low cost of sulfur as an active cathode material, especially when compared to commercial lithium-ion batteries. As global demand for lithium-ion batteries continues to rise, the limited availability and high cost of metals, such as nickel (Ni), cobalt (Co), and manganese (Mn), pose significant challenges for large-scale applications. Furthermore, while lithium has an estimated crustal abundance of only 0.0017% (17 ppm), sodium and potassium are significantly more abundant, with respective crustal abundances of ≈2.6% and 2.4%.[32] This stark difference in availability makes sodium and potassium highly viable alternatives for large-scale energy storage systems. Therefore, the widespread availability of raw materials for alkali

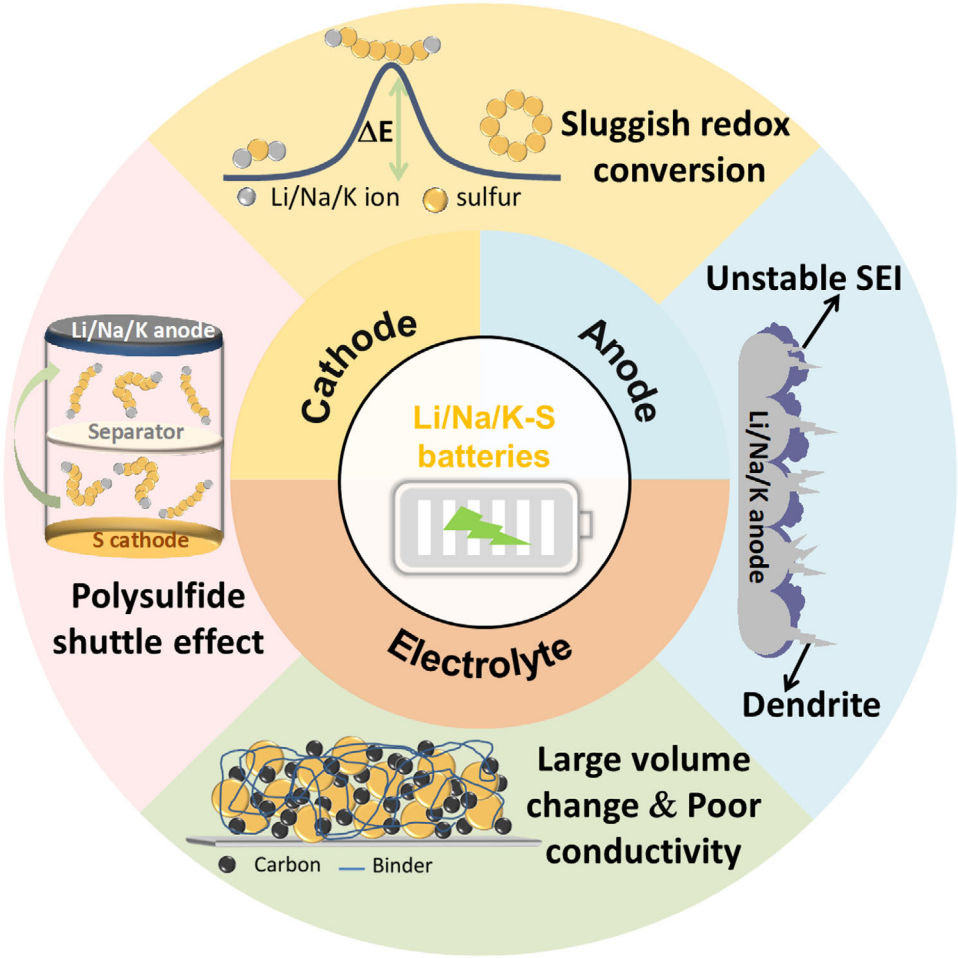

Figure 4. Schematic of the challenges faced by Li-S, Na-S, and K-S batteries.

metal-sulfur batteries, particularly for Na-S and K-S batteries, highlights a clear advantage in terms of long-term resource security and cost efficiency, positioning them as promising candidates for next-generation energy storage solutions.

2.2.2. Higher Theoretical Energy Density

Both Na-S and K-S systems, like Li-S batteries, capitalize on the high theoretical energy density of sulfur as the cathode material. With a theoretical specific capacity of 1675 mAh g^{-1}, sulfur holds the potential for these systems to surpass conventional lithium-ion batteries in terms of energy density, making them promising candidates for next-generation energy storage solutions.

2.3. Challenges and Key Differences between Alkali Metal-Sulfur batteries

While all Li-S, Na-S, and K-S batteries face several common challenges (Figure 4), they also display distinct differences in their electrochemical behavior and performance. The following key aspects highlight both the shared and unique challenges associated with these three battery systems.

2.3.1. Thermodynamics and Reaction Kinetics

Due to the intricate sulfur conversion processes, all Li-S, Na-S, and K-S batteries exhibit relatively slow reaction kinetics. Notably, the larger ionic radii of Na^+ and K^+ ions result in slower diffusion rates and reduced reaction kinetics for sodium and potassium polysulfides (NaPS and KPS) compared to lithium polysulfides (LiPS).[133] In contrast, the smaller Li^+ ion facilitates faster ion diffusion, thereby enhancing ion-transport efficiency and reducing internal resistance, which ultimately promotes a more efficient sulfur reduction process.

Additionally, electrolyte stability and SEI formation critically differentiate these systems. While Li-S batteries benefit from relatively well-formed and stable SEI layers that facilitate efficient charge transfer, Na-S and K-S batteries face considerable challenges due to the larger ionic radii of Na^+ and K^+, which hinder the formation of robust SEI structures and lead to sluggish interfacial kinetics. More precisely, the substantial ionic radius of K^+ imposes severe steric hindrance and sluggish desolvation

kinetics, which significantly impede interfacial charge transfer and thus become a key limiting factor for achieving high power densities.

Furthermore, the relatively low melting point of potassium (63.5 °C), compared to sodium (97.8 °C) and lithium (180.5 °C), presents both advantages and limitations.[35,134] On the positive side, it enables the potential deployment of liquid potassium metal anodes at moderately elevated temperatures, potentially lowering interfacial resistance and facilitating improved electrochemical kinetics. Moreover, this low melting point complicates thermal management under high current densities, where localized heating may induce phase transitions, promote liquid metal infiltration, and compromise both the structural integrity and safety of the cell.

From a thermodynamic perspective, the relatively low melting point of potassium leads to a narrower solid-liquid phase transition window, resulting in more pronounced temperature-dependent fluctuations in ionic conductivity and interfacial stability. These instabilities contribute to non-uniform ion deposition, which accelerates anode expansion and promotes dendrite formation. In contrast, Li-S and Na-S batteries, which leverage the higher melting points of lithium and sodium, exhibit more thermally robust behavior and stable operation across a broader temperature range, thereby reducing the demand for intensive thermal regulation.

Consequently, compared to Li-S systems, both Na-S and K-S batteries are more susceptible to thermal perturbations due to the significantly lower melting points of their respective alkali metals. Notably, lithium remains solid under typical operating conditions, offering enhanced mechanical integrity and a more predictable electrode-electrolyte interface. This thermodynamic stability mitigates the risks of phase transitions and liquid metal infiltration, which are particularly pronounced in potassium-based systems.

2.3.2. Polysulfide Solubility and Shuttle

Effect of polysulfide solubility constitutes a fundamental bottleneck in alkali metal-sulfur battery systems, severely undermining their electrochemical performance and long-term operational stability. During discharge, elemental sulfur undergoes a sequence of reduction reactions, yielding soluble intermediate polysulfide species (e.g., Li_2S_6, Li_2S_4; Na_2S_6, Na_2S_4; K_2S_6, K_2S_4).[32] These intermediates readily diffuse across the electrolyte under the influence of concentration gradients and the internal electric field, migrating toward the anode. There, they are further reduced to lower-order polysulfides or irreversibly converted into solid-phase metal sulfides (Li_2S, Na_2S, or K_2S), which precipitate onto electrode surfaces. This phenomenon, commonly known as the polysulfide shuttle effect, not only causes active material loss, but also initiates parasitic redox reactions at the anode, resulting in continuous charge consumption, self-discharge, and a marked decline in Coulombic efficiency.

The deleterious impact of the shuttle effect manifests through several interconnected degradation pathways. The persistent dissolution and migration of polysulfides progressively deplete the redox-active sulfur content of the cathode, while the deposition of insoluble sulfides at both electrodes passivates electrochemically active sites and impedes the charge-transfer processes. These cumulative effects give rise to pronounced capacity fade, increased polarization, and energy inefficiencies. Over extended cycling, the buildup of inactive byproducts and irreversible electrode surface modifications further exacerbate performance decay. Collectively, these challenges pose formidable barriers to the practical implementation of metal-sulfur battery technologies, underscoring the urgent need for electrolyte innovations and interfacial engineering strategies aimed at suppressing polysulfide dissolution, stabilizing redox pathways, and preserving long-term cell integrity.

The severity of the polysulfide shuttle effect is governed by several interrelated factors, among which electrolyte composition plays a particularly critical role. The solubility of polysulfides is strongly influenced by the nature of the solvent and salt employed in the electrolyte. Generally, ether-based electrolytes typically exhibit higher polysulfide solubility than carbonate-based systems, which exacerbates the dissolution and migration of polysulfide intermediates and consequently intensifies the shuttle effect. In parallel, electrochemical reaction kinetics also substantially affect the extent of polysulfide-related losses. Notably, Na-S and K-S batteries inherently exhibit slower redox kinetics than their lithium-based counterparts, primarily due to the larger ionic radii and lower charge densities of Na^+ and K^+ ions. This kinetic limitation permits extended residence time of soluble polysulfides within the electrolyte, thereby increasing the likelihood of side reactions and accelerating capacity degradation and energy inefficiencies.

Consequently, Li-S, Na-S, and K-S batteries all experience pronounced polysulfide solubility in organic electrolytes, which intensifies self-discharge phenomenon and exacerbates loss of active materials. To alleviate these issues and improve long-term electrochemical stability, it is imperative to implement targeted approaches such as rational electrolyte formulation, strategic modification of electrode surfaces, and the design of effective polysulfide confinement frameworks. These measures collectively contribute to mitigating parasitic reactions and sustaining high-performance battery operation over extended cycles.

2.3.3. Challenges with Metal Anodes

The interaction between the alkali metal anode and the electrolyte constitutes a fundamental determinant of the electrochemical stability and overall performance of Li-S, Na-S, and K-S batteries. In comparison to lithium, sodium and potassium possess higher standard reduction potentials (−2.71 and −2.93 V versus the standard hydrogen electrode, respectively, as opposed to −3.04 V for lithium), weaker metallic bonding strength, and significantly larger ionic radii.[32] These physicochemical attributes render sodium and potassium more susceptible to undesirable reactions with organic electrolyte components, thereby intensifying challenges associated with SEI instability, uncontrolled dendritic growth, and accelerated electrolyte decomposition.

SEI Instability and Electrolyte Decomposition: A stable SEI is essential for protecting the metal anode from continuous reactions with the electrolyte. While lithium-metal anode can form relatively stable SEIs in well-optimized electrolytes, the SEIs on sodium and potassium anodes remain significantly less stable

due to pronounced volume fluctuations during metal deposition and stripping.[134] The stability of lithium SEIs is primarily attributed to the smaller ionic radius and lower chemical reactivity of lithium, which facilitate the formation of dense and uniform interfacial layers. In contrast, sodium and potassium, with their larger ionic sizes and higher reactivities, pose greater challenges, namely, potassium suffers from the most severe interfacial instability owing to its high chemical activity and large ionic radius, which hinder the formation of a compact and resilient SEI. This leads to repeated SEI rupture and reformation, accelerating electrolyte decomposition and causing continuous consumption and side reactions that degrade the anode-electrolyte interface, ultimately compromising long-term electrochemical performance. Sodium, although less problematic than potassium, still suffers from some instability in the SEI, which is primarily enriched with NaF and Na_2O.[134] While this composition helps mitigate electrolyte decomposition, degradation of the interface remains a challenge.

Dendrite Formation and Safety Risks: The instability of the SEI is a principal factor underlying dendrite formation, which remains a formidable barrier to the commercialization of Li-S, Na-S, and K-S batteries, particularly under high current densities or extended cycling. Recurrent SEI fracture exposes fresh metal surfaces, disrupting ion flux uniformity and inducing uneven metal deposition. This promotes the formation of needle-like dendrites capable of penetrating the separator, thereby triggering internal short circuits, thermal runaway, and potential catastrophic failure.

Beyond safety hazards, dendrite growth leads to irreversible capacity loss, as detached metallic filaments contribute to active material depletion and structural degradation of the anode. Simultaneously, the persistent exposure of reactive metal surfaces accelerates electrolyte decomposition and necessitates continuous SEI reformation, progressively consuming electrolyte volume and shortening battery lifespan.[40,48] Among the alkali metals, potassium is particularly susceptible to dendritic instability, owing to its fragile and poorly passivating SEI, which fails to regulate interfacial deposition dynamics. Therefore, the intrinsic instability of Li, Na, and K metal anodes represents a critical limitation in alkali metal-sulfur battery systems. Addressing dendrite growth and SEI failure through advanced interface engineering and rational electrolyte design is imperative to enhance safety, extend cycle life, and realize the full potential of these batteries for large-scale energy storage applications.

2.3.4. Challenges with Cathode

Li-S, Na-S, and K-S batteries encounter critical cathode-related limitations as well, notably pronounced volumetric expansion and inherently low electrical conductivity. These factors collectively undermine structural integrity, hinder charge transport, and constrain long-term cycling stability and electrochemical performance.

Volume Expansion: Sulfur undergoes significant volume changes during cycling as it transitions from elemental sulfur (S_8) to discharge products, such as Na_2S/Na_2S_2 in Na-S batteries, K_2S in K-S batteries, and Li_2S in Li-S batteries. This phase transformation induces substantial mechanical stress on the cathode, with volume expansion varying among the systems. Na-S batteries experience ≈170% volume expansion, while K-S batteries exhibit up to 296% expansion due to the larger ionic radius of K^+ compared to Na^+. Li-S batteries also face ≈80% expansion, though this remains less extreme than that in the Na-S and K-S systems.[32]

Such drastic volume changes result in electrode delamination, microcracking, and loss of electrical contact, all of which contribute to performance degradation. In Na-S batteries, the mechanical stress disrupts cathode integrity, leading to reduced active material utilization. In K-S batteries, the issue is more severe, as the larger K_2S particles exert greater stress on the electrode matrix, further accelerating cathode fracturing and loss of structural stability, which ultimately shortens cycle life. As for Li-S batteries, although the expansion is more moderate, it still contributes to electrode degradation and poor cycling stability over prolonged cycles.

Inferior Conductivity: Both sulfur and its discharge products (Li_2S, Na_2S, and K_2S) are intrinsically insulating, significantly impeding both electron and ion transport, which in turn compromises charge-transfer kinetics and overall electrochemical performance.[32] Notably, K_2S presents a more significant challenge than Na_2S and Li_2S due to its lower ionic conductivity, further hindering K^+ diffusion at the cathode-electrolyte interface and increasing charge-transfer resistance. This results in severe polarization, sluggish reaction kinetics, and incomplete sulfur utilization, ultimately diminishing energy efficiency and rate performance.

Addressing these challenges necessitates the development of advanced strategies, including conductive frameworks, optimized electrode designs, and materials capable of better accommodating volume expansion during cycling. These approaches are critical for enhancing the performance and longevity of metal-sulfur battery systems.

2.3.5. Energy Density and Weight Considerations

Practical energy density remains a significant challenge for Li-S, Na-S, and K-S batteries, with K-S systems exhibiting a slightly lower theoretical specific energy density due to the higher atomic weight and lower reduction potential of potassium. The theoretical gravimetric energy densities of Li-S, Na-S, and K-S batteries are ≈2.600, 1245, and 1023 Wh kg^{-1}, respectively.[35,36] This trend reflects the decreasing electrochemical potential ($Li^+ > K^+ > Na^+$) and increasing molar mass (Li < Na < K). Li-S batteries achieve the highest energy density due to the small ionic radius of Li^+ and its high electrochemical potential, enabling greater sulfur utilization.

However, practical energy density is influenced not only by theoretical values, but also by sulfur utilization, electrolyte formulation, and reaction reversibility. While Li-S batteries theoretically offer the highest energy density, practical limitations, such as polysulfide dissolution, poor conductivity, and volume expansion can reduce their real-world performance. Similarly, Na-S and K-S batteries face similar challenges, their energy densities are inherently lower due to the larger ionic radii and higher atomic weights of Na^+ and K^+ and their corresponding lower electrochemical potentials.

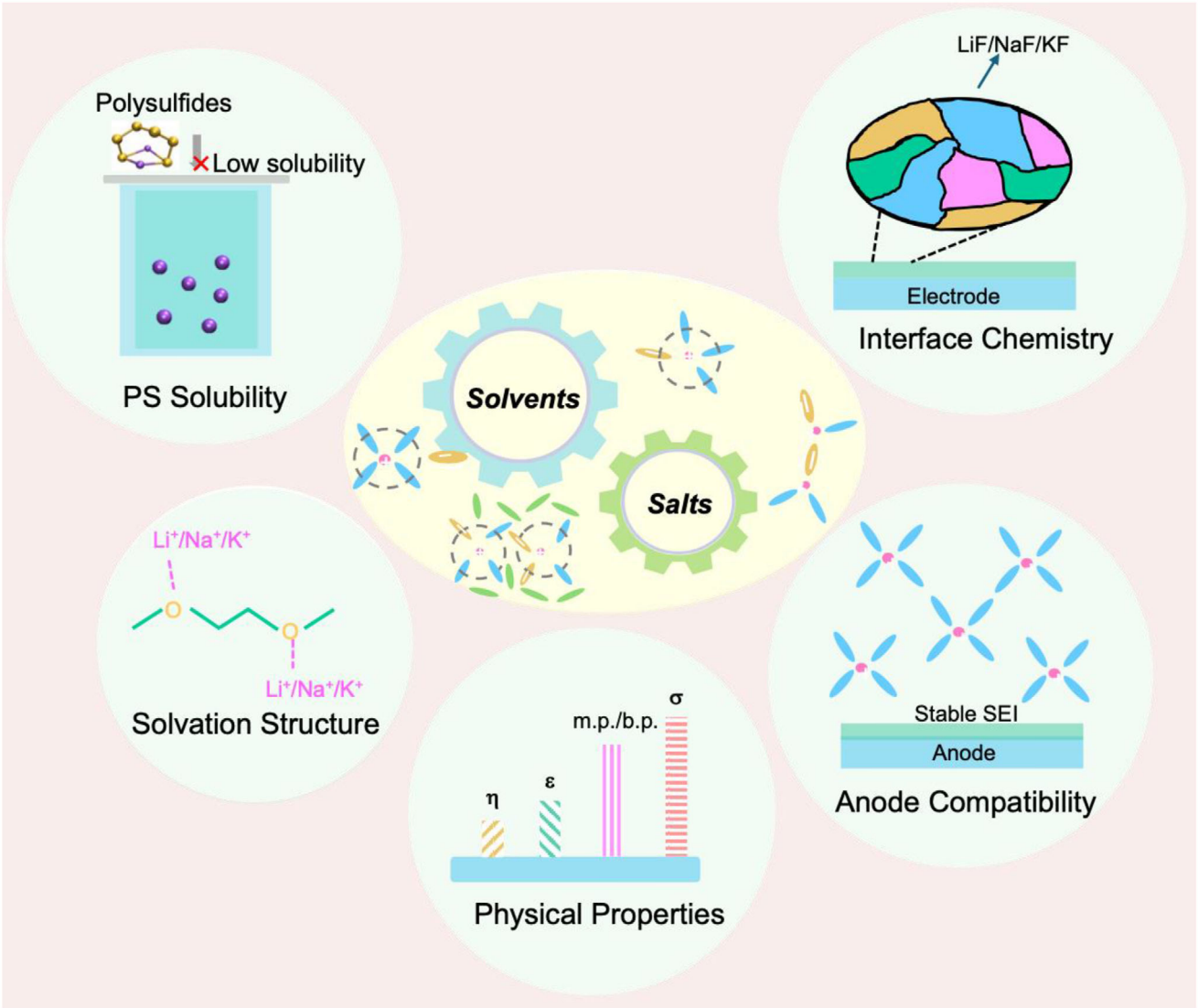

Figure 5. Properties related to the solvents and their corresponding electrolytes, where η, ε, m.p./b.p., and σ represent viscosity, dielectric constant, melting/boiling point, and ionic conductivity, respectively.

To bridge the gap between theoretical and practical energy densities, improvements in electrode architecture, electrolyte design, and interfacial engineering are crucial. These advancements can mitigate the performance limitations of Na-S, K-S, and Li-S batteries, enhancing their real-world applicability and increasing their potential for large-scale energy storage systems.

2.4. Importance of Electrolyte Engineering for High Performance Alkali Metal-Sulfur Batteries

Achieving stable long-term cycling, while maintaining high energy density remains a critical challenge in the development of Li-S, Na-S, and K-S batteries. The performance of these systems is heavily influenced by the polysulfide shuttle effect, dendrite growth, and electrolyte degradation, all of which contribute to capacity fade, increased polarization, and reduced energy efficiency. Among these factors, electrolyte engineering plays a pivotal role, as it directly affects the solubility of polysulfides, stability of SEI, and overall ion-transport properties.[106,135–137]

While strategies to enhance cycling performance, such as minimizing polysulfide dissolution or implementing protective coatings, are essential, they often come at the cost of energy density. For example, concentrated electrolytes or excessive additives can improve cycle life by stabilizing interfaces and suppressing side reactions, but they may simultaneously face reduced ionic conductivity, increased cell resistance, or the addition of unnecessary weight and volume, ultimately undermining energy density. Thus, optimizing electrolyte composition, solvation structure, and functional additives is crucial to mitigating degradation mechanisms, while preserving high energy density. A well-engineered electrolyte must strike an

optimal balance between chemical stability, ionic transport, and polysulfide confinement, ensuring that improvements in cycle life do not compromise power output or practical energy density.

3. Design Principles for Electrolytes for Alkali Metal-Sulfur Batteries

In this section, we provide a concise overview of electrolyte electrochemistry, followed by a discussion on the key physicochemical properties of solvents and electrolytes. The schematic in **Figure 5** showcases the various properties and electrochemical performances of different electrolytes, highlighting their roles in electrolyte stability and overall battery performance. Additionally, we examine how solvent polarity, ionic conductivity, and solvation structures influence cycling stability, rate capability, and Coulombic efficiency.

3.1. Fundamental Properties of Electrolytes

The physicochemical properties of electrolytes critically influence the cycling performance, stability, and safety of Li-S, Na-S and K-S batteries. Key factors, such as melting and boiling points, viscosity, dielectric constant, ionic conductivity, interfacial stability, voltage window, and safety considerations dictate the role of electrolyte in ion transport, interfacial reactions, and thermal management. Strategic electrolyte engineering, including solvent selection, solvation structure optimization, and functional additives, is essential for mitigating the degradation mechanisms and extending battery lifespan.[138]

The melting and boiling points of electrolytes fundamentally delineate their operational temperature windows, determined by lattice strength and intermolecular interactions.[139] A low melting point enables functionality at sub ambient temperatures, whereas a high boiling point enhances thermal robustness under high-power or elevated-temperature conditions. In parallel, viscosity (η) critically governs ion transport and is influenced by van der Waals forces and molecular architecture.[139] Solvents possessing strong dipolar interactions or rigid molecular frameworks typically exhibit higher viscosities, thereby hindering ion mobility. Conversely, linear molecular structures and weakly coordinating solvation environments tend to reduce viscosity, facilitating faster ion diffusion and improved ionic conductivity.

The dielectric constant (ε) also plays a pivotal role in governing ion dissociation and charge transport.[139] A high dielectric constant promotes effective salt dissociation and suppresses ion pairing, thereby facilitating enhanced ionic mobility. However, under high salt concentrations, the value of ε exhibits a bell-shaped dependence due to the interplay between intensified cation–anion coordination and diminished polarization of the solvation shell. Optimizing ionic conductivity thus necessitates a careful balance among solvation energy, dielectric properties, and viscosity to minimize interfacial resistance while preserving electrochemical stability. Through precise modulation of electrolyte composition and physicochemical parameters, researchers seek to improve Coulombic efficiency, suppress parasitic reactions, and prolong cycle life in Li-S, Na-S, and K-S battery systems, thereby advancing their viability for next-generation energy storage applications. The common organic solvents and their properties, along with the various alkali-metal salts and their respective characteristics are outlined in **Tables 1** and **2**.

Table 1. Common organic solvents for electrolytes and their key characteristics.

Solvent	Properties
Dimethoxyethane (DME)	Good solubility, low viscosity, high conductivity
Dioxolane (DOL)	Provides good electrolyte solubility, help in the formation of a stable SEI
Tetrahydrofuran (THF)	High solubility, low viscosity, good conductivity
Tetraglyme (TGDME)	Good solubility ionic conductivity, and high viscosity
Propylene Carbonate (PC)	High polarity, wide electrochemical stability, but relatively high viscosity
Ethylene Carbonate (EC)	High polarity, wider voltage window but more viscous
Dimethyl Carbonate (DMC)	Low viscosity, high conductivity, good solubility
Diethyl Carbonate (DEC)	Good solubility, good electrochemical stability
Fluoroethylene carbonate (FEC)	High electrochemical stability, forms a protective SEI

3.2. Key Electrolyte Design Strategies

During discharge, lithium, sodium, or potassium metal is oxidized at the anode, releasing Li^+, Na^+, or K^+ ions along with electrons. The metal ions migrate through the electrolyte toward the cathode, while electrons flow through the external circuit to generate electric current. At the cathode, elemental sulfur undergoes stepwise reduction to form soluble polysulfides, which are subsequently converted into lower-order species and ultimately precipitate as solid Li_2S, Na_2S, or K_2S.[126] Throughout this redox process, the electrolyte serves not only as the medium for ion transport, but also as a stabilizing agent for the electrode-electrolyte interface, helping to suppress side reactions, mitigate the shuttle effect, and promote long-term cycling stability. However, the electrolyte design principles in the Li-S, Na-S, and K-S systems diverge significantly due to the intrinsic differences in cation size, charge density, and redox reactivity of Li^+, Na^+, and K^+ ions. These variations strongly influence polysulfide solubility and reactivity, thereby determine electrolyte design strategies.

In Li-S batteries, LiPS exhibit moderate solubility in ether-based solvents and a relatively fast redox kinetics due to the small ionic radius and high charge density of Li^+ ion.[32] This may enable efficient sulfur conversion, but also lead to significant shuttle effects. Accordingly, electrolyte design for Li-S batteries aims to balance LiPS solubility and promote interfacial stability. This is often achieved by incorporating $LiNO_3$ additives, fluorinated co-solvents, or high-donor-number solvents to adjust solvation structures and improve SEI formation.

Table 2. Common alkali-ion salts for electrolytes and their properties.

Salt	Properties	Advantages	Disadvantages
$LiPF_6$/$NaPF_6$/ KPF_6	Highly conductive, stable in a wide temperature range	Excellent ionic conductivity, high electrochemical stability.	Sensitive to moisture, can decompose to produce toxic gases
LiTFSI/NaTFSI/KTFSI	High ionic conductivity, excellent stability	Good performance in high and low temperatures	Higher cost than other salts
LiFSI/NaFSI/KFSI	Excellent ionic conductivity, wide electrochemical window	Excellent stability, high temperature performance	Higher cost, sensitive to moisture
$LiClO_4$/$NaClO_4$/ $KClO_4$	Moderate ionic conductivity, inexpensive	Widely used in liquid electrolytes	Decomposes at high voltages, potential for side reactions
$LiBF_4$/$NaBF_4$/$NaBF_4$	Good ionic conductivity, lower reactivity	Less toxic, stable at higher voltages.	Poor electrochemical stability at low temperatures
LiDFOB/NaDFOB/KDFOB	High ionic conductivity, good electrochemical stability	Excellent performance in high voltage systems	Sensitive to moisture, more expensive than $LiPF_6$/$NaPF_6$/ KPF_6
LiOTf/NaOTf/KOTf	High ionic conductivity, good solubility in many solvents	High electrochemical stability, suitable for various electrolytes	Expensive, not as widely used as $LiPF_6$/$NaPF_6$/ KPF_6

As for Na-S batteries, NaPS generally exhibit higher solubility than LiPS owing to the larger ionic radius of Na^+.[116] Furthermore, the redox kinetics is slower, and the resulting SEI is less stable, necessitating stronger polysulfide confinement and better interfacial control. As such, electrolyte systems for Na-S batteries often incorporate solvents or additives that promote inorganic-rich SEI layers and restrict PS mobility. LHCEs and fluorinated carbonates are increasingly explored to stabilize both the anode and cathode interfaces, while suppressing polysulfides crossover.

In K-S batteries, the challenges are even more pronounced. The large ionic radius and low Lewis acidity of K^+ lead to weak solvation strength and sluggish desolvation kinetics.[35] Potassium polysulfides are inherently more reactive and less stable in conventional organic solvents, leading to pronounced interfacial instability. As a result, the SEI formed on the K metal anode is often fragile and poorly passivating, thereby exacerbating dendrite growth and electrolyte decomposition. To address these challenges, electrolyte solvents for K-S batteries should possess low polysulfide solubility, high oxidative stability, and the capability to form robust, KF-rich interphases. Weakly solvating ethers or localized high-concentration electrolyte environments have shown promise in meeting these criteria.

Collectively, these fundamental differences necessitate system-specific electrolyte design strategies. For Li-S batteries, the primary objective is to suppress LiPS shuttling while maximizing sulfur utilization. In Na-S systems, ensuring SEI robustness and attenuating NaPS diffusion are of paramount importance. In contrast, K-S batteries are predominantly constrained by interfacial instability and the poor solvent compatibility of potassium polysulfide species.

Figure 6 summarizes the characteristics of ideal electrolytes for alkali metal-sulfur batteries and their impact on battery performance. The design of an ideal electrolyte for alkali metal-sulfur batteries is dictated by a multitude of interrelated factors, including solvent properties, solvation structure, interfacial chemistry, low-temperature operability, and control over polysulfide solubility. Each of these elements critically influences the overall stability, efficiency, and longevity of the system. The key design principles for developing optimized electrolytes in metal-sulfur batteries are outlined below.

3.2.1. Ideal Solvent Properties

An ideal electrolyte solvent must simultaneously satisfy multiple criteria to ensure optimal electrochemical performance. Low viscosity and moderate solvation strength are essential for facilitating rapid ion transport, while a high dielectric constant or elevated donor number promotes effective salt dissociation, thereby reducing internal resistance.[140] In addition, a broad liquid-phase temperature range and high flash point are critical for maintaining thermal stability and operational safety under variable conditions.

Moreover, for compatibility with high-energy-density battery systems, the solvent must exhibit a wide electrochemical stability window and enable the formation of a robust SEI or CEI, thereby stabilizing the electrode-electrolyte interface. Also, low-molecular-weight solvents with good wettability improve interfacial contact and reduce overall cell mass, which is particularly beneficial for gravimetric energy density. Therefore, from a practical perspective, cost-effectiveness and non-toxicity are also essential, underscoring the need for scalable solvent systems suitable for large-scale battery deployment.

3.2.2. Solvation Structure and Interface Chemistry

The solvation structure within an electrolyte significantly influences ionic conductivity, voltage window, desolvation kinetics, and interface chemistry. The solvation environment at the electrode-electrolyte interface differs from that in the bulk electrolyte due to local ionic interactions. A weakly solvating electrolyte tends to form an anion-rich solvation shell, increasing cation-anion interactions, which can hinder ion transport and elevate internal resistance.[140]

For instance, fluorinated solvents have demonstrated significant potential in enhancing interfacial stability.[136] In

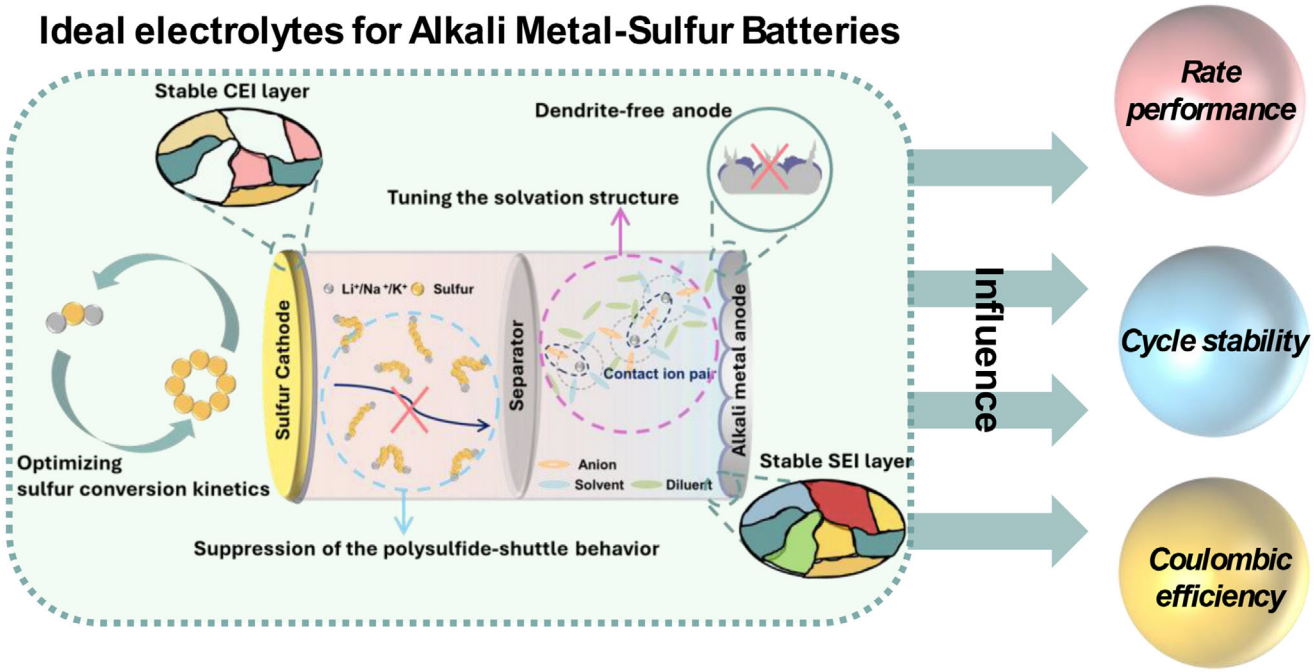

Figure 6. Schematic illustration of the characteristics of ideal electrolytes for alkali metal-sulfur batteries and their impact on battery performance.

low-solvation fluorinated electrolytes, the tailored solvation structures preferentially facilitate the formation of halide-rich interphases, such as LiF, NaF, or KF.[138] These interphases are characterized by their high chemical stability and mechanical integrity, contributing to the development of dense, well-passivated layers at the electrode surface. These interfacial architectures effectively lower interfacial resistance, promote uniform ion flux across the interface, and mitigate dendrite formation, thereby significantly extending the cycling life and reliability of alkali-metal batteries.

3.2.3. Thermal Stability and Flammability Control of Electrolytes

The thermal stability and flammability of electrolytes are key safety concerns for the practical deployment of alkali metal-sulfur batteries, particularly under abuse or elevated-temperature conditions. Conventional ether-based solvents, such as 1,3-dioxolane (DOL) and dimethoxyethane (DME), are widely used due to their compatibility with sulfur species. However, their relatively low flash points (≈0–6 °C) and high volatility make them prone to combustion under thermal runaway conditions.[141] Moreover, their lack of intrinsic flame-retardant properties leads to prolonged self-extinguishing times, thereby posing significant fire hazards.

To address these issues, various strategies have been proposed. Flame-retardant additives, such as trialkyl phosphates, fluorinated carbonates, and ionic liquids, can help suppress flammability by altering combustion pathways or promoting char formation.[111,136,142] HCEs and LHCEs can also reduce solvent activity, thereby mitigating fire risk. Alternatively, the use of non-flammable solvents (e.g., trimethyl phosphate, fluorinated ethers) offers enhanced safety by combining thermal resistance with improved interfacial stability. However, such formulations often face trade-offs in ionic conductivity and compatibility with both electrodes, necessitating further optimization.

Future electrolyte designs for sulfur batteries should balance electrochemical performance with safety by integrating flammability testing metrics, such as flash point, self-extinguishing time (SET), and onset temperature of exothermic reactions (via DSC or ARC), enabling more realistic safety profiling under application-relevant conditions.

3.2.4. Wide-Temperature Performance

The ability of the electrolyte to perform across a broad temperature spectrum is pivotal to ensuring the operational stability and efficiency of Li-S, Na-S, and K-S batteries under varying environmental conditions. At elevated temperatures, the electrolyte must exhibit high thermal stability, low volatility, and strong interfacial compatibility to prevent accelerated capacity fade. Conversely, under sub-zero conditions, it is essential to maintain adequate ionic conductivity, suppress electrolyte freezing, and minimize solvation-induced transport barriers.[106]

Specifically, at high temperatures, ideal electrolytes should possess high boiling points and minimal vapor pressure to sustain ionic conductivity, while mitigating solvent decomposition and interfacial degradation.[143] The formation of a stable SEI/CEI is also essential to prevent metal corrosion, parasitic reactions, and electrolyte depletion. The use of thermally robust components, such as ionic liquids, has proven effective in enhancing the thermal resilience and interfacial stability.

At low temperatures, increased viscosity and sluggish ion dynamics hinder battery performance. In this regime, the solvation structure plays a decisive role: weakly solvating electrolytes can reduce ion–solvent binding strength, thereby

lowering desolvation energy and facilitating cation migration.[139] However, excessive weakening of solvation strength may lead to salt crystallization, which compromises electrolyte homogeneity and ionic transport.[91] Therefore, a well-balanced electrolyte formulation must simultaneously optimize solvation strength, ionic mobility, and salt solubility to ensure reliable performance over a wide thermal operating window.

3.2.5. Polysulfide Shuttle Suppression

As previously discussed, the polysulfide shuttle effect represents a major obstacle to the advancement of sulfur-based batteries, as it induces rapid capacity degradation and self-discharge due to the uncontrolled migration of soluble polysulfide species between the cathode and anode. Suppressing this phenomenon is essential for enhancing long-term cycling stability and preserving electrochemical performance. Effective mitigation strategies typically involve reducing polysulfide solubility, enhancing interfacial interactions between the electrolyte and electrode surfaces, and promoting the formation of robust solid interphases that act as physical and chemical barriers to polysulfide diffusion.[32] In particular, electrolyte engineering and interfacial modification have emerged as critical approaches to curtail shuttle-induced degradation. Continued progress in the rational design of electrolyte systems that simultaneously suppress polysulfide migration and maintain efficient ion transport remains central to the development of high-performance sulfur-based battery technologies.

3.2.6. Comparative Electrolyte Design Strategies for SPAN and C/S Cathodes

Sulfurized polyacrylonitrile (SPAN) has emerged as a compelling alternative to elemental sulfur as the cathode material in metal-sulfur batteries.[116] Fundamentally, its structure features short-chain sulfur atoms chemically integrated into the conjugated pyridinic backbone of the polymer. This covalent configuration effectively mitigates the dissolution of polysulfide species and suppresses the shuttle phenomenon, thereby distinguishing SPAN from conventional sulfur-based cathodes. While SPAN is applied as the alternative cathode material, its electrochemical behavior is solvent-dependent. In ether-based electrolytes (e.g., DME/DOL), the SPAN cathode typically follows a solid-liquid-solid conversion pathway, akin to that of conventional sulfur cathodes, and remains vulnerable to polysulfide dissolution and the resulting shuttle effect.[144] Nevertheless, ether-based systems are still preferred due to their superior compatibility with alkali metal anodes, which facilitates stable SEI formation and improved long-term cycling performance.[92]

By contrast, in carbonate-based electrolytes (e.g., EC/DEC), polysulfide dissolution can be effectively suppressed through the formation of a CEI layer, which promotes a solid-solid reaction pathway. However, interfacial instability between alkali metal anodes and carbonate solvents often results in continuous electrolyte decomposition, unstable SEI formation, and dendritic growth.[116,145] Consequently, SPAN cathodes may exhibit poor reversibility and limited cycle life, primarily due to anode degradation.

Therefore, electrolyte design for SPAN cathodes must balance the suppression of intermediate dissolution with the maintenance of interfacial stability. Although ether-based electrolytes are not entirely immune to shuttle effects, they remain the most practical and extensively studied option due to their favorable compatibility with lithium, sodium, and potassium metal anodes. **Table 3** summarizes the key differences between SPAN and conventional C/S cathodes, emphasizing their divergent mechanisms and electrolyte compatibility.

3.2.7. Perspective on Electrolyte Optimization

To comprehensively evaluate the role of electrolytes in battery performance, it is essential to elucidate their interactions with both the electrode materials and the electrode-electrolyte interface. The influence of electrolytes can be broadly categorized into direct and indirect effects.

Direct effects arise from the intrinsic properties of the electrolyte, such as ionic conductivity, electrochemical stability, and solvation behavior. These characteristics govern key performance metrics, including reaction kinetics, energy density, and operational voltage window. The efficiency of ion transport is directly governed by ionic conductivity, which in turn influences the charge and discharge rates as well as the power output.[138] Moreover, solvent–ion interactions, determined by solvation strength, molecular geometry, and chain length, play a pivotal role in modulating electrode reversibility, working potential, and ion-storage dynamics during cycling.

Indirect effects are predominantly associated with the formation and evolution of the SEI, which is critical for stabilizing the electrode-electrolyte interface. The composition and structural integrity of the SEI are highly sensitive to electrolyte formulation, as different solvents yield distinct decomposition pathways and interphase chemistries. Notably, electrolytes incorporating fluorinated solvents or weakly coordinating solvents can induce the formation of compact, ion-conductive SEI layers, which limit continuous electrolyte degradation and suppress parasitic reactions. A robust SEI not only enhances interfacial charge-transfer kinetics but also plays a pivotal role in inhibiting dendrite growth, thereby improving safety and prolonging cycle life.

In addition, electrolyte–electrode compatibility is vital to mitigate interfacial reactivity and capacity fading. High electrolyte wettability ensures intimate electrode contact, reduces interfacial resistance, and alleviates polarization, thus facilitating faster reaction kinetics and higher energy conversion efficiency. For long-term battery stability, electrolyte systems must be rationally engineered to optimize solvation structure, minimize volatility, and enhance interfacial compatibility, ultimately extending the cycling durability and practical energy density of Li-S, Na-S, and K-S batteries. To further elucidate the critical role of electrolyte design and optimization in metal-sulfur battery systems, representative state-of-the-art electrolytes are discussed in the following sections.

4. Advances in Electrolyte Systems for Alkali Metal-Sulfur Batteries

Ethers and carbonates are commonly used as electrolyte solvents in alkali metal-sulfur batteries due to their suitable

Table 3. Comparison between SPAN cathode and conventional C/S composite cathode in alkali metal-sulfur batteries.

Property / Feature	SPAN Cathode	Conventional C/S Cathode
Sulfur species state	Covalently bonded S (in polymer backbone)	Elemental S_8 physically mixed with carbon host materials
Polysulfide formation	Suppressed to some extent	The formation of soluble long chain polysulfides
Shuttle effect	Moderate	Significant
Electrolyte interaction	Requires solvents that stabilize intermediates	Needs strategies to control polysulfide solubility
Voltage profile	Sloping	Typical two-plateau behavior
Cycle life	Longer and more stable	Shorter due to shuttle and unstable SEI degradation

electrochemical stability, high ionic conductivity, and compatibility with metal electrodes.[32] These solvents facilitate ion transport and may help maintain stable interphases between the electrolyte and electrodes, which is essential for improving battery efficiency and cycle life. The solvation properties of ethers and carbonates also influence the dissolution and diffusion behavior of polysulfides within the electrolyte. Furthermore, while ether-based solvents exhibit favorable polysulfide solubility and good compatibility with alkali metal anodes, carbonate-based solvents are prone to undesirable side reactions with both polysulfides and alkali metals, leading to solvent decomposition and interfacial instability.[144] Therefore, tuning solvent properties to suppress the polysulfide shuttle effect while preserving high ionic conductivity remains a central focus in electrolyte design.

Over the past decade, substantial progress has been made in advancing these electrolyte systems. Researchers have focused on suppressing the solubility of polysulfides and enhancing electrolyte stability through various modifications. This includes the development of hybrid electrolytes that combine carbonates with ethers or other solvents to take advantage of the respective strengths of each solvent type. They not only reduce polysulfide solubility, but also suppress side reactions and enhance cycling efficiency. Moreover, electrolyte additives are often introduced to further mitigate parasitic interactions at the anode interface, thereby fostering more stable and prolonged cycling performance.

Another area of focus lies in the development of novel solvent systems, particularly localized high-concentration electrolytes, which modulate the solvation structure through anion-rich environments to optimize key parameters, such as solubility of polysulfides, interfacial stability, and ionic conductivity.[135,136,146] These advanced electrolyte formulations are intended to address the unique challenges posed by the polysulfide interactions in metal-sulfur systems, ensuring better long-term stability, enhanced rate performance, and more efficient energy storage. While much progress has been made, ongoing research continues to refine these systems, with the goal of improving the overall performance and commercial viability of metal-sulfur batteries for large-scale energy storage applications. **Tables 4–6** present a comparative analysis of the electrochemical performances of various electrolytes reported for Li-S/Na-S/K-S batteries, highlighting key parameters, such as mass loading, capacity retention, current density, and cycle number, to provide a clearer understanding of the impact of electrolyte on battery performance.

4.1. Conventional Liquid Electrolytes

4.1.1. Low Concentration Carbonate-based Electrolytes

Among various liquid electrolytes, low concentration carbonate-based electrolyte systems that use solvents, such as ethylene carbonate (EC), dimethyl carbonate (DMC), and propylene carbonate (PC) are among the most extensively studied and widely adopted in the battery field.[90] These solvents provide relatively high ionic conductivity and a wide electrochemical stability window, both of which are essential for ensuring efficient ion transport during the charge and discharge cycles of the battery. However, one of the major challenges associated with carbonate electrolytes in Li-S, Na-S, and K-S systems is their interaction with polysulfides. During cycling, sulfur undergoes electrochemical conversion to form polysulfides (Li_2S_n, Na_2S_n, K_2S_n), which can react with carbonate solvents through nucleophilic addition or substitution reactions, losing the active sulfur materials and generating undesirable side products that degrade battery performance. To tackle this challenge, researchers have devised sulfur confinement strategies, including embedding sulfur within porous carbon matrices or microporous frameworks, to minimize direct interactions between sulfur species and solvents, thereby mitigating side reactions. Interestingly, during the initial discharge phase, partial decomposition of carbonate solvents may contribute to the formation of a compact CEI, which not only inhibits polysulfide dissolution, but also facilitates reversible solid-state conversion between low-order polysulfides. As such, this intrinsic limitation of carbonate-based electrolytes can potentially be harnessed as a design strategy to regulate interfacial stability and enhance overall cell performance.

Furthermore, to achieve a balance between ionic conductivity, electrolyte stability, and electrode compatibility, mixed solvent systems have been developed by incorporating both cyclic and linear carbonates. Cyclic carbonates, such as EC and PC, are favored for their high electrochemical stability and ability to facilitate the formation of a robust SEI layer, which is crucial for long-term cycling performance. Meanwhile, linear carbonates, including EMC and diethyl carbonate (DEC), help to lower viscosity and enhance ion transport at low temperatures, thereby improving the overall electrolyte performance.[187]

However, the most used solvents EC and PC exhibit certain intrinsic limitations. While EC boasts a high boiling point of 246.7 °C and excellent electrochemical stability, it suffers from poor low-temperature performance and limited compatibility with polysulfides, making it unsuitable as a standalone solvent.

Table 4. Comparison of the electrochemical performances with reported electrolytes for Li-S batteries.

Electrolyte	Cathode	Sulfur content (%) and mass loading [mg cm^{-2}]	E/S [μL mg^{-1}], N/P	Reversible capacity [mA h g^{-1}], cycle number, and C rate	Rate capability [mA h g^{-1}] and C rate	Refs.
LiTFSI-G2 (1:0.8, molar ratio)	S	50, 2.0	-, -	≈900, 100, C/5	–	[147]
1 M LiFSI-DEE	SPAN	-, 3.5	-, -	≈350, 50, C/3	–	[106]
1.5 M LiTFSI-DEC/FEC+TTE (LHCE)	KB/S	70, 1–1.2	30, -	570, 600, 2 C	713, 3 C	[148]
LiFSI-DME/TTE + 2wt% TMS-N_3, additive: TMS-N_3 (LHCE)	SPAN	-, 1.0	50, -	≈600, 800, C/2	320, 3 C	[149]
1.2 M LiTFSI-DME/DOL+$LiNO_3$+F4DMB (LHCE)	S@Ni/S	90, 5.3	15, -	≈500, 150, C/5	–	[150]
LiTFS-THF/toluene, molar ration: THF: LiTFSI = 2:1, (LHCE)	KB/S	70, 1.0	20, -	≈900, 300, C/5	–	[108]
1.5 M LiTFSI-DME/TTE+ 0.05 M $LiBF_4$, additive: $LiBF_4$, (LHCE)	KB-Se/S	70, 2	10, -	≈1000, 200, C/10	–	[109]
1 M LiTFSI-DME/DOL+$LiNO_3$+ 0.2 M $LiTe_3$ (additive: $LiTe_3$)	Li_2S/CNF/Super P	-, 3.8	10, -	≈450, 200, C/5	459, 1C	[151]
1 M LiTFSI-DME/DOL+$LiNO_3$+0.1 M T3Br (additive: T3Br)	KB/S	70, 1.5–2	20, -	780, 350, C/2	≈800, 3C/2	[152]
2 M LiFSI-BME (HCE)	SPAN	-, 1.8	22, -	≈500, 1000, 1 C	–	[144]
1 M LiTFSI-DME/DOL+$LiNO_3$+ 0.1 M 4Mpy (additive: 4Mpy)	CNT/S	70, 1.3	38, -	598, 400, 1C	712, 4 C	[153]
1 M LiTFSI-DME/DOL+$LiNO_3$+HME (LHCE)	CNT/S	70, 4.4	8, -	≈500, 113, C/10	919, 0.3 C	[145]
LiFSI-DME/TFTFE++$LiNO_3$ (LiFSI:$LiNO_3$:DME: TFTFE = 1.9:1.0:18.5:3.8), LHCE	–	-, 3.8	8, -	≈600, 160, C/10	–	[154]
2.2 M LiFSI-THP/TTE (LHCE)	SPAN	-, 2	15, -	353, 1000, C/2	–	[155]
2 M LiFSI-PE (LHCE)	SPAN	-, 1	40, -	≈400, 1200, 3C	–	[156]
1 M LiTFSI-DME/DOL+$LiNO_3$+HMPA (additive: HMPA)	G/S	80, 3.2	10, -	799, 100, C/10	≈750, 3 C	[157]
1 M LiTFSI-CPME+ 50 mM BTDS (additive: BTDS)	KB/S	70, 3.2	10, -	1000, 300, C/5	494, 16 C	[110]
1 M LiTFSI (DOL:DME) + 1 wt% $LiNO_3$ + 0.1 M TTCA (additive: TTCA)	Li_2S/MWCNTs	80, 1.5	20, -	473, 800, 1 C	660, 4 C	[158]
1 M LiTFSI (DOL:DME) + 1 wt% $LiNO_3$ + 1 wt% CuL (additive: CuL)	sulfur	, 2.0	20, -	601, 250, 1 C	583, 5 C	[159]
1 M LiTFSI in DBE/TMS+ 0.2 M NH_4TFA (additive: NH_4TFA)	KB/S	-, 4.0	7.5, -	715, 0.063, 250, C/5	601, 1 C	[160]
1 M LiTFSI (DOL:DME) + 5 wt% ISDN (additive: ISDN)	CNT/S	70, 4.0	10, -	793, 100, C/10	720, C/2	[161]
1 M LiTFSI (DOL:DME:THF) +0.2 M SnI_2-LiI (additive: SnI_2-LiI)	Super P +MWCNT/Li2S	65, 4.0	5, -	≈2 mA h cm^{-2}, 100, C/10	≈1.25 mAh cm^{-2}, 0.6 C	[162]
1 M LiTFSI (DOL:DME:) + 0.1 M LiI (additive: LiI)	CNT/S	70, 1.2	15.7, -	≈600, 250, 2 C	655, 4 C	[163]
1 M LiTFSI (DOL:DME:1,4 BDT) + 1 wt% $LiNO_3$, (additive: BDT)	carbon paper/ S	-, 3.5	11.4, -	909, 500, C/2	1200, 1 C	[164]
1 M LiTFSI (DOL:DME) + 2 wt% $LiNO_3$ + 10 mM DPDSe (additive: DPDSe)	CNT/S	70, 1.2	15.7, -	720, 0.091, 350, C/2	–	[165]
1 M LiTFSI (DOL:DME:DCBQ) + 0.2 M $LiNO_3$ (additive: DCBQ)	CMK3/S	60, 1.2	-, -	≈800, 100, 1 C	622, 2 C	[166]
1 M LiTFSI (DOL:DME) + 0.1 M $LiNO_3$ + 50 mM DBBQ (additive: DBBQ)	carbon/S	78, 2.0	-, -	850, 500, 1 C	745, 10 C	[167]
0.8 M LiTFSI + 0.2 M CH_3TFA (additive: CH_3TFA)	carbon/S	67.5, 4.8	10, -	750, 40, C/10	–	[168]
1 M LiTFSI (DOL:DME) + 2 wt% $LiNO_3$ +10 wt% PES*n* (additive: PES*n*)	MWCNT/S	70, 1.2	21, -	748, 100, C/2	–	[169]

(*Continued*)

Table 4. (Continued)

Electrolyte	Cathode	Sulfur content (%) and mass loading [mg cm^{-2}]	E/S [µL mg^{-1}], N/P	Reversible capacity [mA h g^{-1}], cycle number, and C rate	Rate capability [mA h g^{-1}] and C rate	Refs.
1 M LiTFSI (DOL:DME) + 1 wt% $LiNO_3$ + 0.5 wt% N-CD (additive: N-CD)	super P/S	70, 2.0	-, -	589, 500, C/2	547, 2 C	[170]
1 M Li (DOL:DME) + 2 wt% $LiNO_3$ + 0.1 M DTbDS (additive: DTbDS)	MWCNT/S	70, 5.0	15.6, -	≈300, 150, 4 C	566, 4 C	[171]
1 M Li (DOL:NiDME) + 1 wt% $LiNO_3$	CMK3/S	70, 1.0	-, -	784, 500, 1 C	635, 3 C	[172]

On the other hand, PC has low ionic conductivity and poor low-temperature performance, in addition to its reduced compatibility with metal anodes, which poses challenges for long-term cycling stability.[190] These drawbacks necessitate careful formulation and the inclusion of functional additives to optimize carbonate electrolyte performance in Li-S, Na-S and K-S battery systems.

Li-S Batteries with LCCEs: As previously noted, the use of carbonate-based electrolytes in Li-S batteries presents significant challenges. The high reactivity between lithium metal and carbonate solvents often results in the formation of a thick, unstable SEI, which promotes dendrite growth and compromises interfacial stability.[144] This degradation at the anode-electrolyte interface leads to capacity loss, shortened cycle life, and elevated internal resistance. Addressing these issues necessitates the development of functional electrolyte additives, advanced anode protection techniques, and rational SEI design to ensure long-term stability and high-performance operation in Li-S systems employing carbonate-based electrolytes.

In 2018, Sun et al. achieved a breakthrough by engineering sulfur cathodes to undergo a solid-phase Li-S redox reaction via a well-designed electrolyte (1 M $LiPF_6$ in EC:DEC with 20 vol%

Table 5. Comparison of the electrochemical performances with reported electrolytes for Na-S batteries.

Electrolyte	Cathode	Sulfur content (%) and mass loading [mg cm^{-2}]	E/S [µL mg^{-1}], N/P	Reversible capacity [mA h g^{-1}], cycle number, and C rate	Rate capability [mA h g^{-1}] and C rate	Refs.
1 M $NaClO_4$-0.2 M Na_2S/P_2S_5 TEGDME	KB/S	50, 2.0	-, -	200, 1000, -	–	[173]
2 M NaTFSI-PC/FEC + InI_3 (HCE, additive 10 mM InI_3)	S@MPCF	60, 0.36	50, -	581, 500, 1 C	867, 2 C	[36]
2 M NaTFSI/TMP+FEC (LCE)	SPAN	-, 1.2–1.5	100, -	788, 300, 1 C	300, 4 C	[111]
NaFSI-DME/TTE LHCE (DME:NaFSI:TTE = 1:1.2:1 molar ratio), LHCE	MWCNT/S	80, 2.0	15, -	922, 300, C/10	–	[112]
Na_3SbS_4/PETEA (mass ratio of 1.5:1)	Na_2S_6/CNF	-, 1.0	25, -	804, 80, 0.6 mA h cm^{-2}	–	[174]
BASE/Na[OTf]-Cs[TFSA]	S/carbon paper	-, -	-, -	355, 1000, 0.5 mA	250, 2.0 mA	[175]
1 M NaTFSI-FDMA/MTFE+FEC, LHCE	porous carbon/S	63, 1.0	60, -	724, 200, C/10	486, 2 C	[113]
1 M NaTPB in PC/FEC (7wt%) + PETA (1.5wt%) + AIBN (0.5wt%)	SPAN	70, 3.1	-, -	644, 2500, 2 C	590, 4 C	[176]
2 M NaFSI-MeTHF/TTE (LHCE)	KB/S	-, 1.8	18, -	530, 200, C/10	402, 1 C	[114]
2 M NaFSI-DME/Toluene(LHCE)	SPAN	-, 2–2.5	13.5, -	530, 300, 1 C	690, 1 C	[115]
1 M NaTFSI in FEC	S@MRP	40, 0.65	-, -	456, 1000, C/2	379, 2 C	[177]
1 M NaTFSI in EMIFSI with 10 wt.% FEC	S@C	–	-, -	565, 500, 0.2 A g^{-1}	140, 2 A g^{-1}	[178]
NaFSI in DME/TTE with C3mpyrFSI (NaFSI: DME: TTE molar ratio = 1:1.3:1), additive: 0.3 M C3mpyrFSI	SPAN	-, 2	15, -	586, 250, 1 C	573, 3 C	[179]
2 M NaFSI-DMP/TFTFE (LHCE)	SPAN	-, 2.2	13.5, -	530, 500, C/2	608, 1 C	[116]
2 M NaFSI-THP/ETFE (LHCE)	SPAN	-, 2.2	13.5, -	517, 500, 1C	743, 1 C	[180]
2 M NaFSI-DMP/CPME (LHCE)	SPAN	-, 2.2	13.5, -	490, 800, C/2	≈600, 1 C	[181]

Table 6. Comparison of the electrochemical performances with reported electrolytes for K-S batteries.

Electrolyte	Cathode	Sulfur content (%),Sulfur mass loading [mg cm^{-2}]	E/S [μL mg^{-1}], N/P	Reversible capacity [mA h g^{-1}], cycle number, and C rate	Rate capability [mA h g^{-1}] and C rate	Refs.
1 M KCF_3SO_3/TEGDME	S/CNF	-, 1.0	65, -	500, 50, 0.2 A g^{-1}	800, C/3	[182]
0.8 M KPF_6 in EC/DEC	SPAN	38.0, 1.0	-, -	147, 100, C/2	218, 3 C	[183]
0.3 M $Cu(TFS)_2$-0.1 M KTFS in Me-Im	S_8/VC	-, 1–1.2	40, -	≈500, 200, 0.48 C	500, 1. 2 C	[184]
1 M KSO_3CF_3 in EC:DEC (1:1, v/v)	CCS	39.3, 1.0–1.5	120, -	253, 300, 0.15 A g^{-1}	94, 1 A g^{-1}	[185]
0.8 M KPF_6 in EC/DEC	Microporous C/S	18.6, 0.5–1.0	10, -	870, 150, 0.02 A g^{-1}	741, 2 A g^{-1}	[186]
3 M KFSI in DME (LCE)	ACF-1500@S	15.0, 1.3	46, -	157, 250, 0.05 A g^{-1}	100, 2 A g^{-1}	[187]
4.34 mol kg^{-1} KFSI in DME (LCE)	SPAN	80.0, 2.0	13, 2.01	2.5 mA h cm^{-2}, 700, C/2	480, 5 C	[118]
1 M KFSI in EC/DEC	FS-SPAN	33.2, 7.0	-, -	313, 300, 0.33 A g^{-1}	148, 1.6 A g^{-1}	[188]
3 M KTFSI in EC (LCE)	S@MHCF	–	-, -	654, 800, 0.5 A g^{-1}	295, 1 A g^{-1}	[119]
KTFSI in DME/TFTFE, molar ratio of 1:2.33:1 (KTFSI/DME/TFTFE). (LHCE)	S@Bi_2S_3–rGO	75, 1	-, -	448, 80, 0.5 A g^{-1}, 0.2C	–	[189]

FEC), completely avoiding polysulfide formation (**Figure 7a**).[191] In-operando sulfur K-edge XANES (Figure 7c) confirmed a direct conversion from cyclo-S_8 to Li_2S in this electrolyte, unlike the typical ether-based systems where soluble polysulfides dominate (Figure 7b). Time-of-flight secondary ion mass spectrometry (TOF-SIMS) further validated the absence of polysulfide migration to the anode, indicating effective suppression of the shuttle effect. Fluoroethylene carbonate (FEC) was introduced as a critical cosolvent to reduce polarization and stabilize the Li metal anode by forming a uniform SEI layer. This enabled a capacity of 670 mAh g^{-1} over 100 cycles with minimal fade (0.11% per cycle). Moreover, pouch cells with double-sided electrodes delivered 200 Wh kg^{-1} at the electrode level, demonstrating practical feasibility. Importantly, the approach is compatible with industrial carbon materials (e.g., BP800, BP1300), highlighting its scalability. This work redefines Li-S battery design in carbonate electrolytes by enforcing a solid-phase reaction mechanism. Eliminating polysulfide dissolution bridges the gap between high-energy Li-S chemistry and the inherent safety of carbonate electrolytes, paving the way for next-generation energy storage.

Also, Lu et al. developed a cyclic carbonate-based electrolyte (2 M lithium bis(fluorosulfonyl)imide (LiFSI) in EC) to address interfacial issues in practical Li-S batteries using sulfurized polyacrylonitrile (SPAN) cathodes.[192] Replacing traditional ether solvents like DME with EC, the new electrolyte promotes the formation of a uniform polycarbonate-rich CEI on SPAN cathode (**Figure 8a**). This CEI, composed mainly of organic components, such as polycarbonates and $-(CH_2CH_2O)_n-$, effectively prevents polysulfide dissolution and supports SPAN's solid-phase redox process (Figure 8b). In contrast, ether-based electrolytes (e.g., 1 M LiFSI/ dimethoxyethane (DME)) yield heterogeneous, inorganic-rich CEIs (e.g., LiF and Li_2CO_3), which exacerbate the shuttle effect. Also, ^{17}O NMR confirms enhanced Li^+-EC coordination in the EC-based electrolyte, directing CEI formation. At the same time, it promotes a bilayered SEI on lithium metal anodes, consisting of a dense Li_2O outer shell and a nanocrystalline Li_2O/Li_2CO_3 inner layer, as observed via cryo-TEM. This structured SEI layer improves Li^+ transport, suppresses dendrite growth, and enables a high Li Coulombic efficiency of 97.45% over 400 cycles. Moreover, practical Li-SPAN pouch cells with high sulfur loading (4.08 mAh cm^{-2}) and

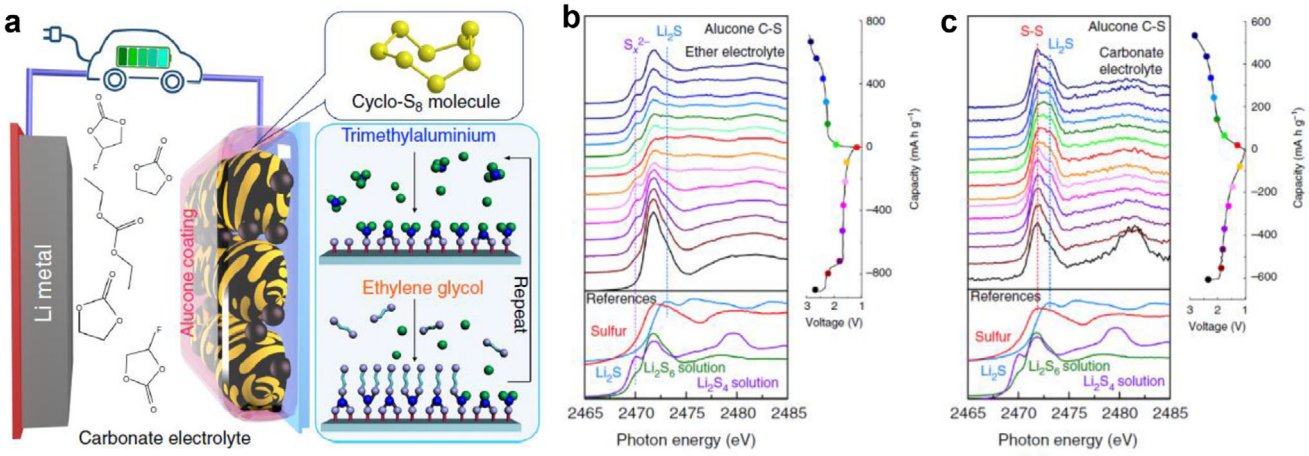

Figure 7. a) Schematic of a Li-S battery with carbonate-based electrolyte. In situ X-ray absorption study within (b) ether and (c) carbonate electrolytes. Reproduced with permission.[191] Copyright 2018, Springer Nature.

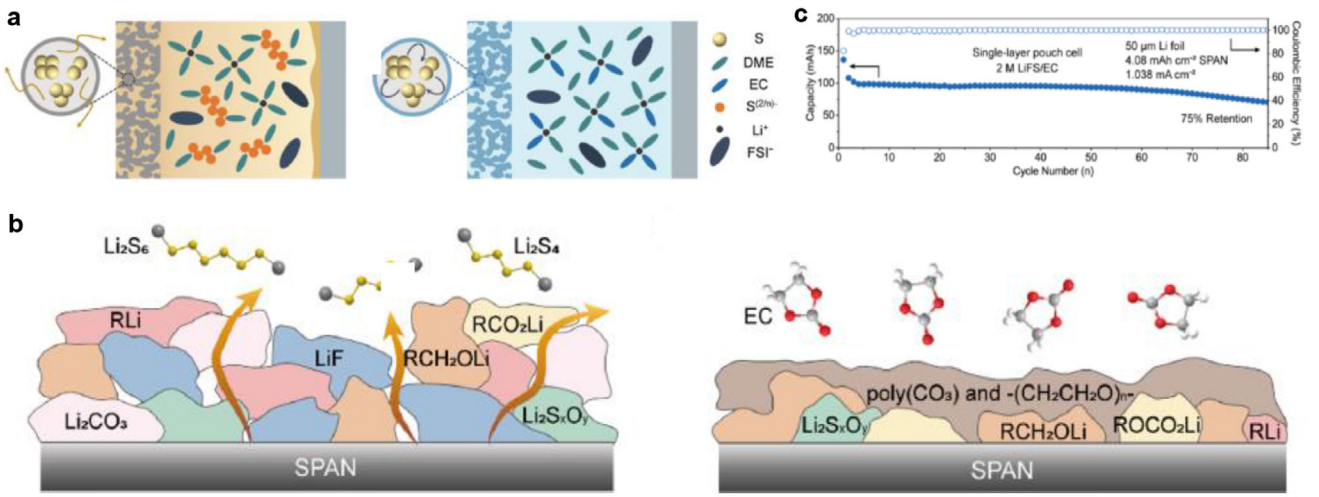

Figure 8. a) Schematic illustrations of the sulfur redox process in 1 M LiFSI/DME and 1 M LiFSI/DME-EC. b) Schematic illustrations of the structure of CEIs formed in 1 M LiFSI/DME and 1 M LiFSI/DME-EC. c) Cycling performance of pouch-type Li-SPAN full batteries at a 100 mAh capacity. Reproduced with permission.[192] Copyright 2018, American Chemical Society.

lean Li anodes (N/P = 1.22) achieve a volumetric energy density of 615 Wh L^{-1} (Figure 8c), offering a sevenfold improvement in cycle life over conventional carbonate-based systems (e.g., 1 M LiFSI in EC-DEC). This performance underscores the importance of interfacial engineering, particularly the synergy between the solvation properties of EC and the decomposition behavior of LiFSI, in optimizing both energy density and cycling stability.

Na-S Batteries with LCCEs: As for Na-S systems, Guo and colleagues proposed a ternary carbonate electrolyte (1 M $NaClO_4$ dissolved in PC/EC at a 1:1 volume ratio, with 2 wt% FEC) for a cathode composed of activated porous carbon fibers and small sulfur molecules (S_{2-4}).[193] In this electrolyte, S_{2-4} molecules are confined within ultra micropores and undergo a single-step reaction with Na_2S during discharge. After 400 cycles at a rate of C/10, a reversible capacity of 997 mAh g^{-1} was achieved. Moreover, Ahn and his team investigated S_{2-4} molecules using a different ternary electrolyte (1 M $NaClO_4$ dissolved in a 1:1:1 volume ratio of PC/EC/DEC) without the addition of FEC.[194] During the first discharge, a small peak at 2.2 V was observed, attributed to the conversion of surface sulfur into long-chain polysulfides. It is noteworthy that the significant capacity loss from the first to the second discharge cycle may be due to side reactions during the first discharge and the formation of carbonate-based sulfur SEI and CEI layers. The C/S_{2-4} cathode demonstrated a reversible capacity of 790 mAh g^{-1} after 60 cycles at a rate of C/10, indicating a high degree of reversibility.

Recently, Wu's group developed a 1 M sodium bis(fluorosulfonyl)imide (NaTFSI) in FEC electrolyte (denoted as FECE) to investigate the role of FEC in room-temperature Na-S batteries (**Figure 9a**).[177] FEC plays a multifaceted role in enhancing battery performance by modulating interfacial properties. The study reveals that FEC promotes the formation of a unique double-layered CEI, which effectively suppresses the shuttle effect and supports solid-to-solid sulfur conversion. The CEI is formed via rapid nucleophilic reactions and electrolyte decomposition, yielding a structure primarily composed of NaF, Na_2CO_3, and $ROCO_2Na$. The outer NaF-rich layer provides strong protection against polysulfide dissolution, thereby stabilizing the interface between the electrolyte and sulfur cathode, improving sulfur utilization, and enhancing cycling stability. Likewise, on the sodium anode, FEC facilitates the formation of a robust SEI later enriched with NaF and C–F bonds. This SEI layer helps prevent dendrite growth, mitigates side reactions, and enables reversible sodium plating and stripping (Figure 9b). These interfacial enhancements lead to high Coulombic efficiency, extended cycle life, and reduced polarization. Overall, the findings underscore the critical role of FEC as a carbonate electrolyte solvent for safe, long-lasting, and high-performance Na-S batteries, offering valuable insights for future electrolyte design for energy storage applications.

K-S Batteries with LCCEs: K-S batteries are a promising energy storage system, yet the use of low-concentration carbonate-based electrolytes in K-S system remains relatively underexplored. As mentioned, carbonate-based solvents are rarely applied in Li/Na-S systems, especially for C/S cathodes, due to their vulnerability to nucleophilic attack by highly reactive lithium and sodium polysulfides. However, their use in K-S batteries may be potential compared to ether-based electrolyte. Compared to ether solvents, potassium polysulfides generally exhibit a lower solubility in carbonate-based organic solvents, which can intrinsically prevent shuttle effect during cycling process.[119] Furthermore, with the formation of CEI layers on the surface of cathode materials via nucleophilic reaction, the redox processes in those K-S systems are dominated by solid-solid or quasi-solid-state conversion reactions, effectively further circumventing the formation of soluble long-chain polysulfide intermediates that are highly reactive with potassium anode. Moreover, due to its weaker Lewis acidity compared to Li^+ and Na^+, K^+ exhibits a smaller Stokes radius (3.6 Å versus 4.8 and 4.6 Å, respectively) in carbonate-based solvents.[32] As a result, potassium demonstrates the highest ionic conductivity, and transport number among the three alkali metal ions in carbonate electrolytes. Therefore, the adoption of carbonate solvents in K-S batteries reflects a strategic trade-off

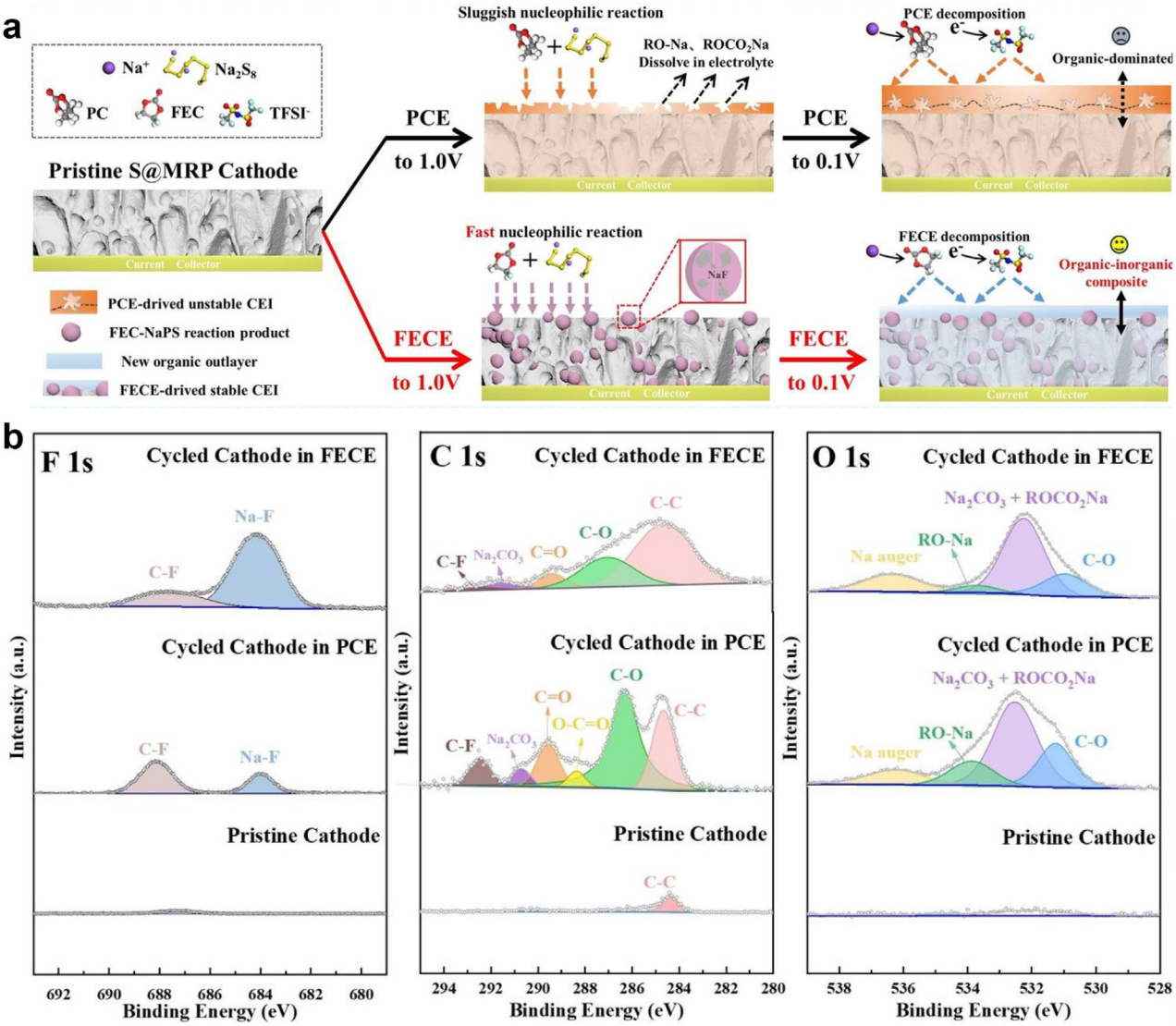

Figure 9. a) Schematic illustration of the working mechanism of Na-S batteries in FECE electrolyte. b) XPS results of F 1s, C 1s, and O 1s. Reproduced with permission.[177] Copyright 2024, Wiley-VCH.

that leverages the unique chemical behavior of potassium polysulfides to suppress shuttle effects, while taking advantage of the high ionic conductivity and stable-operating window offered by carbonate electrolytes.

To address these issues, researchers are exploring modifications to carbonate-based electrolytes by tailoring their solvation structures. The use of multifunctional electrolytes, which integrate multiple solvents to optimize physicochemical properties, has shown promise in overcoming these challenges. Further details on electrolyte optimization strategies for K-S systems are discussed in the subsequent sections.

4.1.2. Low Concentration Ether-based Electrolytes

Ether solvents have been widely used in alkali-sulfur battery systems due to their favorable solvation ability for metal salts and good compatibility with sulfur species and alkali-metal anode. Particularly, in Li-S batteries, ether solvents effectively dissolve lithium salts and are well-suited for interacting with sulfur species, facilitating efficient electrochemical performance. However, despite the significant advantages of ether-based electrolytes in Li-S batteries, they also face various challenges, which are even more pronounced in Na-S and K-S batteries.

In Li-S batteries, ether solvents with strong lithium-ion solvation capability promote LiPS dissolution, enhancing electrochemical activity and conversion kinetics. However, this also intensifies the shuttle effect, leading to active material loss, low Coulombic efficiency, and rapid capacity fading. Conversely, ether solvents with weak solvation ability can suppress LiPS dissolution, but result in sluggish sulfur conversion, ultimately compromising battery performance.[107,145,195] Therefore, a balance between LiPS dissolution and sulfur conversion kinetics is important, which is mainly determined by the electrolyte

composition. Similar challenges are encountered with Na-S and K-S batteries. To be specific, the larger ionic radii and higher electrochemical reactivity of sodium and potassium complicate solvation stability and electrolyte selection. For instance, in K-S systems, the weak solvation ability and large size of potassium ions lead to sluggish ion conductivity. Although ether solvents with strong solvating power can enhance this conversion, they also aggravate the shuttle effect, compromising battery performance.

Therefore, regulating the solvation structure of ether electrolytes is a key strategy for enhancing metal-sulfur battery performance. Approaches, such as modifying ether solvent structures, employing low donor-number solvents, or introducing sterically hindered molecules, can effectively weaken the solvation strength for lithium ions, polysulfides, and related species. This helps suppress long-chain polysulfide dissolution, while maintaining good ionic conductivity. Such strategies not only mitigate the shuttle effect, but also stabilize the electrode–electrolyte interface, reducing parasitic reactions and improving cycling stability and safety. As a result, moderately solvating ether-based electrolytes may present a promising pathway for advancing metal-sulfur batteries and offer valuable insights for future electrolyte design.

Li-S Batteries with LCEEs: LCEEs have been extensively studied as standard electrolyte systems for Li-S batteries. A typical LCEE for Li-S consists of DME and 1,3-dioxolane (DOL) in 1 M LiTFSI, owing to their low viscosity, high ionic conductivity, and ability to dissolve intermediate LiPS, which enhances the redox kinetics.[149] Nevertheless, the intrinsic drawbacks of ether solvents limit their practical application. In addition to the shuttle effect, the highly reactive lithium-metal anode is susceptible to uncontrolled dendrite growth and interfacial side reactions in ether solvents, leading to an unstable SEI and potential safety risks.

To address these challenges, recent research has focused on regulating the solvation structure of lithium ions and polysulfides in ether-based electrolytes to mitigate the shuttle effect and stabilize the electrode–electrolyte interface. Specifically, the design of weakly solvating electrolytes has emerged as an effective strategy to inhibit polysulfide dissolution and suppress undesired parasitic reactions. By incorporating low-donor-number solvents, weakly coordinating molecules, or sterically hindered ether solvents, the solvation strength between Li^+ and solvent molecules can be significantly reduced.[195–197] This weak solvation environment promotes the formation of a more stable interphase, inhibits the dissolution of long-chain polysulfides, and encourages the deposition of insoluble short-chain species near the cathode. Additionally, weakly solvating electrolytes help regulate the desolvation process at lithium-metal surface, enabling a uniform lithium deposition and enhancing SEI stability. These electrolyte systems offer new opportunities to enhance cycling stability, Coulombic efficiency, and safety of Li-S batteries, representing a crucial development direction for future electrolyte engineering.

Zhang's research group systematically investigated the role of solvent–diluent interactions in tuning the solvation structure of lithium polysulfides (LiPSs) and their effect on electrode kinetics. The study focused on electrolytes composed of DME as the primary solvent and hydrofluoroether (HFE) as the diluent.[196] Binding energy analysis revealed that Li_2S_6 exhibits a stronger interaction with DME (−2.59 eV) compared to HFE (−1.36 eV), underscoring DME's superior solvation capability arising from its pronounced electron-donating characteristics. In contrast, HFE weakens LiPS–solvent interactions by acting as a weakly coordinating diluent. Also, molecular dynamics (MD) simulations revealed a dual-shell solvation structure. DME coordinates LiPSs in both inner (3.9–5.5 Å) and outer (> 5.5 Å) shells, while HFE occupies only the outer shell. Notably, as the HFE content increases, it displaces DME in the outer shell (**Figure 10**a–c), reducing the overall solvation strength. This adjustment lowers Li_2S_8 solubility from 4.3 M (0% HFE) to 1.8 M (30% HFE), which correlates with a 60% reduction in shuttle current and a significant increase in Coulombic efficiency (81.8% versus 38.2% without HFE). By occupying the outer shell, HFE also reduces LiPS reactivity toward lithium anode, promoting uniform Li deposition. A moderate HFE ratio (20%) offers a balanced solvation structure that supports favorable redox kinetics, enabling 146 stable cycles in coin cells with a high sulfur loading of 4.3 mg cm^{-2} and 30 cycles in pouch cells with a specific energy of 338 Wh kg^{-1}. This work highlights how controlling solvent–diluent interactions can guide electrolyte design for long-life and high-performance Li-S batteries.

Similarly, Huang et al. proposed a novel encapsulated lithium-polysulfide electrolyte (EPSE) using hexyl methyl ether (HME) as a co-solvent to address a trade-off between rate capability and parasitic reactions in Li-S batteries.[145] The HME-based EPSE (HME EPSE) features a bilayer solvation structure, where DME and DOL form the inner solvent shell to dissolve and stabilize LiPSs, while HME constitutes the outer shell and kinetically suppresses parasitic reactions at the lithium-metal anode owing to its weak solvating ability and high reductive stability (Figure 10d). The outer HME layer reduces the reactivity of LiPSs with lithium metal, thereby mitigating the shuttle effect and preserving active material. This effect is supported by X-ray photoelectron spectroscopy (XPS) analysis, which shows lower sulfur content on cycled lithium anodes in the HME EPSE compared to conventional DOL/DME electrolytes. The electrolyte delivers a high specific capacity of ≈1040 mAh g^{-1} at C/10 and prolongs cycle life to 113 cycles under demanding conditions, in contrast to 65 cycles with conventional electrolytes (Figure 10e). MD simulations confirm the bilayer solvation structure and emphasize HME's critical role in maintaining cathode redox kinetics, while protecting the anode interface. This study demonstrates that the deliberate selection of co-solvents, such as HME, enables the simultaneous optimization of rate performance and cycling stability, thereby advancing the development of practical high-energy-density lithium–sulfur batteries.

Furthermore, Zhang et al. investigated the electrolyte solvation structure with lithium polysulfides (PSs) by introducing anti-reductive solvent shells to mitigate parasitic reactions with lithium-metal anode.[198] The key strategy involved employing diisopropyl ether (DIPE) as a co-solvent with conventional solvents, such as DOL and DME (Figure 10f). MD simulations and nuclear magnetic resonance (NMR) spectroscopic analyses revealed a dual-solvation shell configuration surrounding PSs. The inner shell, composed of DOL and DME, facilitates PS dissolution and supports cathode redox kinetics. The outer shell, predominantly formed by DIPE, provides resistance to reduction decomposition by lithium metal. Due to its low

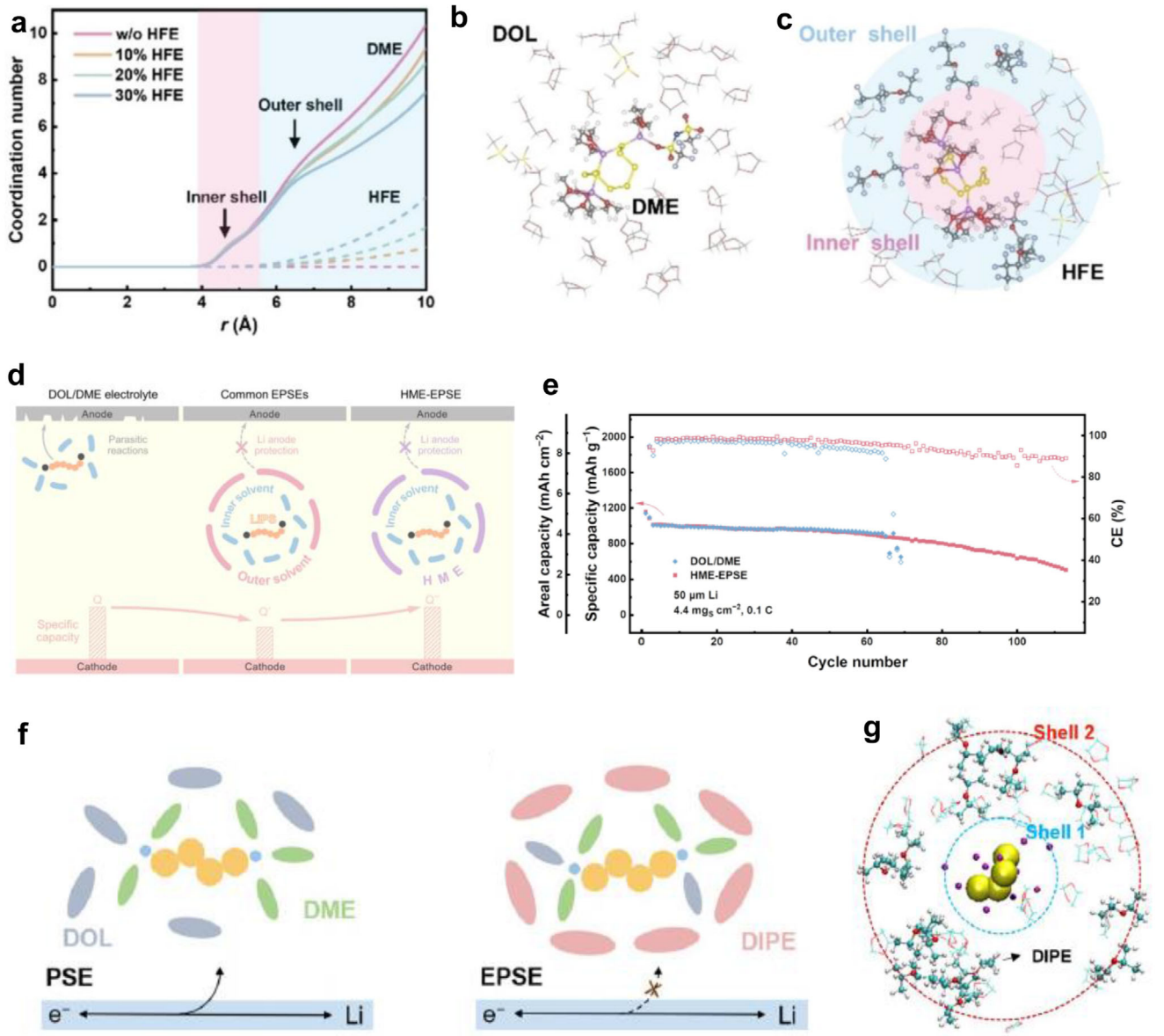

Figure 10. a) Coordination number (CN) profiles of DME and HFE molecules surrounding S_8^{2-} in different electrolyte systems derived from MD simulations. MD snapshots illustrating the solvation environment of S_8^{2-} in the electrolytes b) without HFE and c) containing 30% HFE. Reproduced with permission.[196] Copyright 2023, Wiley-VCH. d) Schematic illustration of the working principles of different electrolyte systems. e) Cycling stability of Li-S coin cells employing DOL/DME electrolyte or HME-EPSE under harsh testing conditions. Reproduced with permission.[145] Copyright 2024, Wiley-VCH. f) Schematic illustration of the electrolyte structure of PS species in PSE and EPSE. g) Representative MD simulation snapshots showing the molecular configuration surrounding S_4^{2-} in EPSE. Reproduced with permission.[198] Copyright 2024, Wiley-VCH.

solvating ability and high carbon-to-oxygen ratio, DIPE preferentially occupies the outer shell, effectively encapsulating PSs and reducing their direct interaction with the lithium surface. This encapsulation is illustrated in Figure 10g, showing that DIPE limits PS exposure to the lithium anode, whereas conventional DOL-rich outer shells remain highly reactive. NMR spectra further confirmed that DIPE exhibits weaker ion-dipole interactions compared to DOL and DME, which is consistent with the MD simulation results. This anti-reductive outer shell significantly decreased sulfur deposition on the lithium surface, suppressing parasitic reactions and enhancing battery performance. Li-S cells with the DIPE-based electrolyte achieved 120 stable cycles under practical conditions, including thin lithium metal (50 μm) and high sulfur loading (4.0 mg cm^{-2}), whereas cells with conventional electrolytes delivered only 62 cycles. Additionally, the study showcased a 300 Wh kg^{-1} pouch cell, emphasizing the practical applicability of the approach. These results underscore the critical role of solvent shell engineering in optimizing electrolyte design, with DIPE serving as a functional diluent to realize a balance between PS solubility and anode stability. This work offers valuable insights into electrolyte development for conversion-type batteries.

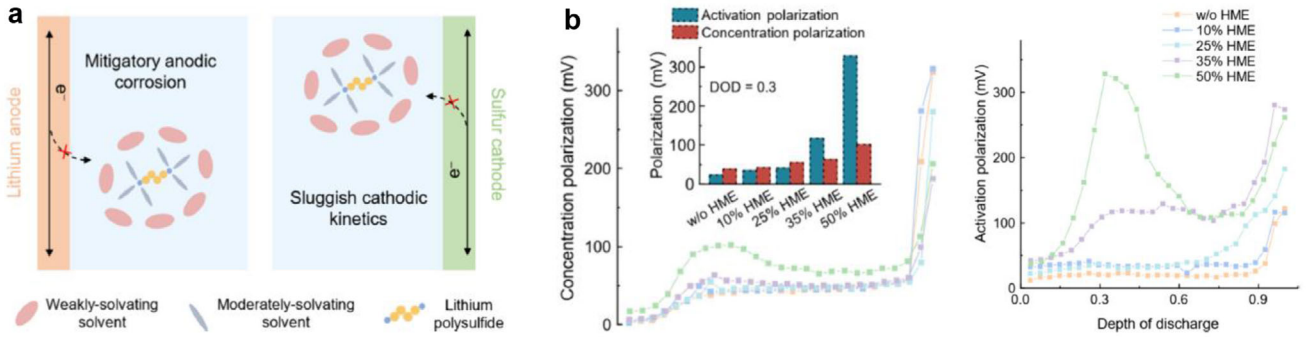

Figure 11. a) Schematic illustration of LiPS redox reactions at the anode and cathode in a weakly solvating electrolyte. b) Variations of concentration polarization (left) and activation polarization (right) with depth of discharge (DOD), along with their comparison at DOD = 0.3. Reproduced with permission.[195] Copyright 2018, American Chemical Society.

By employing low-polarity, low-density solvents, such as HME, weakly solvating electrolytes (WSEs) effectively reduce the solvation strength of LiPSs. This weakened solvation suppresses parasitic side reactions, mitigates LiPS shuttling, and promotes stable lithium deposition (**Figure 11a**).[195] However, this inherent advantage of WSEs is accompanied by a significant drawback. The diminished solvation environment not only lowers the solubility of LiPSs, but also alters the interfacial reaction pathways and increases the energy barrier for charge transfer during LiPS redox conversion, thereby severely hindering cathodic reaction kinetics. Zhang et al. systematically investigated the kinetic degradation mechanism of LiPSs in WSEs, revealing that activation polarization (η_{act}), rather than ohmic resistance or concentration polarization, is the dominant factor contributing to voltage hysteresis and limited sulfur utilization in WSE-based Li-S batteries (Figure 11b). Through a combination of electrochemical analysis and density functional theory (DFT) calculations, the study shows that the weakened solvation environment increases the charge-transfer activation energy and shifts the rate-determining step of LiPS conversion, resulting in sluggish redox kinetics and significant polarization.

To address this intrinsic kinetic limitation while maintaining the anode protection benefits of WSEs, a titanium nitride (TiN) electrocatalyst was rationally introduced to accelerate the interfacial charge-transfer process. The TiN catalyst enhances LiPS adsorption and facilitates efficient electron transfer, reducing η_{act} by ≈70% (from 115 to 35 mV), thereby enabling a high reversible capacity of 1200 mAh g^{-1} and excellent cycling stability over 100 cycles in coin cells. Furthermore, this electrocatalytic approach was successfully extended to high-loading 2.5 Ah Li-S pouch cells, delivering a practical energy density of 381 Wh kg^{-1} based on the total cell mass and stable performance over 35 cycles with a high Coulombic efficiency of 95%. This work not only elucidates the fundamental kinetic limitations of LiPS conversion in WSEs, but also presents an effective electrocatalytic strategy to resolve a trade-off between anode protection and cathode performance, thereby advancing the practical development of high-energy-density and long-cycle-life Li-S batteries.

In 2023, Cui et al. proposed an electrolyte with moderate polysulfide solubility by tailoring the composition of solvent and diluent to achieve a balance between rapid reaction kinetics and effective shuttle suppression.[150] Traditional ether-based electrolytes with ultrahigh or high LiPS solubility (> 200 mM [S]), such as DOL/DME systems (≈1100 mM [S]), enable fast kinetics, but suffer from severe polysulfide shuttling (**Figure 12a**). In contrast, a moderate solubility range (50–200 mM [S]) was identified as optimal, allowing sufficient LiPS dissolution for efficient sulfur conversion, while minimizing the shuttle effect. To achieve this balance, the authors developed single-solvent, single-salt, moderate-solubility electrolytes (S_6MILE) using fluorinated ethers (Figure 12b).

Fluorination weakens the interaction between solvent molecules and lithium ions, which reduces polysulfide solubility, while retaining adequate ionic conductivity. MD simulations indicated that fluorination promotes Li_2S_6 clustering, correlating with lower solubility. As a result, the fluorinated 1,4-dimethoxybutane (F4DMB)-based S_6MILE enabled a fivefold improvement in cycle life (150 cycles with 99.89% Coulombic efficiency at 0.2C rate) compared to the conventional DOL/DME under lean electrolyte conditions (E/S = 5 μL mg^{-1}). Moreover, the formation of LiF-rich SEIs facilitated stable lithium plating and stripping, maintaining over 98% Coulombic efficiency. This study identifies moderate LiPS solubility (50–200 mM [S]) as a key electrolyte design parameter for Li-S batteries. Fluorinated ether-based S_6MILE electrolytes, especially those based on F4DMB, deliver high capacity, extended cycle life, and excellent calendar stability, offering a clear molecular strategy for advancing Li-S battery technology toward practical applications.

Na-S/K-S Batteries with LCEEs: In Na-S/K-S batteries, commonly used ether-based solvents include diethylene glycol dimethyl ether (DEGDME) and tetraethylene glycol dimethyl ether (TEGDME).[112] Similar to the Li-S system, the shuttle effect remains a primary challenge. Moreover, due to the higher reactivity of the sodium/potassium anode compared to lithium anode, controlling polysulfide solubility and suppressing the shuttle effect is even more critical in the Na-S/K-S system. Therefore, the research on LCEEs for Na-S/K-S Batteries is still in the early stage and most of them are focused more on the sulfur conversion behavior within LCEEs.

Dou et al. investigated the redox mechanisms of sulfur in room-temperature Na-S batteries.[199] They found that sulfur confined within the pores of a carbon matrix undergoes a solid-to-solid phase transition, whereas sulfur dispersed on the carbon surface tends to experience a solid-to-liquid transition. These

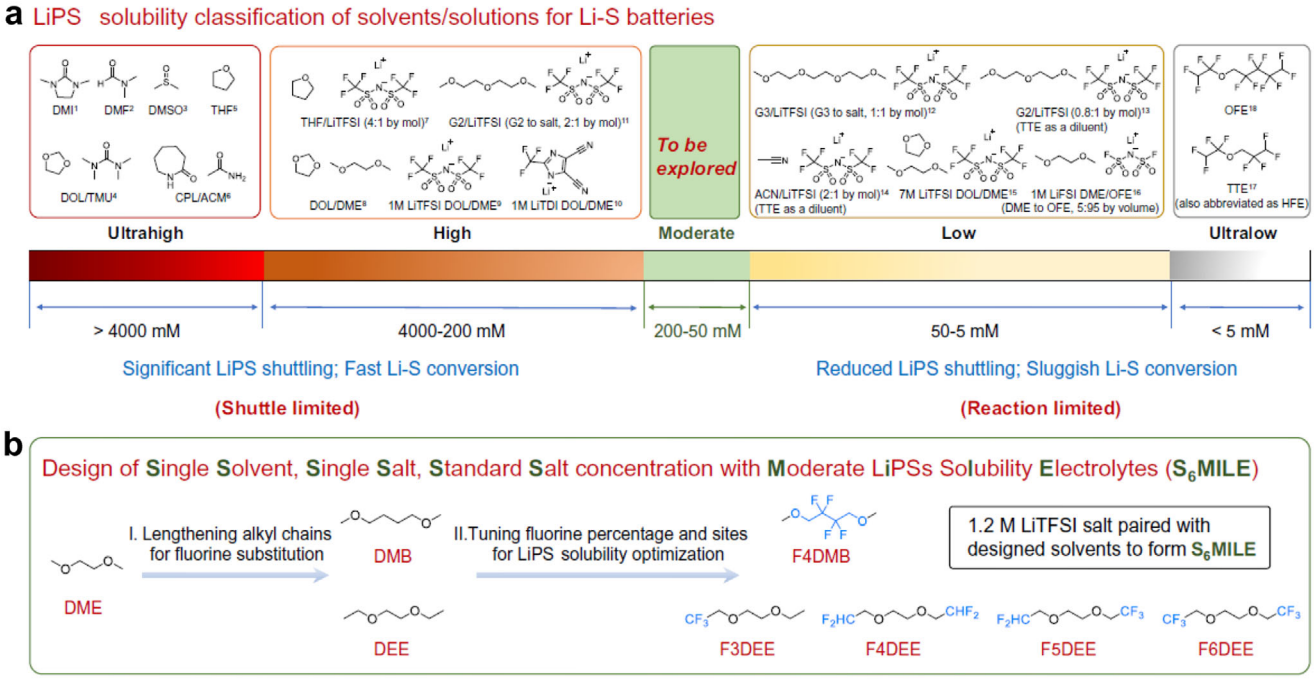

Figure 12. a) Classification of solvents and electrolytes in Li-S batteries based on LiPS solubility. b) Design strategy of S_6MILE electrolytes with controlled LiPS solubility for stable and high-performance Li-S batteries. Reproduced with permission.[150] Copyright 2023 National Academy of Sciences.

distinct phase transition pathways result in markedly different voltage–capacity profiles. Specifically, the solid-to-solid transition is characterized by a discharge capacity below 1.8 V (**Figure** 13a), while the solid-to-liquid process exhibits three discharge plateaus at ≈2.0, 1.5, and 1.0 V (Figure 13b). This divergence in electrochemical behavior is primarily governed by the sulfur distribution: sulfur embedded in carbon pores is isolated from the bulk electrolyte, with Na^+ transport occurring through the CEI, whereas surface-deposited sulfur is in direct contact with the solvent, resulting in either side reactions in carbonate electrolytes or dissolution into ether-based systems.

Hwang and colleagues synthesized a series of K_2S_x polysulfides ($1 \leq x \leq 6$) and systematically investigated their solubility in diethylene glycol dimethyl ether (DEGDME). In contrast to lithium polysulfides, short-chain K_2S_x species ($x < 5$) exhibit negligible solubility in DEGDME, whereas long-chain species ($x \geq 5$) dissolve readily, forming a dark brown solution. This distinct solubility trend provides critical insights into the physicochemical behavior of potassium polysulfides in K-S battery systems. The solubility disparity among different chain lengths likely arises from variations in polysulfide molecular structure, intermolecular interactions, and solvent-specific selectivity. Such behavior plays a pivotal role in governing polysulfide dissolution, mobility, and the shuttle effect, which collectively determine the electrochemical performance and stability of K-S and Na-S batteries.

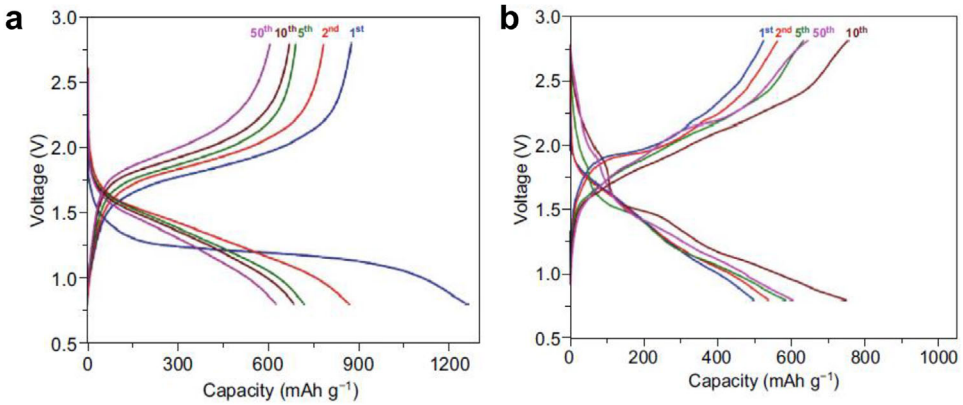

Figure 13. a,b) Discharge-charge profiles of S in the pores and surface of the cathode host, respectively. Reproduced with permission.[199] Copyright 2021, Springer Nature.

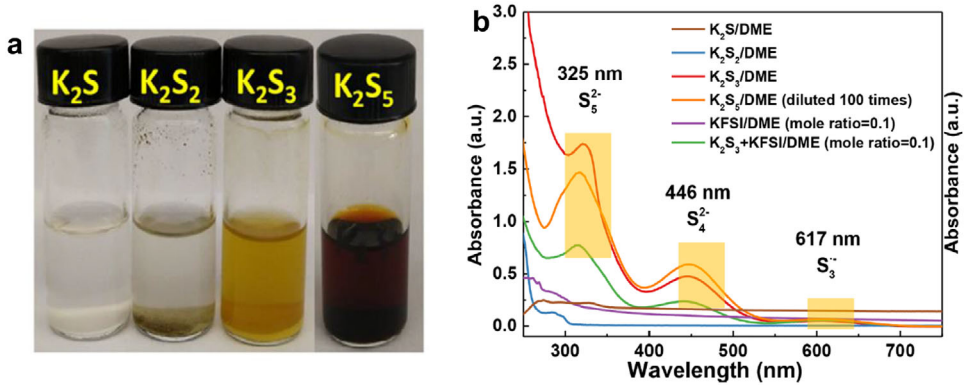

Figure 14. a) Digital photos of K_2S_x dissolved in DME solvents. b) UV–vis spectra of K_2S_x in different solutions. Reproduced with permission.[200] Copyright 2018, American Chemical Society.

Further advancing this understanding, Wu et al. examined the solubility and redox behavior of short-chain K_2S_x species ($1 \leq x \leq 3$) in potassium bis(fluorosulfonyl)imide (KFSI)-based dimethyl ether (DME) electrolytes.[200] They quantified the solubility of K_2S_3 and K_2S_2 in DME as 71.4 mg/100 g and 12.6 mg/100 g, respectively. Despite the relatively low solubility, K_2S_3 forms pale yellow solutions containing soluble polysulfide species, such as S_5^{2-}, S_4^{2-}, and $S_3^{\bullet-}$, as evidenced by UV–vis spectroscopy (**Figure 14**a,b). Notably, S_5^{2-} undergoes disproportionation into S_6^{2-} and S_4^{2-}, indicating a complex equilibrium involving species like K_2S_6, K_2S_4, K_2S_5, and potentially K_2S and K_2S_2. Interestingly, the presence of KFSI salt suppresses the solubility of K_2S_3, attributed to the co-ion effect arising from increased ionic strength. In addition, NMR spectroscopy confirmed that FSI^- anions remain chemically stable in the presence of K_2S_3, highlighting the compatibility of the KFSI–DME electrolyte with polysulfides.

Although these findings shed light on the solvation chemistry and redox dynamics of sodium/potassium polysulfides, research on LCEEs design for Na-S/K-S batteries remains in its infancy. Future efforts should emphasize a deeper mechanistic understanding of polysulfide speciation and solubility behavior, address shuttle-related challenges, and explore alternative systems, such as ionic liquids and high-concentration electrolytes to enable high-performance Na-S/K-S batteries.

4.2. High-Concentration Electrolytes and Localized High-Concentration Electrolytes

Conventional ether-based electrolytes provide high ionic conductivity and efficient sulfur utilization. However, their high polysulfide solubility leads to continuous dissolution and diffusion between electrodes, resulting in capacity fading, low Coulombic efficiency, and poor cycling stability. These drawbacks hinder the practical application of metal-sulfur batteries. To address this issue, advanced electrolyte designs, such as high-concentration electrolytes (HCEs) and localized high-concentration electrolytes (LHCEs) have been developed (**Figure 15**a).

Figure 15b presents three representative solvation structures in electrolytes: solvent-separated ion pairs (SSIPs), contact ion pairs (CIPs), and aggregates (AGGs). In conventional low-concentration electrolytes, SSIPs dominate due to the abundance of free solvent molecules and weak ion–ion associations.[201] As the salt concentration increases, the number of free solvent molecules decreases and the ion–ion interactions strengthen. At sufficiently high salt concentrations, the electrolyte enters the HCE regime, where the limited solvent environment favors the formation of CIPs and AGGs. These compact solvation structures enhance electrolyte stability, facilitate the formation of an inorganic-rich interphase, and reinforce the structural integrity of both electrodes.

By tuning the salt concentration, solvent composition, and additives, the solvation environment can be effectively regulated to suppress polysulfide dissolution and stabilize the electrode–electrolyte interface in HCEs. Although HCEs are effective in inhibiting polysulfide diffusion and promoting an anion-rich solvation structure that favors the formation of a stable inorganic-rich SEI, their practical use is limited by high viscosity, poor wettability, and increased cost. To overcome these limitations, LHCEs have been developed by incorporating inert diluents with low permittivity and donor ability into the HCE matrix. This design maintains the presence of CIPs and AGGs, while significantly reducing viscosity and salt content. As a result, LHCEs offer improved ionic conductivity and lower cost compared to conventional HCEs. Together, HCEs and LHCEs effectively mitigate the shuttle effect, enhance interfacial stability, and improve the cycling performance, safety, and long-term viability of metal-sulfur batteries.

4.2.1. Li-S Batteries with HCEs and LHCEs

Nazar's group proposed a novel HCE system that addresses both cathode and anode challenges in Li-S batteries. This system utilizes diglyme (G2) as the solvent, lithium bis(trifluoromethanesulfonyl)imide (LiTFSI) as the lithium salt, and 1,1,2,2-tetrafluoroethyl 2,2,3,3-tetrafluoropropyl ether (HFE) as the diluent.[147] By tuning the solvent-to-salt molar ratio to 0.8:1, the electrolyte forms a 3D network that significantly reduces solvent activity and suppresses polysulfide dissolution. This structural change shifts the sulfur redox mechanism from the conventional dissolution–precipitation pathway to a quasi-solid-state conversion, allowing for reduced electrolyte volumes.

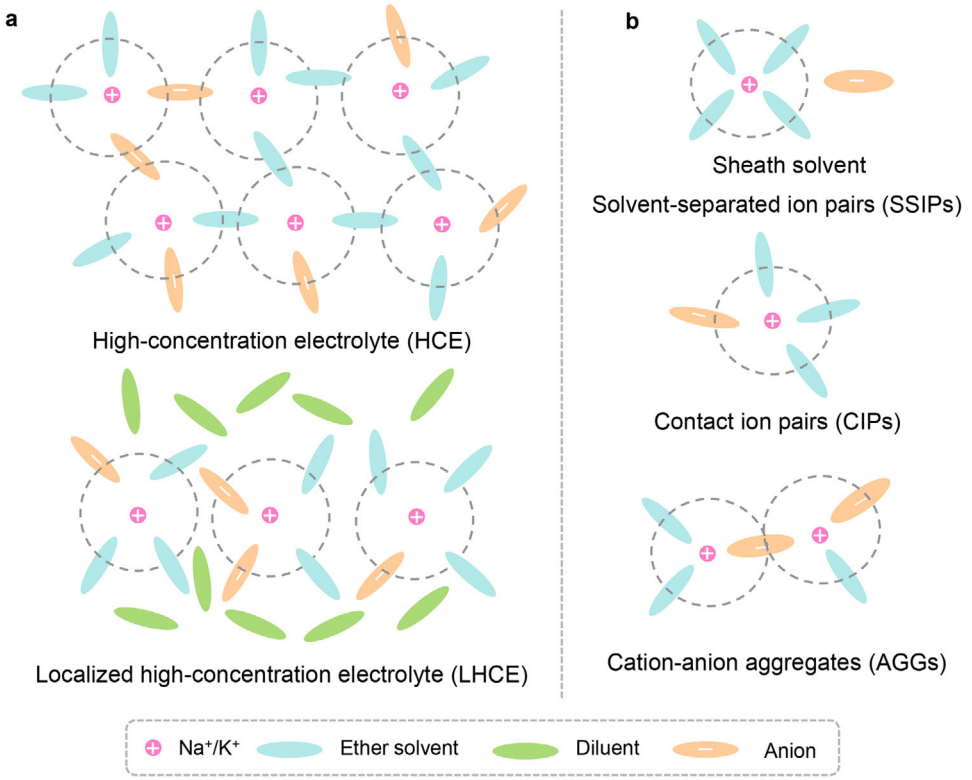

Figure 15. a) Schematic illustration of the solvation structures of ether-based HCE and LHCE. b) Schematic illustration of three solvation structures.

The proposed electrolyte features a high Li^+ concentration (≈4.2 M) and an elevated lithium-ion transference number (t_{Li+} = 0.73), which together alleviate localized space charge effects and suppress dendrite formation. Notably, the SEI is enriched with ion-conductive Li_2O, as confirmed by XPS, rather than organic decomposition products, contributing to enhanced interfacial stability (**Figure 16**a–d). In symmetric Li||Li cells, this electrolyte enables stable cycling for over 400 h at 1 mA cm^{-2} with minimal polarization. Moreover, in Li-S full cells with an electrolyte-to-sulfur (E/S) ratio of 5 µl mg^{-1}, a high reversible capacity of 720 mAh g^{-1} is retained after 100 cycles (Figure 16e). This work presents a promising strategy for realizing high-energy, long-cycle-life Li-S batteries by fine-tuning the solvation environment to synergistically stabilize both the sulfur cathode and lithium metal anode.

Intriguingly, Wang's group introduced a novel lightweight electrolyte for Li-S batteries with SPAN cathode, addressing the key challenges in energy density and cyclability through engineered solvation structures and interfacial chemistry.[202] The electrolyte consists of 1.7 M LiFSI in triethyl phosphate (TEP) and dibutyl ether (DBE) (1:3 v/v, referred to as TD; Figure 16f), achieving a low density of 1.04 g mL^{-1}, which is 40%–50% lighter than conventional LHCEs like LiFSI-TEP/1,1,2,2-tetrafluoroethyl 2,2,3,3-tetrafluoropropyl ether (TTE). This reduction in weight yields a 12%–20% improvement in cell-level energy density, which is especially advantageous for high-capacity Li/SPAN systems wherein the electrolyte mass constitutes a dominant fraction. Notably, DBE acts as a diluent that enhances its affinity with TEP, drawing TEP away from the Li^+ solvation shell and encouraging FSI^- anion coordination. Spectroscopic analyses (FT-IR, Raman, PFG-NMR) confirm this unique solvation structure, which promotes the formation of robust, inorganic-rich interphases (e.g., LiF and Li_3N) on both electrodes. These interphases are essential for accommodating large volume changes (> 40% for SPAN) and suppressing side reactions. Compared to TTE-based LHCEs, the TD electrolyte shows reduced solvent decomposition and greater reductive stability, delivering a high Li plating/stripping Coulombic efficiency (99.4%) and long cycling life (> 200 cycles at a lean electrolyte condition of 5 g $(Ah)^{-1}$). It also demonstrates low volatility and thermal stability, which is comparable to TTE-based systems under abuse conditions. Mechanistically, the strong interaction between TEP and DBE mitigates solvent decomposition, retards electrolyte consumption, and sustains efficient ion transport (1.32 mS cm^{-1}), thereby enabling lean-electrolyte operation at 3 g Ah^{-1}. In pouch cells, this translates to a projected energy density of 205 Wh kg^{-1}. Overall, this work underscores the importance of lightweight diluent selection, solvation design, and interphase engineering for advancing high-energy Li-metal batteries.

Furthermore, Pang's group developed an innovative tetrahydrofuran (THF)–LiTFSI–toluene electrolyte that enables a quasi-solid-state sulfur reaction under lean electrolyte conditions, effectively mitigating polysulfide shuttling and sluggish redox kinetics.[108] By incorporating low-cost, low-density toluene into a concentrated THF–LiTFSI solvate, the original 3D solvation network is disrupted, forming two distinct microdomains (**Figure 17**a), including (1) aromatic-rich regions that partially dissolve elemental sulfur (S_8, ≈3 mg mL^{-1} at 35 °C) to

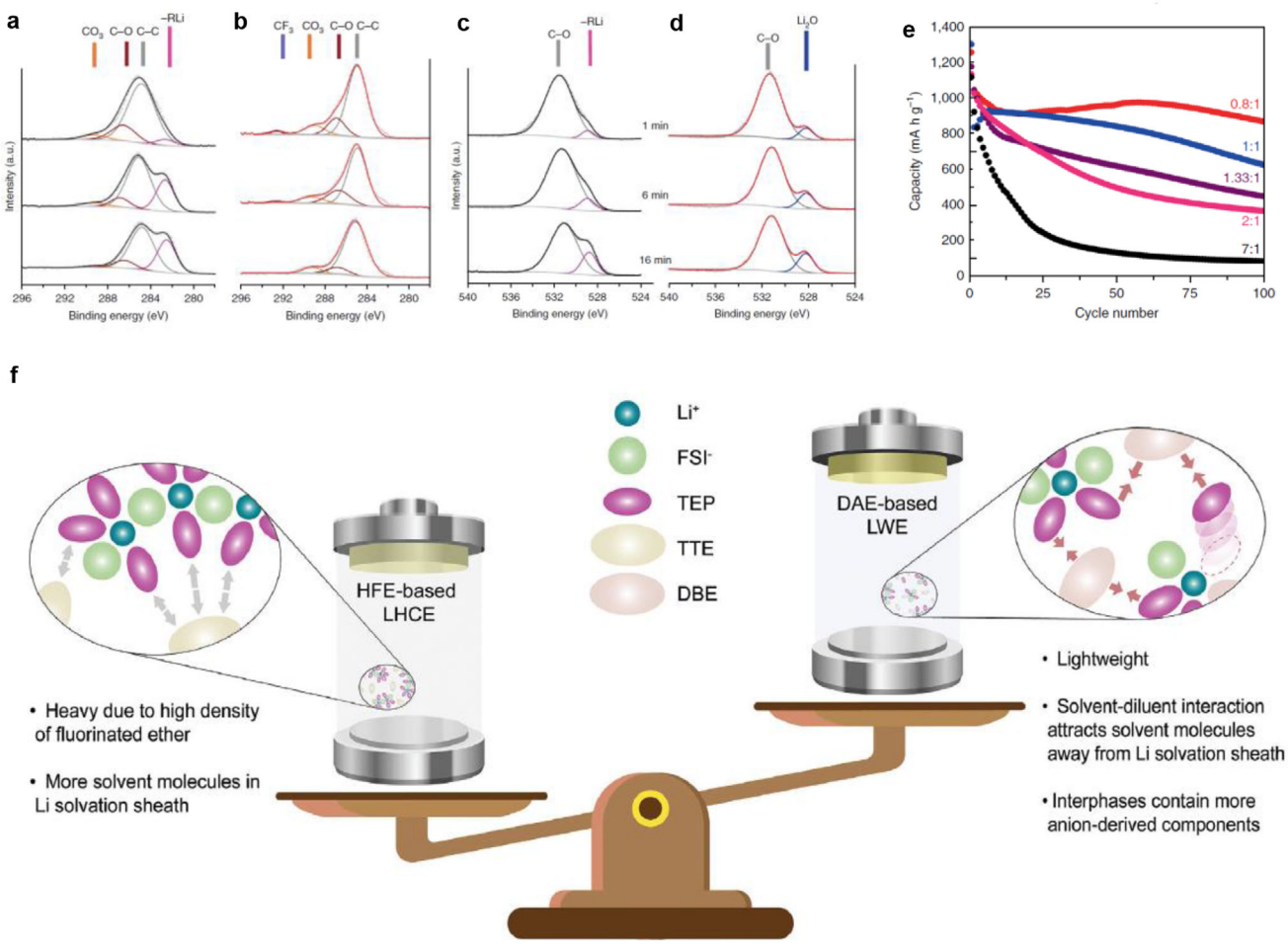

Figure 16. XPS analysis of the SEI on the Li-metal anode after complete stripping following ten cycles in Li-Cu cells. The (a,b) C 1s and (c,d) O 1s spectra. e) Cycling performance of Li-S batteries with different G2:LiTFSI electrolytes at C/2 rate. Reproduced with permission.[147] Copyright 2018, Springer Nature. f) Schematic illustration of the lightweight electrolyte concept and its main advantages over traditional LHCEs. Reproduced with permission.[202] Copyright 2024, Wiley-VCH.

enhance redox kinetics, and (2) THF–$TFSI^-$ coordinated domains that retain ultra-low polysulfide solubility (< 2%), while preserving efficient Li^+ transport pathways. MD simulations reveal that toluene's electron-donating aromatic rings interact with the electron-deficient –CF_3 groups of $TFSI^-$ anions, breaking up the THF–LiTFSI aggregates. This restructured solvation environment favors $TFSI^-$ reduction over THF decomposition, leading to the formation of an inorganic-rich SEI composed of LiF, Li_3N, and Li-S species. Through solvent-driven microstructure engineering, this electrolyte system decouples sulfur redox kinetics from electrolyte volume, offering a promising strategy for high-energy, lean-electrolyte Li-S batteries.

Kim et al. developed a DME–fluorinated ether (FE) electrolyte system to address polysulfide shuttling and electrolyte depletion in lean-electrolyte Li-S batteries.[154] The degree of fluorination in the FE molecules modulates the Li^+ solvation structure through H–F interactions with DME. As shown in Figure 17b, increasing fluorination weakens the Lewis basicity of DME, reducing its coordination with Li^+ and enhancing anion (FSI^- and NO_3^-) participation in the solvation shell. This transition adjusts the electrolyte from a strongly solvating to a moderately solvating regime, achieving a balance between suppressing polysulfide solubility and maintaining sulfur redox kinetics. Moreover, the moderate solvation promotes the preferential reduction of FSI^- and NO_3^-, forming an inorganic-rich SEI composed of LiF and Li_3N, with 25% lower carbon content compared to conventional DME-based systems. The optimized DME–TFTFE electrolyte enables a 0.5-Ah Li-S pouch cell with a gravimetric energy density of 405 Wh kg^{-1} at an ultra-lean electrolyte-to-sulfur (E/S) ratio of 2 µL mg^{-1}, maintaining 70% capacity after 80 cycles. This study highlights the crucial role of solvent–cosolvent interactions in tuning solvation structures, providing a framework for designing electrolytes that offer a balance among interfacial stability, redox kinetics, and practical scalability.

Notably, Cui et al. establishes a quantitative relationship between solvation properties and performance in Li-S battery electrolytes by analyzing the solvation free energy (ΔG_{solv}) of Li^+. Their work demonstrates how ΔG_{solv} influences voltage profiles, polysulfide solubility, and cycling stability.[203] The study investigates several ether-based solvents, including DME, DOL,

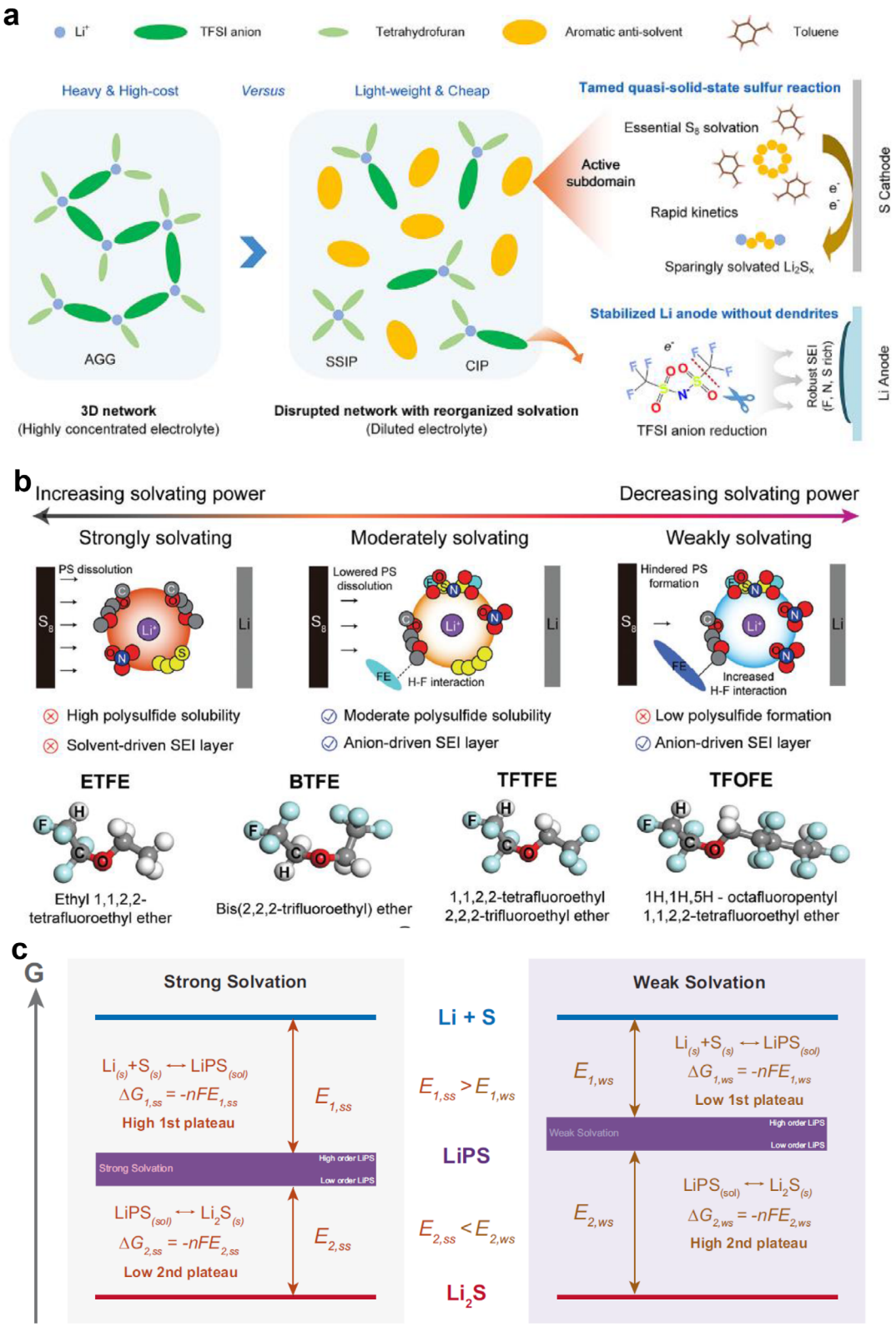

Figure 17. a) Anti-solvent engineering of sparsely solvating electrolytes toward sulfur-solvation-enhanced quasi-solid-state electrochemical processes. Reproduced with permission.[108] Copyright 2023, Elsevier. b) Schematic representation of DME-FE electrolytes with distinct solvation capabilities and chemical configurations of the FE cosolvents applied. Reproduced with permission.[154] Copyright 2024, Wiley-VCH. c) Illustration of the influence mechanism of solvation free energy on the voltage behavior of Li-S batteries. Reproduced with permission.[203] Copyright 2024, Springer Nature.

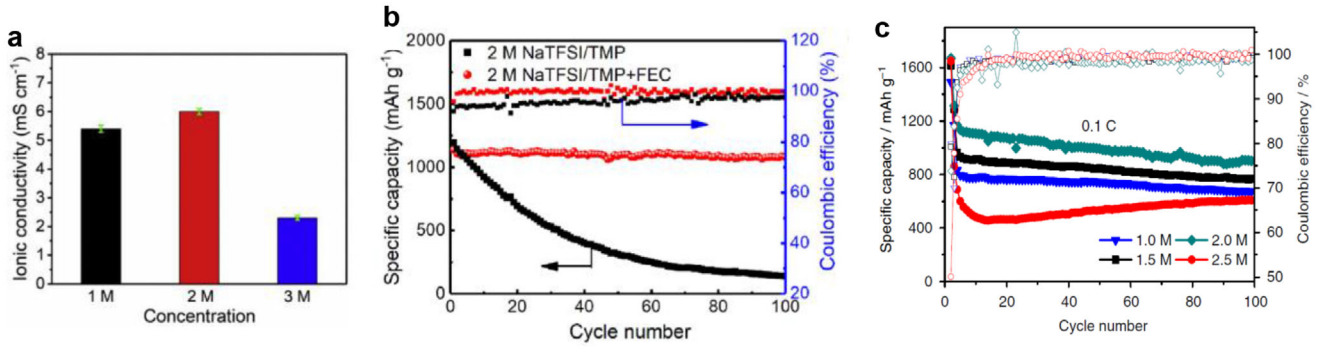

Figure 18. a) Ionic conductivities of electrolyte with different salt concentrations. b) Cycle performance of Na-S batteries with different electrolytes. a,b) Reproduced with permission.[111] Copyright 2019, Elsevier. c) Cycle performance of Na-S batteries with different salt concentrations. Reproduced with permission.[36] Copyright 2018, Springer Nature.

and tetraethylene glycol dimethyl ether (G4), with fluorinated diluents like TTE. Figure 17c illustrates that weaker solvation, achieved through high salt concentrations or TTE addition, reduces the first discharge plateau (Li/S → LiPS) and elevates the second plateau (LiPS → Li_2S). This change is due to the destabilization of LiPS intermediates in weakly solvating electrolytes. Remarkably, DME-TTE mixtures form LHCE that reduce LiPS solubility and shuttle effects, while improving Coulombic efficiency. However, excessive weakening of solvation (e.g., pure TTE) hinders redox kinetics. Generally, the free-energy term ΔG_{solv} governs the thermodynamic stability of lithium polysulfides. Strongly solvating electrolytes, such as DME and G4 lower the polysulfide free energy, thereby elevating the voltage of the first discharge plateau. Conversely, weakly solvating mixtures like DME–TTE raise the polysulfide energy level, reshaping the voltage profile and markedly reducing polysulfide solubility. This balance between thermodynamic stability and kinetics emphasizes the importance of electrolyte design, with fluorinated diluents like TTE offering a promising approach to optimizing performance by tuning solvation structures.

4.2.2. Na-S Batteries with HCEs and LHCEs

As mentioned above, the severe polysulfide solubility and high reactivity of the sodium-metal anode pose significant challenges for operating Na-S batteries with low-concentration electrolytes. Notably, recent studies have shown that adjusting electrolyte concentration and constructing localized solvation structures can effectively control ion diffusion and interfacial reaction dynamics, thereby regulating Na metal deposition behavior, inhibiting dendrite growth, and suppressing NaPS shuttling. These strategies offer valuable insights into electrolyte engineering for Na-S systems, opening new avenues toward achieving high energy density, enhanced cycling stability, and improved safety.

Previously, Wu et al. presented a non-flammable electrolyte system comprising 2 M NaTFSI dissolved in a trimethyl phosphate (TMP) and FEC solvent mixture (7:3 v/v), designed for high-performance room-temperature Na-S batteries.[111] As the electrolyte concentration increases from 1 M to 2 M, the ionic conductivity improves accordingly (**Figure 18a**). However, a further increase to 3 M results in reduced conductivity due to elevated viscosity. Generally, TMP is strategically chosen for its low viscosity (2.3 mPa·s), wide liquid-phase temperature window (−46 to 197 °C), and intrinsic non-flammability, thus addressing the safety concerns posed by volatile carbonate solvents. Ab initio molecular dynamics (AIMD) simulations and XPS depth profiling further indicate that FEC preferentially decomposes due to its lower LUMO energy relative to TMP, leading to the generation of uniform NaF nanocrystals and organic species (e.g., O–C = O groups) within the SEI. This fluorine-rich SEI effectively suppresses dendrite growth and minimizes interfacial resistance. When the proposed electrolyte is paired with the SPAN cathode, the cells deliver a reversible capacity of 788 mAh g^{-1} after 300 cycles at 1C rate (Figure 18b), exhibiting a minimal capacity decay rate of just 0.04% per cycle, which substantially outperforms conventional carbonate-based electrolytes. This work underscores the synergistic effect of phosphate solvents and fluorinated additives in engineering stable electrode–electrolyte interfaces, offering a scalable pathway toward safe, dendrite-free Na-S battery technologies.

Also, Wang's research group demonstrated the cycling performance of room-temperature Na-S batteries using electrolytes with varying NaTFSI salt concentrations (1.0–2.5 M) in a PC:FEC (1:1 by volume) solvent.[36] The optimal capacity retention and highest reversible capacity (907 mAh g^{-1} after 100 cycles at C/10 rate) were achieved at 2 M NaTFSI (Figure 18c). This improvement is attributed to the high salt concentration effectively suppressing polysulfide dissolution and stabilizing the Na anode by inhibiting dendrite growth. However, increasing the concentration beyond 2 M, such as to 2.5 M, results in excessive electrolyte viscosity, which diminishes ionic conductivity and causes capacity degradation. Therefore, a concentration of 2 M provides an optimal balance between polysulfide suppression and ionic transport, thereby maximizing electrochemical performance.

In 2019, our research group was the first to explore the potential advantages of LHCEs in Na-S batteries (**Figure 19a**).[112] By increasing the salt concentration and reducing the amount of free DME solvent, we engineered a distinctive solvation structure that optimizes interactions with anion species. Subsequently, the LHCE was prepared by introducing the "inert" solvent TTE to dilute the high-concentration electrolyte, thereby reducing viscosity, enhancing ionic conductivity, and improving electrode wettability. Notably, Na-S batteries employing this LHCE demonstrated

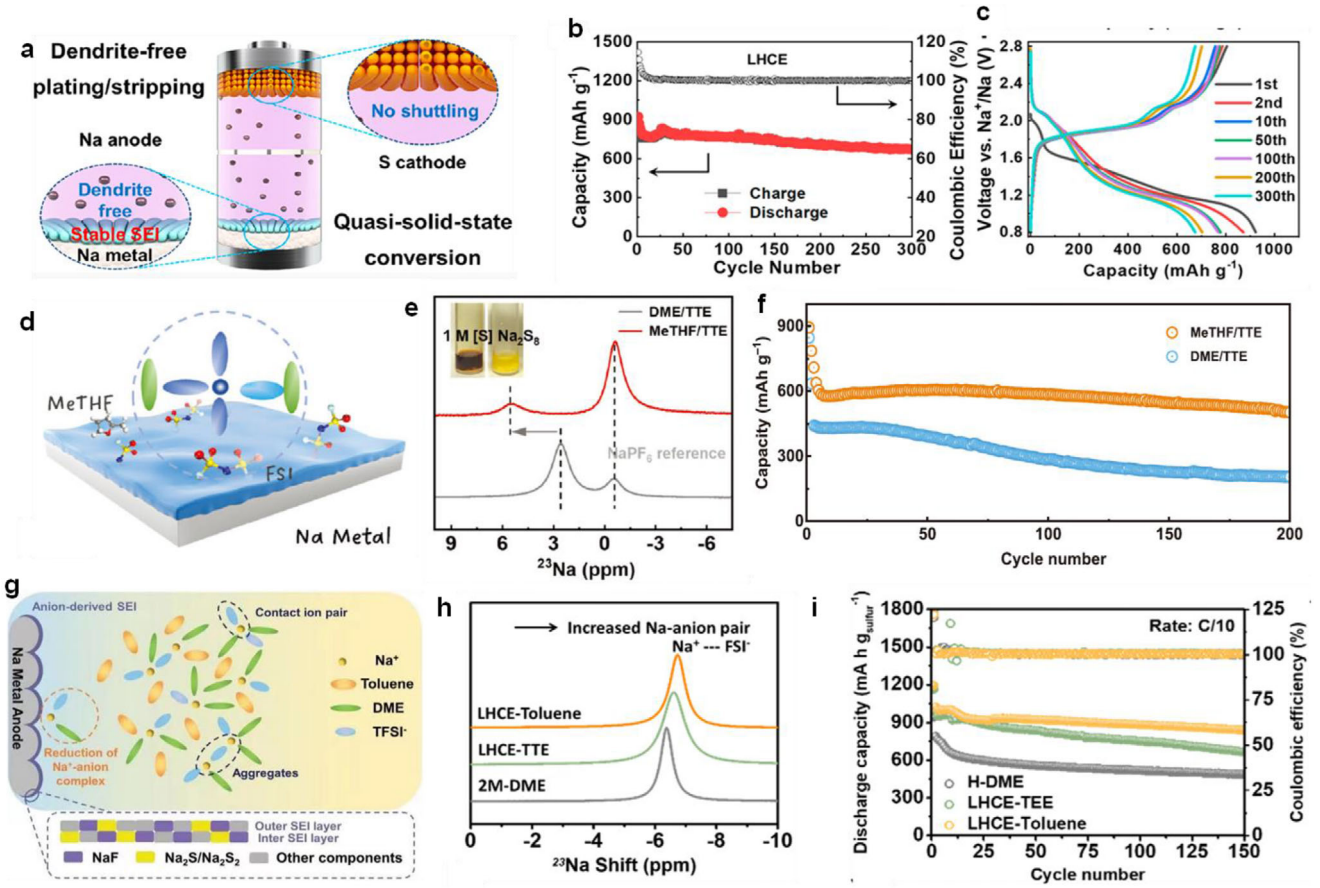

Figure 19. a) Schematic illustration of DME/TTE LHCE electrolyte working mechanism of Na-S battery. b,c) Cycle performance and discharge-charge profiles of DME/TTE LHCE electrolyte-based Na-S batteries at C/10. a–c) Reproduced with permission.[112] Copyright 2021, American Chemical Society. (d) Schematic illustration of MeTHF/TTE LHCE electrolyte working mechanism. e) ^{23}Na NMR spectra of polysulfides-based electrolytes. f) Cycle performance of MeTHF/TTE and DME/TTE-based electrolytes at C/10. d–f) Reproduced with permission.[114] Copyright 2023, Wiley-VCH. g) Schematic illustration of DME/Toluene LHCE electrolyte working mechanism of Na-S battery. h) ^{23}Na NMR spectra of various electrolytes. i) Cycle performance of Na-SPAN batteries with different electrolytes. g–i) Reproduced with permission.[115] Copyright 2024, Wiley-VCH.

an impressive initial discharge capacity of up to 922 mAh g^{-1}. Even after 300 cycles, the capacity remains at 675 mAh g^{-1}, corresponding to a low-capacity decay rate of only 0.10% per cycle (Figure 19b,c). The average Coulombic efficiency approaches 100%, indicating minimal polysulfide shuttling within the LHCE system. This performance suggests a sulfur redox mechanism distinct from the traditional dissolution–precipitation pathway. As illustrated in Figure 19c, the voltage profile during the initial discharge cycle exhibits a brief sloped region associated with polysulfide formation, comprising merely 7% of the total discharge capacity. This observation indicates a highly suppressed generation of soluble polysulfides. In subsequent cycles, the redox behavior transitions to a single, well-defined voltage plateau, characteristic of a solid-to-solid sulfur conversion pathway. The sustained stability of this profile throughout extended cycling underscores the high reversibility and distinctive electrochemical characteristics enabled by the LHCE formulation.

Furthermore, most inner-shell solvents are typically strong solvating molecules, such as DME. Achieving an ideal coordination structure often requires a high salt-to-solvent ratio (SSR) and a substantial diluent-to-solvent ratio (DSR), which inevitably leads to reduced ionic conductivity and increased cost.[114] To overcome these limitations, our research group compared conventional linear ethers like DME with cyclic ethers. Notably, methyl furan (MeTHF) exhibits a lower solvation energy and slightly greater steric hindrance, offering a promising balance between solvation strength and spatial configuration.[114] This property allows anions to approach the inner-coordinated Na^+ more closely, while positioning the solvent molecules nearer to the outer diluent. Such spatial arrangement enables the electrolyte to transition from a LHCE to a locally saturated electrolyte (LSE) under low SSR and DSR conditions (Figure 19d). In this electrolyte system, a more robust and efficient SEI forms on the sodium-metal anode without altering the lithium-like growth behavior. Concurrently, sulfur conversion at the cathode shifts from a conventional dissolution–precipitation mechanism to a quasi-solid-state reaction. ^{23}Na NMR spectroscopy further elucidates the Na^+ environment in the electrolyte. As shown in Figure 19e, the ^{23}Na resonance peak for Na_2S_8 in LHCE appears at 2.8 ppm, whereas in the LSE system, this peak shifts significantly downfield to 5.7 ppm. This shift indicates that due to the stronger electron-donating ability of the solvent relative to S_8^{2-}, more polysulfide species

coordinate around Na^+, promoting the formation of a quasi-solid-state structure in the LSE. Notably, 1.0 M Na_2S_8 exhibits poor solubility in LSE (inset in Figure 19e), and thus only the saturated upper-layer solution was collected for NMR analysis. The MeTHF/TTE-based LSE demonstrates excellent electrochemical performance. The Na-S battery employing this electrolyte delivers a high discharge capacity of 530 mAh g^{-1} after 200 cycles at a C/10 rate, with an average Coulombic efficiency of ≈100% (Figure 19f). This performance markedly surpasses that of DME-based LHCE systems.

To date, most diluents used in LHCE systems are fluorinated solvents due to their low dielectric constants and strong donor capabilities. However, fluorinated solvents are expensive, and their higher density poses challenges for overall energy density. Furthermore, fluorinated ether diluents have been reported to decompose during cycling, with organic fragments, such as CF_2 and CF_3 potentially integrating into the SEI layer, which may adversely impact battery performance. Therefore, we introduced a novel Na-S battery LHCE composed of 2 M NaFSI dissolved in a mixture of DME and toluene.[115] Toluene serves as a diluent in the LHCE system with weaker solvation capability, thereby contributing to the formation of a unique solvation structure with the electrolyte, as shown in Figure 19g. Additionally, the ^{23}Na NMR spectra in Figure 19h provide detailed insights into the interaction strength between Na^+ and FSI^- in the proposed electrolyte. Compared to the 2 M DME system, the ^{23}Na NMR peak in the LHCE shifts upfield, with the toluene-containing LHCE showing the most prominent chemical shift. This indicates that the introduction of the diluent enhances the interaction between Na^+ ions and FSI^- ions. The FSI^- ions tend to surround the Na^+ ions, increasing electron density and thereby enhancing a shielding of Na^+, which results in the observed upfield shift. Overall, the addition of toluene leads to the formation of more Na^+–FSI^- complexes in the electrolyte, which is a significant feature of the LHCE system. As shown in Figure 19i, replacing 2M-DME with LHCE significantly enhances the cycling stability of Na-S cells with SPAN cathode. Notably, the LHCE-toluene system outperforms LHCE-TTE, retaining 82% of its initial capacity and delivering 840 mAh g^{-1} after 150 cycles at C/10 rate, compared to only 64% retention with 2M-DME.

Impressively, Wang et al. introduced an innovative all-fluorinated electrolyte system composed of 2,2,2-trifluoro-N,N-dimethylacetamide (FDMA) as the solvent, 1,1,2,2-tetrafluoroethyl methyl ether (MTFE) as the anti-solvent, and fluoroethylene carbonate (FEC) as the additive (**Figure 20a**).[113] This electrolyte enables a "quasi-solid-phase" Na-S conversion reaction, effectively suppressing the polysulfide shuttle and significantly enhancing the reversibility and cycle life. Similarly, the use of FDMA solvent in combination with FEC enables the in situ formation of a NaF- and Na_3N-rich CEI, which stabilizes the sulfur redox process by facilitating a solid-state conversion from sulfur to Na_2S. Simultaneously, the MTFE anti-solvent provides additional stabilization to the sodium metal anode by altering the Na^+ solvation structure, thus lowering polysulfide solubility and enhancing ion transport at the interface. This approach reduces the formation of soluble polysulfides, which are a primary contributor to capacity degradation and poor cycling stability in Na-S batteries. Consequently, this electrolyte not only ensures high ionic conductivity, but also exhibits non-flammability, thereby enhancing both electrochemical performance and safety. With this rational design, the system delivers a high reversible capacity of 1114 mAh g^{-1} at C/10 and retains ≈65% capacity after 200 cycles (Figure 20b).

Recently, our group developed an asymmetric solvent-based electrolyte for Na-S batteries with SPAN cathode, employing a dual-sheath solvation structure to simultaneously suppress polysulfide dissolution and shuttle effects.[116] This system utilizes 1,2-dimethoxypropane (DMP) as the primary solvent and 1,1,2,2-tetrafluoroethyl-2,2,2-trifluoroethyl ether (TFTFE) as the fluorinated diluent. In contrast to conventional DME-based electrolytes, which strongly solvate NaPS and thus suffer from severe shuttle effects, the designed electrolyte creates a distinct asymmetric solvation environment. Specifically, the inner solvation sheath dominated by DMP ensures stable Na^+ coordination, while the outer sheath enriched with TFTFE effectively suppresses the migration of NaPS species. (Figure 20c). This dual-sheath architecture confines NaPS near the cathode side, significantly reducing parasitic reactions at the anode. Moreover, the tailored solvation structure fosters the formation of a robust, inorganic-rich CEI, enhancing the interfacial stability and accelerating polysulfide conversion kinetics. Electrochemical testing confirms that Na-S batteries with this electrolyte exhibit high Coulombic efficiency, excellent cycling stability, and improved capacity retention. (Figure 20d). Altogether, this study underscores solvation engineering as a powerful strategy for advancing electrolyte design in high-performance Na-S battery systems.

Furthermore, the pivotal role of the electrical double layer (EDL) structure in Na-S batteries was investigated by our research group, focusing on how polysulfide solvation modulates interfacial chemistry and overall electrochemical performance (Figure 20e,f).[180] The solvation–desolvation dynamics critically influence the formation of both the SEI and CEI layers, thereby governing ion transport behavior and interfacial stability. A well-regulated EDL structure effectively suppresses polysulfide dissolution, mitigates the shuttle effect, and enhances long-term cycling performance. Among the solvents examined, tetrahydropyran (THP) demonstrates superior performance compared to conventional ether-based systems owing to its finely tuned solvation environment that balances polysulfide confinement with efficient Na^+ transport (Figure 20g). THP-based electrolytes promote the formation of a stable, optimally composed CEI that minimizes parasitic side reactions and improves sulfur utilization. DFT calculations and MD simulations further reveal that THP enables controlled Na^+ desolvation, facilitating uniform sodium deposition and enhanced interfacial stability. Collectively, this study underscores the critical role of solvation engineering in modulating EDL structures for Na-S batteries, offering a comprehensive framework that integrates theoretical insights and experimental validation to advance electrolyte design for next-generation energy storage systems.

4.2.3. K-S Batteries with HCEs and LHCEs

Similar to Na-S batteries, the high solubility of polysulfides and the pronounced reactivity of the potassium-metal anode present considerable challenges for the operation of K-S batteries with low-concentration electrolytes. The development of HCEs and

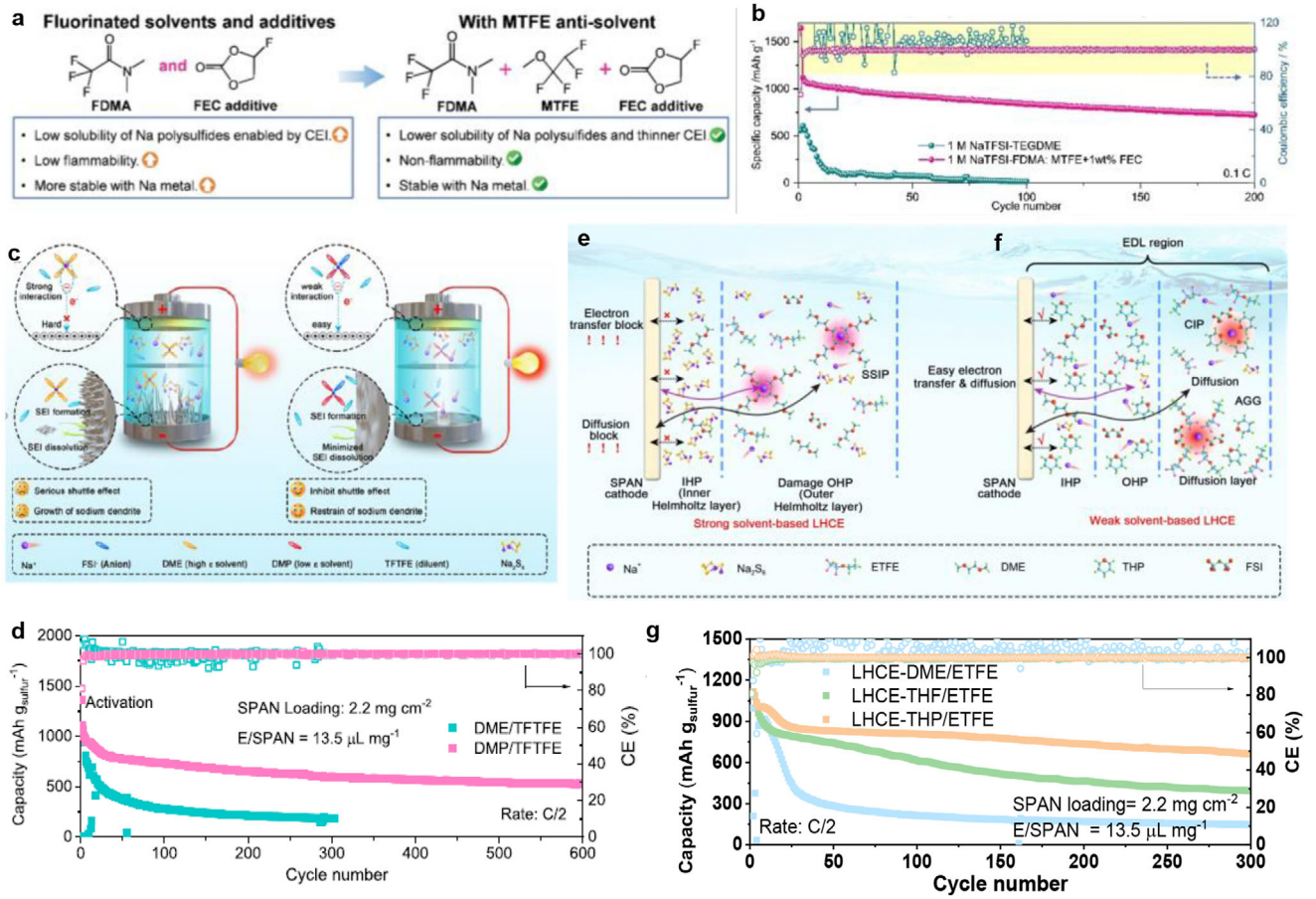

Figure 20. a) Schematic illustration of fluorinated solvents, additives, and anti-solvent solvents. b) Cycle performance of different electrolytes at C/10. a,b) Reproduced with permission.[113] Copyright 2025, Wiley-VCH. c) Schematic diagram of Na-S batteries with different LHCEs. d) Cycle performance of different LHCEs at C/2. c,d) Reproduced with permission.[116] Copyright 2025, American Chemical Society. e,f) Schematic illustration of the EDL structure with different LHCEs. g) Cycle performance of different LHCEs at C/2. e–g) Reproduced with permission.[180] Copyright 2025, Wiley-VCH.

LHCEs offers promising pathways to address these issues and expand the practical applicability of K-S systems.

Sun et al. have developed a concentrated electrolyte composed of 5 M potassium trifluoromethanesulfonimide (KTFSI) in DEGDME, which effectively mitigates the shuttle effect in K-S batteries.[117] This electrolyte enables an average discharge voltage of 2.1 V, corresponding to an energy density of ≈1270 Wh kg^{-1} and an output power of about 700 Wh kg^{-1}. As shown in **Figure 21**a,b, the initial cycle curves of three different K-S systems demonstrate a significant improvement in reversible capacity with increasing electrolyte concentration. In the case of the 5 M electrolyte, the reversible capacity reaches ≈527 mA h g^{-1} with an initial CE of 86.96%, reflecting a substantial suppression of polysulfide dissolution and the shuttle effect. Visual experiments further confirm the impact of electrolyte concentration on performance. As depicted in Figure 21c, with 1 and 3 M electrolytes, the discharge voltage ranges from 2.38 to 2.10 and 1.20 V, respectively, with noticeable diffusion of brown color indicative of polysulfide dissolution. In contrast, the 5 M electrolyte results in a pale-yellow appearance on the anode side, suggesting significantly reduced dissolution at higher concentration. Beyond its role in suppressing polysulfide dissolution, this concentrated electrolyte also plays a crucial role in inhibiting dendrite growth, thus significantly improving the performance and cycle life of K-S batteries.

Moreover, Yu et al. proposed a high-concentration carbonate-based electrolyte of 3 M KTFSI in EC, which effectively regulates the dissolution behavior of polysulfides and enhances potassium-metal stability.[119] The solvent with the highest dielectric constant, such as EC, can significantly reduce the interactions between K^+ and $TFSI^-$. Also, MD simulations and Raman spectroscopy confirmed that most of the $TFSI^-$ exists as CIPs and AGGs rather than SSIPs in a 3 M KTFSI DEC electrolyte. This bifunctional electrolyte enables a "solid–liquid–solid" conversion mechanism, minimizing side reactions and stabilizing sulfur redox chemistry. The EC-based electrolyte forms a more compact and uniform CEI layer on the sulfur cathode, effectively suppressing the shuttle effect, as confirmed by the TEM and XPS analysis (**Figure 22**a–f). The electrolyte also facilitates the formation of a stable potassium-metal anode with a KF-rich SEI that prevents dendrite growth. The cells with designed electrolyte demonstrated impressive long-term cycling stability, with 654 mAh g^{-1} retained after 800 cycles at 0.5 A g^{-1} (Figure 22g). This work underscores the potential of high-concentration carbonate

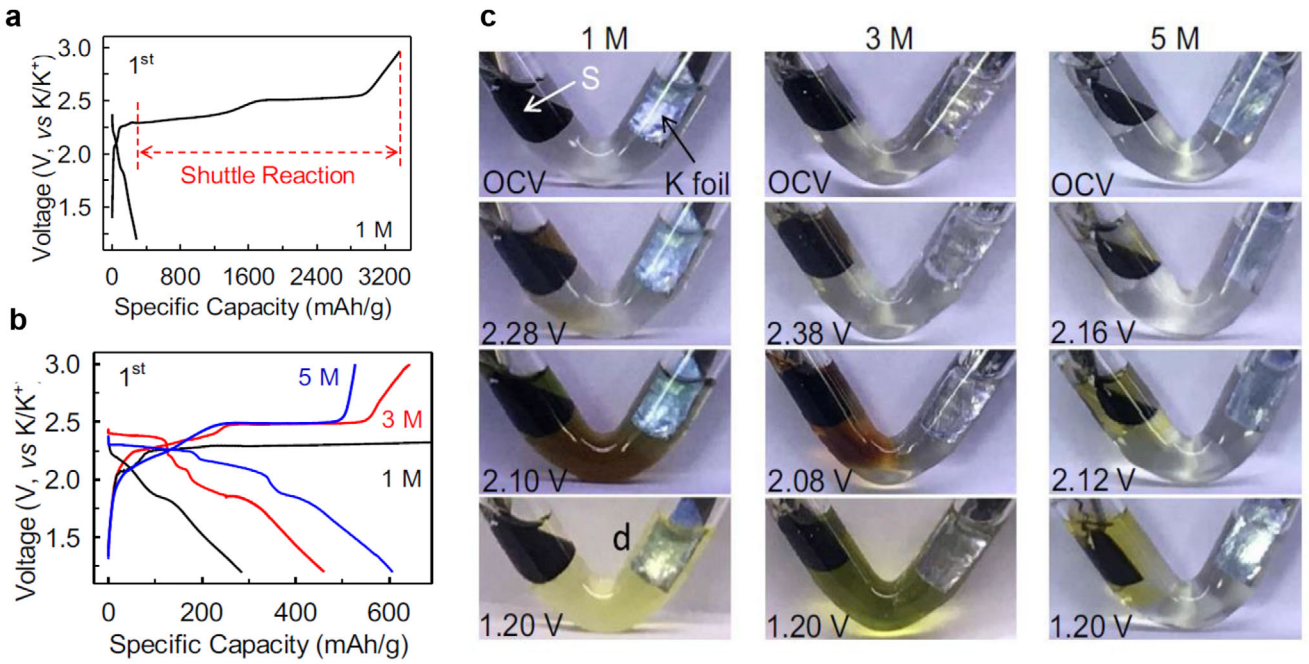

Figure 21. a,b) Discharge-charge profiles of K-S batteries under different salt concentrations at 10 mA g^{-1}. c) Dissolution test of polysulfides in various salt concentrations. Reproduced with permission.[117] Copyright 2019, Elsevier.

electrolytes in stabilizing K-S battery performance, presenting an effective alternative to ether-based systems.

Qin's research group developed an ether LHCE for K-S batteries. (**Figure 23a**).[189] By incorporating a fluoroether cosolvent with low polarity and high polysulfide stability, the electrolyte significantly reduces the solubility of KPS, thereby improving cathode stability and suppressing shuttle effects. The anion-derived SEI, enriched in inorganic components like KF, enhances ionic conductivity and reduces interfacial resistance. The K-S cell with S@Bi_2S_3-rGO cathode utilizing this LHCE demonstrates a reversible capacity of 448 mAh g^{-1} with 81% retention after 80 cycles (Figure 23b). However, the study also highlights that continuous anode corrosion and byproduct accumulation still limit long-term stability. These findings provide insights into electrolyte design for high-energy-density K-S batteries.

Analogously, Huang et al. investigated a HCE system for K-S batteries, incorporating a SPAN cathode to address the persistent challenges, such as polysulfide dissolution and potassium anode instability.[118] The 4.34 mol kg^{-1} KFSI/DME electrolyte significantly enhances the cycling stability by mitigating dendrite formation and improving interfacial kinetics (Figure 23c). Phase-field modeling and operando imaging demonstrate that this concentrated electrolyte effectively suppresses potassium ion depletion, promoting uniform K deposition and reducing dendritic growth (Figure 23d). Furthermore, MD simulations and Raman spectroscopy reveal a solvation structure dominated by CIPs and AGGs, which contributes to the formation of a more stable and robust SEI. These findings underscore the synergistic effect between SPAN cathodes and HCEs in modulating interfacial reactions and improving the overall electrochemical performance of K-S batteries.

Min et al. investigated the interaction strengths of fluorinated ether compounds with PC.[120] They found that the interaction between HFE and PC was significantly stronger than that between TFTFE and PC, which effectively diminished the interaction between K^+ and PC (**Figure 24a**). This enhanced interaction promotes the reversible insertion and extraction of K^+, while also imparting non-flammable properties to the electrolyte. The proposed interfacial model elucidates the kinetic and thermodynamic properties of the K^+-solvent complexes, thereby improving the stability of both the electrolyte and the electrode and significantly enhancing the performance of K-S batteries. Additionally, they observed that upon adding HFE and TFTFE as diluents to the original PC-based electrolyte, the chemical shifts in the ^{39}K NMR spectra shifted from −0.35 to −0.302 and −0.315 ppm, respectively. This shift indicates that the diluents weaken the interaction between K^+ and PC (Figure 24b).

Furthermore, the shift induced by HFE (−0.302 ppm) was more pronounced compared to TFTFE (−0.315 ppm), suggesting a stronger interaction between HFE and PC. The reduction in K^+-PC coordination and the enhanced coordination between K^+ and FSI^- resulted in an increased electron density around the oxygen in the S = O bond, leading to a shift toward higher field values in the NMR spectra (Figure 24c). A comparison with TFTFE also revealed that the shielding effect of S = O was more pronounced with HFE, indicating a stronger interaction between K^+ and FSI^-. Also, in the PC/HFE-based electrolyte, the binding energy between K^+ and PC was −222.36 kJ mol^{-1}, which is higher than that in the original PC-based electrolyte (−308.12 kJ mol^{-1}) and in the PC/TFTFE-based electrolyte (−257.89 kJ mol^{-1}) (Figure 24d). This further confirms that the addition of diluents weakens the K^+-PC binding, with HFE proving to be the most effective. The advantages of the designed electrolyte (0.3 M KFSI in PC/HFE)

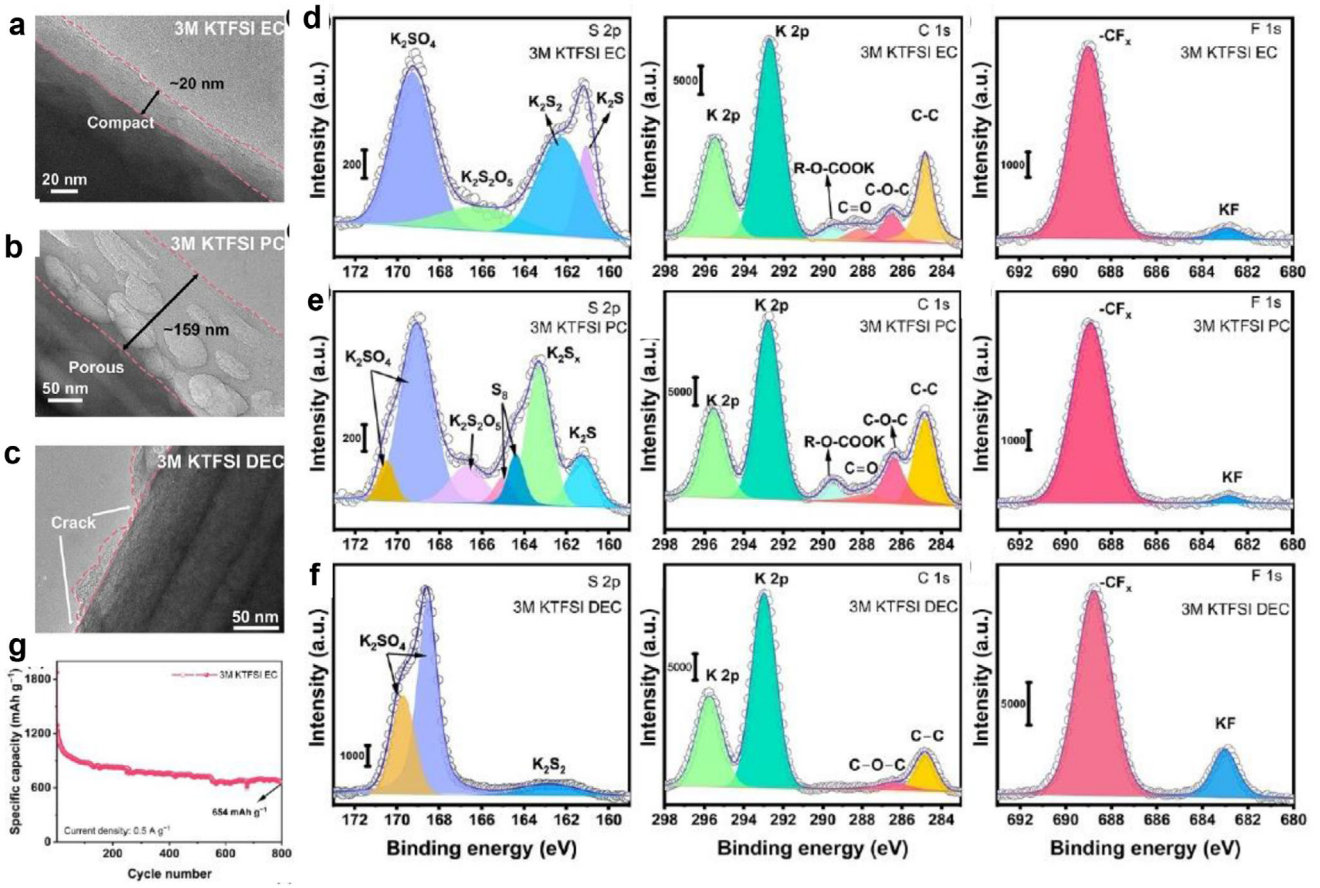

Figure 22. a–c) TEM images of the cathode after 30 cycles in different electrolytes. d–f) XPS data of the cathode. g) Cycling performance of K-S batteries with EC-based electrolyte. Reproduced with permission.[119] Copyright 2023, Wiley-VCH.

were validated by assembling KC_8-SPAN cells (Figure 24e). After 200 cycles at a current density of 100 mA g−1, the battery exhibited a high capacity retention of 73.3%, demonstrating excellent cycling stability of cells with proposed electrolyte (Figure 24f).

4.3. Functional Electrolyte Additives

In recent years, functional electrolyte additives have emerged as one of the most promising strategies for overcoming the critical challenges faced by alkali metal-sulfur batteries. The incorporation of these additives into electrolyte systems provides multifaceted regulation at both the cathode and anode interfaces. At the anode, additives can undergo preferential reduction or decomposition to form robust and ion-conductive SEI/CEI layers, thereby stabilizing metal surfaces and mitigating dendrite growth. At the cathode, additives with tailored chemical functionalities can interact with soluble polysulfides via chemical adsorption, coordination, or catalytic transformation, effectively suppressing their migration and promoting rapid redox kinetics. Furthermore, certain advanced additives possess the ability to modulate the solvation structure of metal ions, regulate interfacial ion transport, and homogenize the spatial distribution of electrochemical reactions within the electrode matrix. Consequently, rational design of functional electrolyte additives plays a pivotal role in establishing stable electrode–electrolyte interfaces, enhancing sulfur utilization, suppressing the shuttle effect, and improving the overall electrochemical performance. In the subsequent sections, recent advancements in functional additives for alkali metal-sulfur batteries will be systematically reviewed, with particular emphasis on their interfacial regulation mechanisms and structure–function relationships.

4.3.1. Li-S Batteries with Functional Electrolyte Additives

Functional electrolyte additives offer multifaceted regulation in Li-S batteries by anchoring polysulfides, enhancing redox kinetics, and stabilizing lithium anodes through SEI formation. Their ability to modulate solvation structures and reaction pathways makes them key to suppressing the shuttle effect and improving cycling performance.

In 2024, Amine et al. explored the unexpected role of Lewis acid additives (LAAs), specifically $LiBF_4$, in suppressing spatial reaction heterogeneity and enhancing the performance of Li-S batteries with high sulfur loading and lean electrolyte conditions (**Figure 25a**).[109] Contrary to conventional system, the controlled

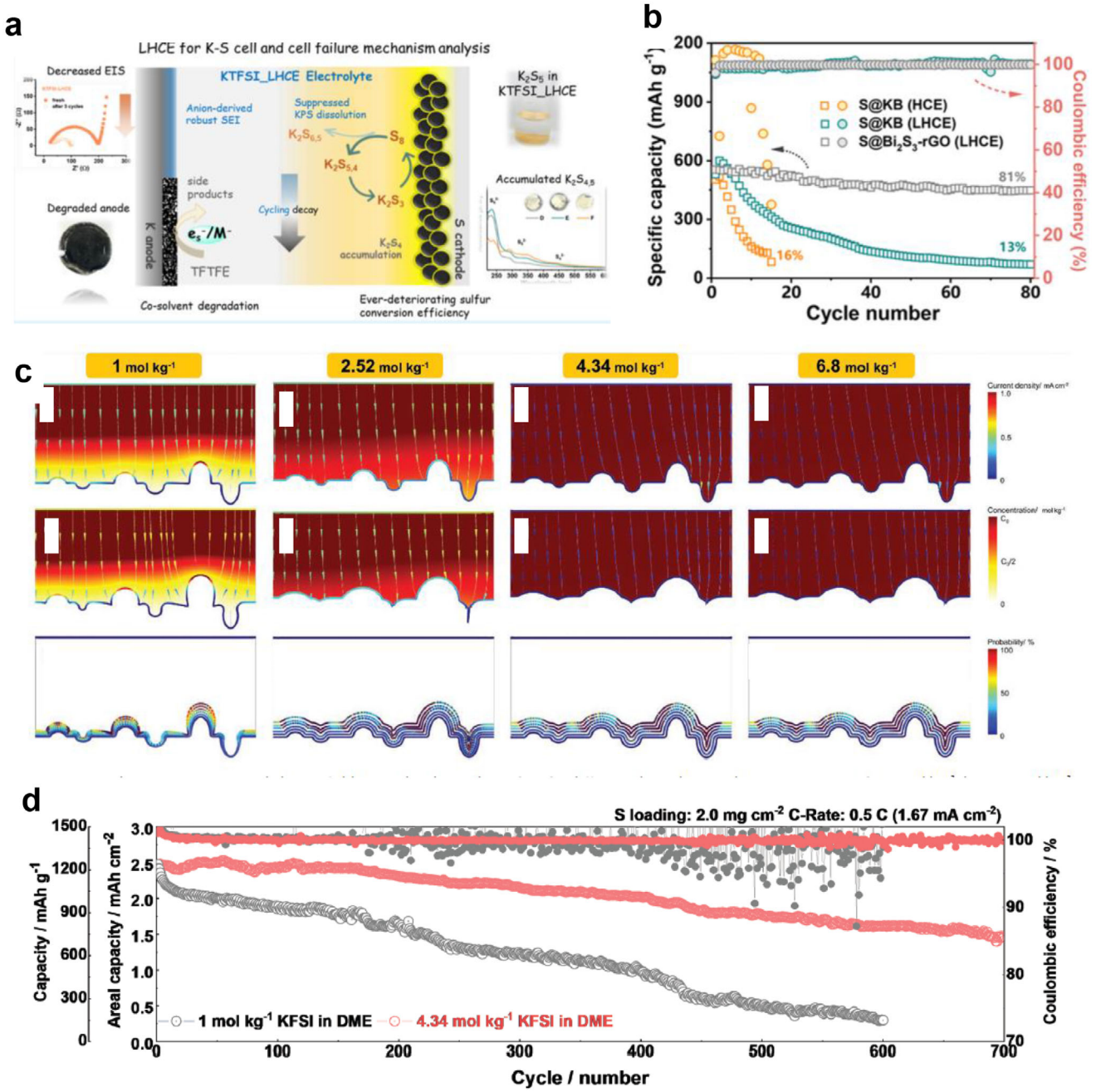

Figure 23. a) Schematic illustration of LHCE electrolyte in K-S batteries. b) Cycle performance of K-S batteries at C/5. a,b) Reproduced with permission.[189] Copyright 2024, American Chemical Society. c) Electrolyte concentration and electric field distribution near the electrode surface. d) Long cycle performance of HCE electrolyte at C/2. c,d) Reproduced with permission.[118] Copyright 2022, Wiley-VCH.

reaction between sparingly solvated polysulfides and $LiBF_4$ induces an in situ formation of a homogeneous CEI, which promotes electrolyte wetting and ion transport. The designed electrolyte composed of 1.5 M LiTFSI in TTE/DME (10:3 v/v) with 0.05 M $LiBF_4$ (denoted LAA-0.05) demonstrates superior electrochemical performance, including higher specific capacity, improved Coulombic efficiency, and extended cycling stability.

A key highlight is the synchrotron X-ray absorption spectroscopy (XAS) analysis (Figure 25b,c), which reveals distinct redox pathways in the LAA-0.05 electrolyte compared to conventional DME/DOL. While DME/DOL exhibits concurrent formation of soluble LiPS and Li_2S, the LAA-0.05 electrolyte facilitates a quasi-solid-solid transition, eliminating LiPS intermediates and ensuring complete sulfur utilization. This is further supported by in situ Se K-edge XANES showing no LiPSe formation and a sharp edge shift at full discharge, confirming efficient active material conversion. Also, the ToF-SIMS and XPS confirm the uniform distribution of F-rich

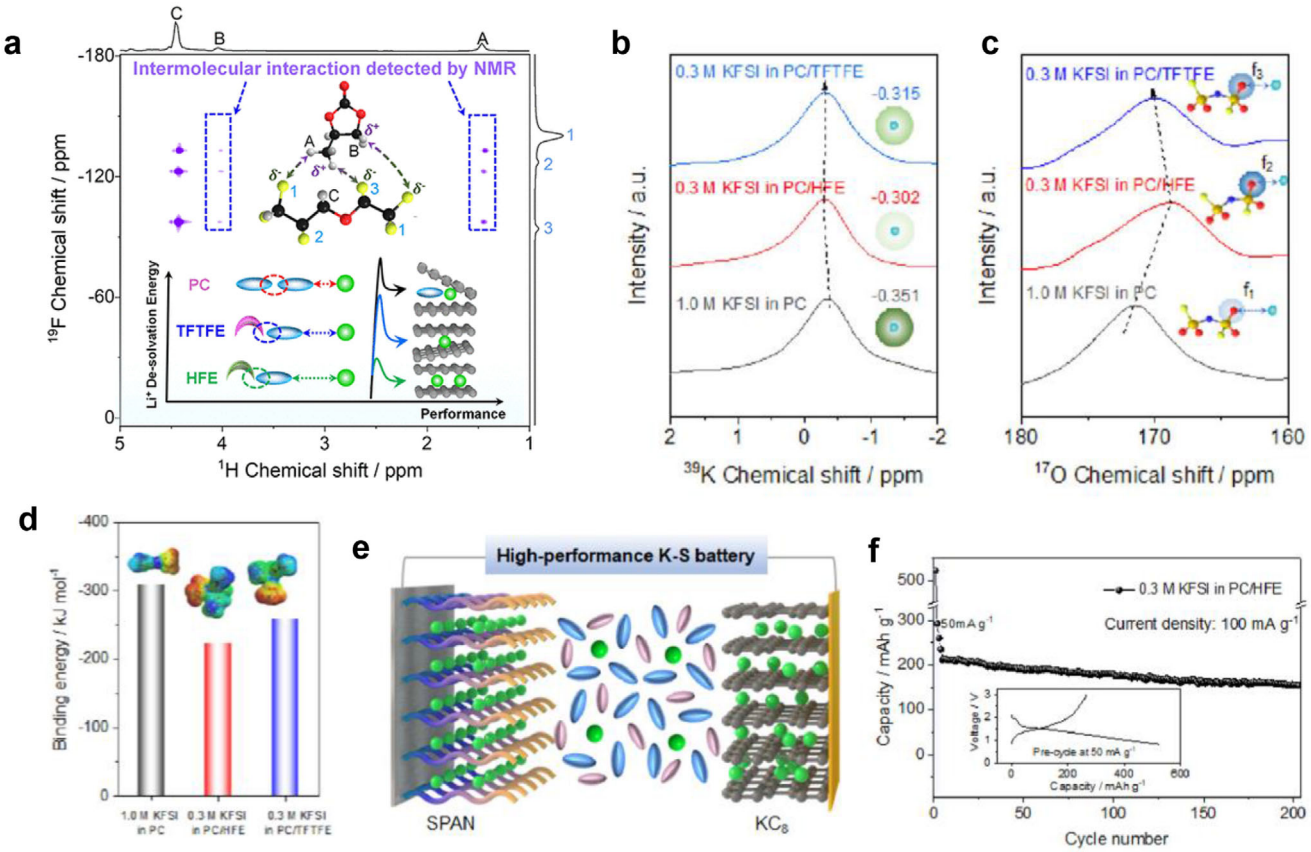

Figure 24. a) Schematic illustration of PC/TFTFE and PC/HFE electrolyte working mechanism in a K-S battery. b) ^{39}K and (c) ^{17}O NMR spectra of different electrolytes. d) The HOMO-LOMO energy gap between Na^+-solvents/ Na^+-anion. e) Schematic illustration of K-S battery consisted of SPAN cathode and graphite anode. f) Cycle performance of K-S battery at 100 mA g^{-1}. a–f) Reproduced with permission.[120] Copyright 2024, American Chemical Society.

CEI, which enhances ion transport and suppresses polysulfide shuttling. Pouch cell evaluations demonstrate reduced reaction heterogeneity with homogeneous Li_2S distribution and negligible sulfur residuals, validating the practical applicability of this electrolyte design. Overall, this work redefines the utility of polysulfide-incompatible additives, offering a promising strategy to achieve high-energy, long-cycle Li-S batteries by tailoring interfacial chemistry and reaction uniformity.

Furthermore, Liang's research group introduced a novel electrolyte additive, tetrapropylammonium bromide (T3Br), to enhance the performance of Li-S batteries by leveraging a radical conversion pathway and stabilizing the lithium anode.[152] The T3Br additive facilitates the formation of tri-sulfur radicals ($S_3^{\bullet-}$), which promote 3D nucleation of Li_2S, thereby improving sulfur utilization and redox kinetics. Unlike conventional high donor number (DN) solvents, T3Br mitigates the reactivity of lithium metal while preserving the benefits of the $S_3^{\bullet-}$ radical pathway. Impressively, the UV/Vis spectroscopic analysis (Figure 25d,e) demonstrates the presence of $S_3^{\bullet-}$ radicals in T3Br-containing electrolytes, evidenced by distinct absorption peaks at 618 nm. This contrasts with the yellowish polysulfide-dominated spectra of other additives, underscoring the unique ability of T3Br to stabilize $S_3^{\bullet-}$ intermediates. Furthermore, the potentiostatic deposition tests (Figure 25f–h) reveal that T3Br additive facilitates the formation of tri-sulfur radicals ($S_3^{\bullet-}$) to promote a 3D nucleation of Li_2S and showcase an improved kinetics compared to conventional electrolytes. Notably, Li || Li symmetric cells with T3Br exhibit stable cycling performance and reduced overpotential attributed to the formation of a LiF-rich SEI derived from the proposed additives. Also, MD simulations further confirm that T3Br alters the Li^+ solvation structure, increasing $TFSI^-$ coordination and enhancing SEI stability. Ultimately, the cell demonstrates exceptional performance, including a high initial capacity (1132 mAh g^{-1}), long cycle life over 700 cycles at 1C rate, and compatibility with lean electrolytes (5 µL mg^{-1}). This work provides a strategic approach to designing electrolyte additives that simultaneously enhance sulfur redox kinetics and lithium anode stability, paving the way for practical high-energy Li-S batteries.

Xi et al. presented a novel electrolyte strategy for Li-S batteries by incorporating 4-mercaptopyridine (4Mpy) as an organic sulfur-based redox regulator (RR) additive. This multifunctional additive simultaneously accelerates LiPS conversion kinetics (**Figure 26**a) and suppresses the shuttle effect, thereby addressing two major challenges that limit the performance and stability of Li-S battery systems.[153] Unlike conventional redox mediators (RMs) (e.g., LiI), which suffer from additive shuttling

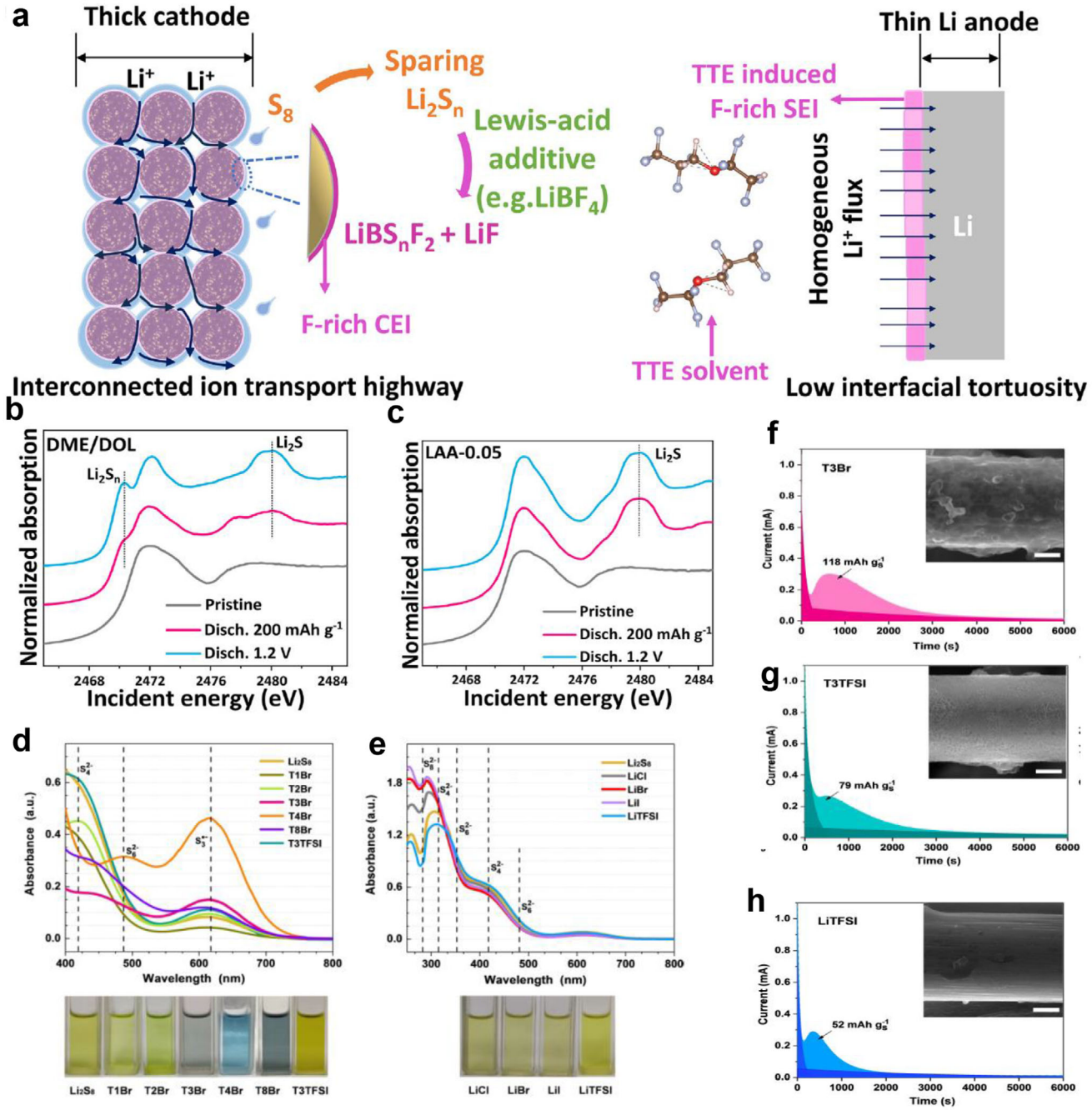

Figure 25. a) Electrochemical processes in LAA-0.05-based Li-Se/S cells. b,c) In situ S K-edge spectra during discharge: DME/DOL versus LAA-0.05 systems. a–c) Reproduced with permission.[109] Copyright 2024, Elsevier. UV/Vis absorption spectra and optical images of Li_2S_8 solutions following exposure to (d) QAS additives (T1Br, T2Br, T3Br, T4Br, T8Br, and T3TFSI) and (e) different lithium salts featuring various anions. Potentiostatic Li_2S_8 deposition profiles on carbon paper in electrolytes containing (f) T3Br, g) T3TFSI, and (h) LiTFSI without additives. d–h) Reproduced with permission.[152] Copyright 2024, Wiley-VCH.

and low Coulombic efficiency (89.73%), 4Mpy achieves a high Coulombic efficiency of 99.14% over 500 cycles (Figure 26b). This stability stems from its unique redox mechanism. First, 4Mpy reacts with LiPS to form lithium-pyridinethiolate (Li-pyS) during discharge procedure. Then, it is further oxidized to 4,4′-dipyridyl disulfide (4,4′-pyS_2) during the charging process. This unique electrochemical behavior creates a reversible cycling process to minimizes LiPS dissolution (Figure 26c). Therefore, this work pioneers a dual-functional organic additive that regulates LiPS conversion, while stabilizing the lithium anode, offering a scalable strategy for high-energy Li-S batteries.

Notably, our group introduced lithium tritelluride ($LiTe_3$) as a novel electrolyte additive to simultaneously address unstable lithium deposition and sluggish sulfur redox kinetics in Li-S

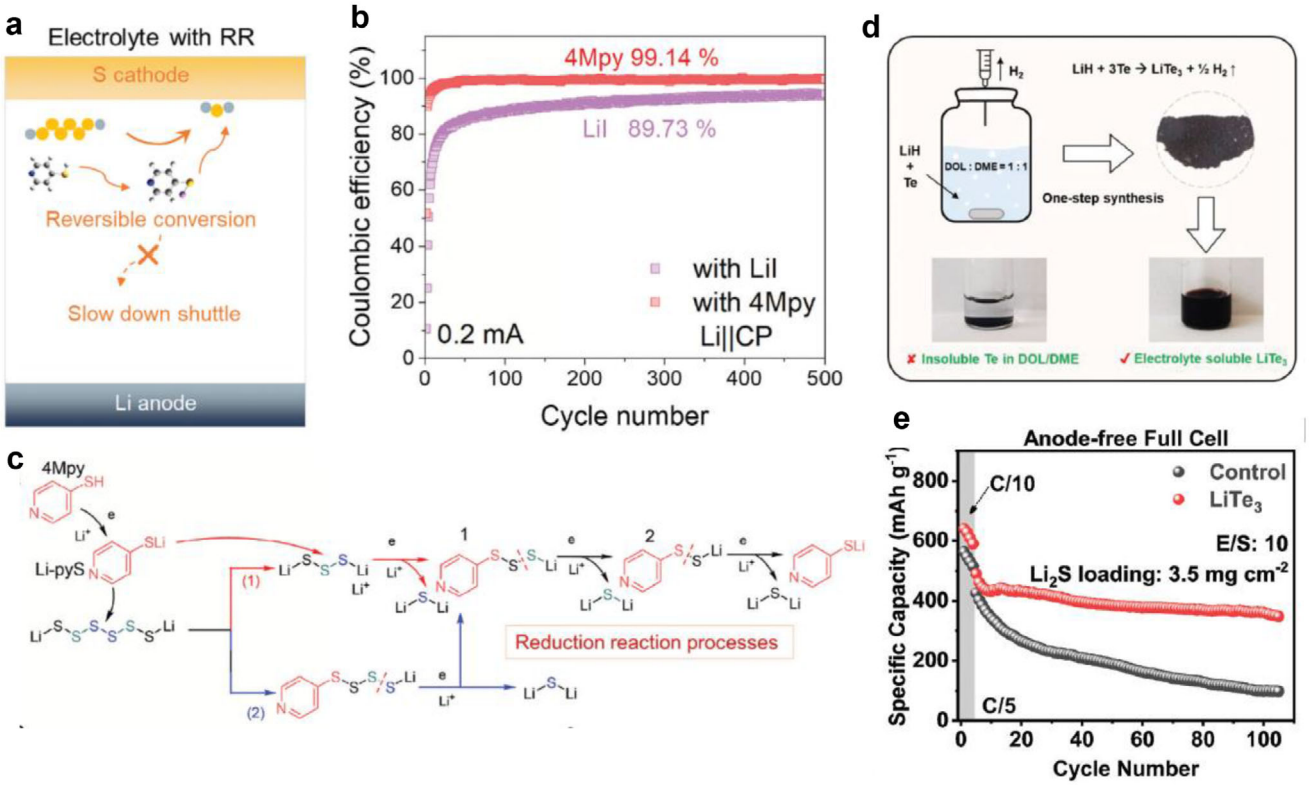

Figure 26. a) The designed Li-S batteries electrolyte additive with a LiPS RR additive suppresses the LiPS and additive shuttle. b) Comparison of Coulombic efficiency between LiI and 4Mpy additives. c) Schematic illustration the possible reaction processes during the discharge reduction process in Li-S batteries with 4Mpy additive. a–c) Reproduced with permission.[153] Copyright 2024, Wiley-VCH. d) Preparation and solubility of $LiTe_3$ in ether-based electrolyte. e) The comparative cycling performance of anode-free Li–S batteries with/without the additive at C/5. d,e) Reproduced with permission.[151] Copyright 2024, Wiley-VCH.

batteries. Synthesized through a one-step solution-based method, $LiTe_3$ performs a dual role by facilitating the formation of polytellurosulfides that act as redox mediators to enhance cathode kinetics, while also promoting the development of a Li_2TeS_3/Li_2Te-rich SEI layer that stabilizes the lithium-metal anode (Figure 26d). Furthermore, $LiTe_3$ lowers the activation barrier for Li_2S oxidation and facilitates uniform lithium deposition.[151] As a result, in anode-free Ni || Li_2S full cell systems, the $LiTe_3$-containing cell delivers an initial capacity of ≈500 mAh g^{-1}, 15% higher than the control cell. Moreover, it retains 71% of its capacity after 100 cycles at a C/5 rate, while the control cell retains only 23% (Figure 26e). Overall, $LiTe_3$ significantly improves cyclability and sulfur utilization, especially under lean electrolyte conditions, offering a scalable and practical strategy for next-generation energy storage systems.

4.3.2. Na-S Batteries with Functional Electrolyte Additives

Na-S batteries face greater challenges than Li-S systems due to the larger Na^+ radius and lower reduction potential, which lead to severe polysulfide dissolution and unstable anode interfaces. Functional electrolyte additives offer an effective solution by forming stable SEI layers, suppressing dendrite growth, and interacting with NaPS to inhibit shuttling and enhance redox kinetics. Thus, rational additive design is key to improving interfacial stability and electrochemical performance in Na-S batteries.

Wang et al. presented a "cocktail optimized" electrolyte system for high-performance RT Na-S batteries. The proposed electrolyte consists of 2 M NaTFSI in a co-solvent mixture of PC and FEC with an indium triiodide (InI_3) additive. (**Figure** 27a).[36] In this study, the electrolyte containing 2 M NaTFSI in a PC:FEC (1:1 by volume) mixture achieves the highest reversible capacity of 907 mAh g^{-1} after 100 cycles at C/10 rate, outperforming both lower (1–1.5 M) and higher (2.5 M) salt concentrations (Figure 27b). The improved performance at 2 M is attributed to two key mechanisms: (1) the high salt concentration reduces polysulfide solubility through a "solvent-in-salt" effect, suppressing shuttle behavior and stabilizing the sodium-metal anode with a fluorine-rich SEI, and (2) the FEC co-solvent lowers polysulfide dissolution by weakening the binding energy with Na_2S_x, while promoting a stable SEI. Intriguingly, the InI_3 additive acts synergistically. Iodide ions (I^-) oxidize to triiodide (I_3^-) during charging, promoting the conversion of insoluble Na_2S back to polysulfides, while In-ions form a protective indium layer on the anode to mitigate corrosion. This design of multifunctional electrolyte enables a stable cycling performance of 648 mAh g^{-1} after 500 cycles at C/2 rate, addressing critical challenges in room-temperature Na-S batteries.

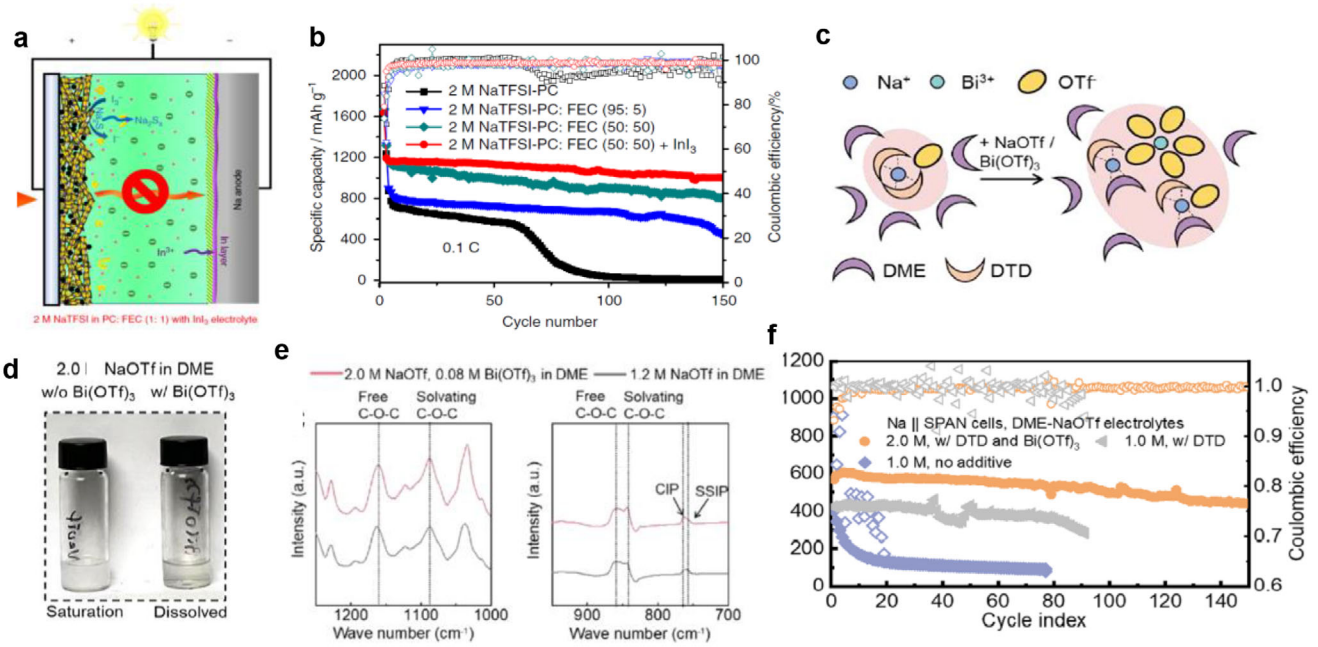

Figure 27. a) Schematic illustration of NaTFSI-PC/FEC+InI_3 electrolyte in a Na-S battery. b) Cycle performance of Na-S batteries with different electrolytes. a,b) Reproduced with permission.[36] Copyright 2018, Springer Nature. c) The facilitation of sodium salt dissolution by Bi^{3+} cations. d) Solvation structure changes induced by Bi^{3+} cations. e) FT-IR spectra of various electrolytes. f) Cycle performance of Na-SPAN batteries with different electrolytes. c–f) Reproduced with permission.[204] Copyright 2023, American Chemical Society.

Moreover, our research group demonstrated that incorporating bismuth triacetate ($Bi(OAc)_3$) with the 1,3,2-dithiolane-2,2-dioxide (DTD) additive in conventional ether-based electrolytes enables a Coulombic efficiency exceeding 99% for sodium metal, while fully suppressing the dissolution of sodium polysulfides.[204] The addition of DTD significantly weakens the interaction between Na^+ and OTf^- and increases the solubility of NaOTf. As a result, the electrolyte contains a higher concentration of NaOTf, where Na^+ is more prone to form CIPs with OTf^- (Figure 27c). When $Bi(OTf)_3$ is present at a concentration of 0.08 M, the solubility of NaOTf reaches 2.1 M. In addition to promoting salt solubility, Bi forms Na_3Bi with sodium, which is a highly efficient mixed conductor with a high Na^+ diffusion rate (Figure 27d). The FT-IR spectrum of the electrolyte shows an enhanced peak at 763 cm^{-1}, indicating that OTf^- ions are in a CIP state, and an enhanced peak at 753 cm^{-1}, implying that OTf^- ions are in a SSIP state (Figure 27e). This suggests that under high salt solubility conditions, OTf^- ions are more readily incorporated into the solvation shell to form CIPs, which is thermodynamically favorable. Therefore, the battery retains 79% of its initial capacity (535 mAh g^{-1}) after 150 cycles (Figure 27f). In contrast, the battery using ether-based electrolyte without additives experiences a 50% decrease in capacity after just 10 cycles.

In 2024, Yu's group systematically investigated the incorporation of Tin(II) trifluoromethanesulfonate ($Sn(OTf)_2$) as a functional additive in non-flammable phosphate-based electrolytes for Na-S batteries, highlighting its synergistic contributions to electrochemical performance and safety.[205] Generally, $Sn(OTf)_2$ modulates the Na^+ solvation environment by coordinating with solvent molecules and anions, thereby attenuating the interaction between Na^+ and polysulfides (**Figure** 28a,b). This adjustment effectively suppresses polysulfide solubility and mitigates the shuttle effect. Furthermore, the in situ formation of $Na_{15}Sn_4$ from $Sn(OTf)_2$ decomposition markedly enhances Na^+ transport across the SEI, as evidenced by its exceptionally low diffusion energy barrier of 0.093 eV (Figure 28c). This facilitates homogeneous sodium deposition, suppresses dendritic growth, and reinforces interfacial stability. In parallel, $Sn(OTf)_2$ exhibits catalytic activity toward sulfur redox reactions, promoting the reversible conversion of polysulfides to lower-order sulfur species, thereby improving sulfur utilization and minimizing capacity degradation. Collectively, these multifaceted functionalities render $Sn(OTf)_2$ a compelling additive candidate for advancing the safety, efficiency, and durability of next-generation Na-S battery systems.

Wu et al. reported the development of a nonflammable dual-functional electrolyte for RT Na-S batteries, integrating FEC with 1-ethyl-3-methylimidazolium bis(fluorosulfonyl)imide (EMIFSI) ionic liquid (IL) to address key electrochemical and safety limitations.[178] This tailored electrolyte simultaneously mitigates sodium dendrite growth, polysulfide shuttle effects, and inefficient sulfur conversion. On the sodium anode, the synergistic effect of FEC and EMIFSI promotes the formation of an inorganic-rich SEI, which suppresses dendritic deposition and ensures homogeneous sodium plating. The inherent nonflammability of the IL significantly enhances battery safety by mitigating fire hazards associated with organic electrolytes. Meanwhile, at the cathode, the combination of $FSI^-/TFSI^-$ anions and FEC facilitates a direct solid–solid transformation from S_8 to Na_2S, effectively bypassing the formation of soluble long-chain Na_2S_x intermediates. This transition is pivotal for suppressing polysulfide dissolution and minimizing the shuttle phenomenon. Furthermore,

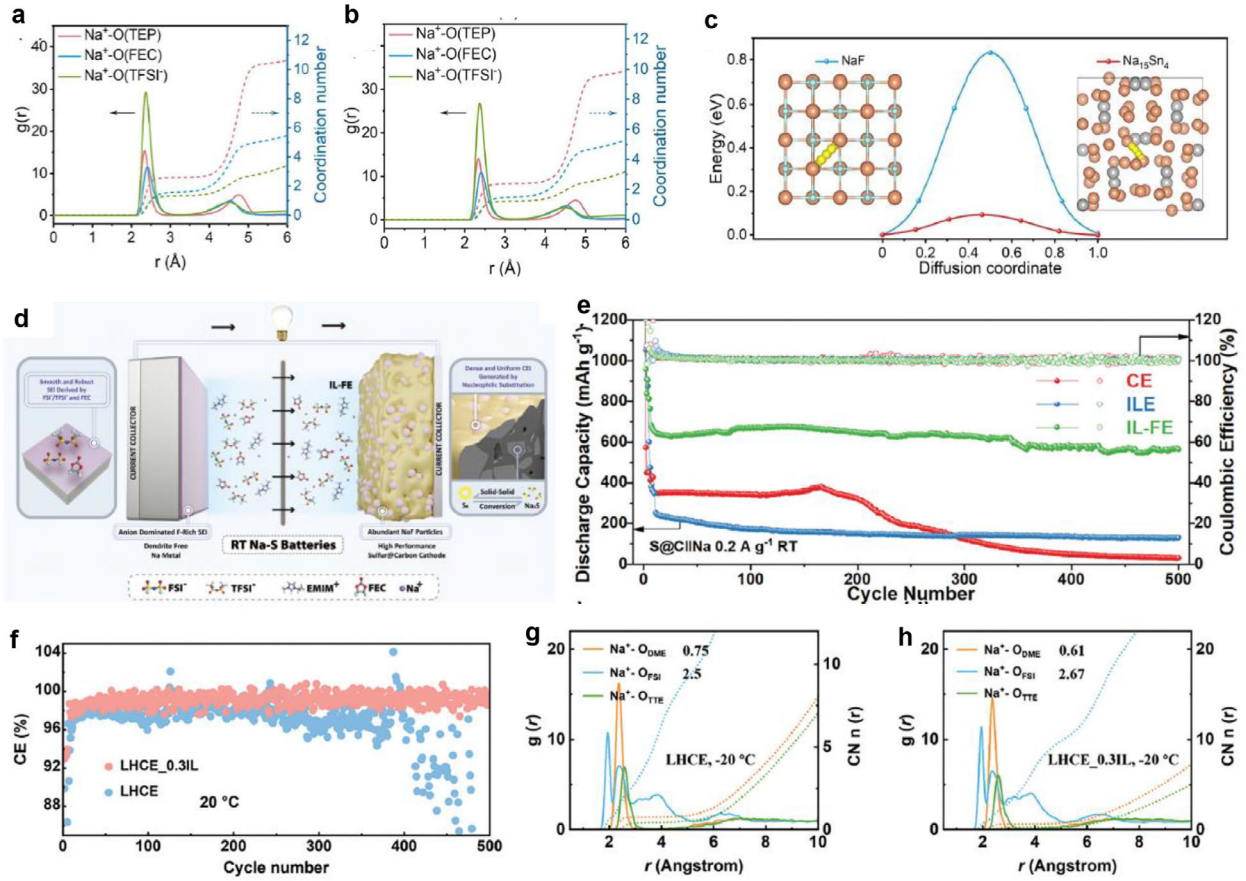

Figure 28. a,b) RDF plots of the baseline electrolyte and the electrolyte with $Sn(OTf)_2$ additive from MD simulation. c) The migration paths of Na and the migration energy of NaF and $Na_{15}Sn_4$. Reproduced with permission.[205] Copyright 2024, Wiley-VCH; d) Na-S battery configuration employing ionic liquid-enhanced electrolyte. e) Long-term cycling stability at 0.2 A g^{-1}. Reproduced with permission.[178] Copyright 2024, Wiley-VCH. f) CE test of Na-Cu batteries with different electrolytes. g,h) RDF profiles from MD simulations under −20 °C. Reproduced with permission.[179] Copyright 2024, Wiley-VCH.

the electrolyte enables the formation of a NaF-enriched CEI, which not only confines active sulfur species, but also improves the redox reversibility and sulfur utilization during cycling. The optimized solvation environment arising from the interplay between IL anions and FEC enhances ionic conductivity, lowers interfacial impedance, and accelerates reaction kinetics. Crucially, the IL-based electrolyte minimizes sulfur leaching and side reactions, promoting a compact and robust SEI/CEI architecture. These combined benefits yield outstanding electrochemical performance, evidenced by a high specific capacity of 565 mAh g^{-1} with nearly 100% Coulombic efficiency over 500 cycles at 0.2 A g^{-1} (Figure 28e). Overall, this dual-functional electrolyte represents a significant advancement toward the practical deployment of safe, long-lasting RT Na-S batteries.

Our group presented low-temperature Na-S batteries by introducing an ionic liquid (IL)-mediated LHCE. The IL of N-Propyl, N-methyl pyrrolidinium bis(fluorosulfonyl)imide (C3mpyrFSI) serves as a functional diluent additive to reconstruct the solvation structures, enabling a stable operation of the cells at −20 °C.[176] The key advancement is demonstrated in Figure 28f, which compares the Coulombic efficiency (CE) of Na plating/stripping in Cu||Na cells with different electrolytes. While traditional LHCE achieves a CE of ≈97.5%, the IL-modified LHCE (LHCE_0.3IL) significantly improves this to ≈99.1% over 500 cycles at 20 °C. This enhancement stems from the unique role of C3mpyrFSI in restructuring the electrolyte solvation environment. This IL reduces solvation cluster sizes and strengthens Na^+-FSI^- coordination, while weakening Na^+-solvent interactions, as revealed by MD simulations (Figure 28g,h). This enables faster ion transport and forms a stable, inorganic-rich SEI dominated by NaF, which is crucial for low-temperature performance. The IL also stabilizes the anode interface by forming an inorganic-rich NaF-based SEI layer, which lowers the activation energies for Na^+ desolvation and transport. Consequently, Na-S pouch cells with LHCE_0.3IL achieve 450 mAh g^{-1} at −20 °C (82% capacity retention after 140 cycles), outperforming conventional LHCEs. This work pioneers a solvation-tuning strategy for extreme-condition batteries, emphasizing the dual role of IL in bulk electrolyte optimization and interfacial engineering.

In summary, functional electrolyte additives have emerged as a pivotal strategy for modulating interfacial chemistry and enhancing the electrochemical performance of alkali metal-sulfur batteries. In Li-S systems, extensive research has demonstrated that tailored additives can effectively stabilize the lithium-metal anode, suppress polysulfide shuttling, and facilitate the formation of robust SEI/CEI layers. Similarly, in Na-S batteries, functional

additives have shown great promise in tuning the Na^+ solvation structure, inhibiting NaPS dissolution, and regulating sodium deposition behavior. In contrast, the application of such additives in K-S batteries remains in its infancy, with limited systematic studies on interfacial regulation. Given the distinct physicochemical characteristics of potassium metal and KPS species, future research should focus on rational design of advanced additives capable of concurrently modulating solvation environments, stabilizing electrode interfaces, and mitigating shuttle phenomena. The establishment of universal design principles and mechanistic insights into additive-induced interfacial modulation across Li-, Na-, and K-S systems will be instrumental in advancing the development of high-energy, long-life alkali metal-sulfur batteries.

5. Summary and Perspectives

Electrolytes are pivotal to the overall electrochemical performance of metal-sulfur batteries, including Li-S, Na-S, and K-S systems. In addition to their fundamental role in ion transport, electrolytes critically influence the stability of the electrode–electrolyte interface, regulate electrochemical reactions, and address major challenges, such as dendrite growth and the polysulfide shuttle effect. Therefore, the composition of electrolytes and the characteristics of their solvation structures determine the charge–discharge behavior, cycle life, rate capability, and overall efficiency of metal-sulfur batteries. In particular, the solvation/desolvation properties of the electrolyte, along with its compatibility with both the alkali-metal anode and the sulfur cathode, are critical for improving the performance and stability of metal-sulfur batteries.

Recent advancements in electrolyte systems have demonstrated promising improvements in both performance and stability. The well-designed electrolytes incorporating functional additives or novel solvents with tailored solvation behavior have showcased significant potential in enhancing ionic conductivity, stabilizing the electrode–electrolyte interface, and minimizing parasitic reactions. For example, LHCEs can effectively suppress polysulfide shuttle while maintaining ion conductivity compared to HECs. Similarly, electrolyte additives have been introduced to form protective layers on the anode and cathode surface to further improve the cycling stability and battery lifetime.

Despite these advances, significant challenges persist for practical metal-sulfur batteries, particularly in achieving an optimal balance between sulfur conversion kinetics and long-term electrolyte stability, especially under demanding cycling conditions. Another critical challenge lies in addressing the mechanical and chemical instability at the electrode-electrolyte interface, which can lead to dendrite growth and polysulfide dissolution. As a result, development of multifunctional electrolytes that not only enhance ionic conductivity, but also stabilize the electrode–electrolyte interface, is essential for advancing battery safety, efficiency, and longevity. Consequently, ongoing research is required, and the ultimate goal of designing electrolytes is to achieve high ionic conductivity, superior interfacial stability, and robust chemical resistance to side reactions, while ensuring they are cost-effective and scalable for real-world applications. The following outlines the design concept, requirements and key considerations for developing future metal-sulfur electrolytes.

5.1. Low N/P Ratio and E/S Ratio

The N/P (negative to positive) ratio and E/S (electrolyte to sulfur) ratio are crucial factors for practical metal-sulfur batteries, impacting key aspects, such as cycle life, stability, and energy efficiency. A low N/P ratio, which represents the amount of negative electrode (metal anode) relative to the positive electrode (active sulfur cathode), is often preferred in metal-sulfur batteries. Generally, limited N/P configurations demand highly efficient alkali-metal deposition and stripping behavior, which strongly depends on SEI formation. Therefore, electrolytes with optimized solvation structures that promote uniform alkali-metal nucleation, suppress dendritic growth, and stabilize the SEI layer are beneficial for meeting low N/P ratio requirements.

Similarly, the **E/S ratio** also has a significant impact on the electrochemical performance of metal-sulfur batteries. A reduced electrolyte volume in low E/S ratio cells significantly slows down the sulfur redox kinetics due to limited ionic transfer. This can lead to incomplete sulfur conversion, increased polarization, and poor rate performance. As a result, electrolyte systems that can enhance ion transport, reduce viscosity, and stabilize intermediate species are essential to facilitate fast redox reactions and ensure high sulfur utilization under lean electrolyte conditions. Therefore, achieving a balance between the electrolyte amount and sulfur content necessitates advanced electrolyte systems capable of providing high ionic conductivity and stability with a reduced electrolyte volume.

Notably, tailored electrolyte systems, such as HCEs, LHCEs or functional additives, can mitigate these challenges by enhancing sulfur utilization, minimizing active material dissolution, and promoting the formation of stable, ion-conductive interphases on both electrodes. Consequently, a rational electrolyte design is indispensable for achieving high Coulombic efficiency and long-term stability in metal-sulfur cells operating under practical conditions.

5.2. Advanced Characterization Techniques

Designing electrolytes for metal-sulfur batteries requires a comprehensive understanding of electrolyte behavior under operational conditions. Advanced characterization techniques can offer valuable insights into the chemical composition, solvation structure, and dynamic interfacial processes occurring during battery cycling, thereby elucidating the mechanisms behind rationally designed electrolytes.

XPS is one of the most powerful surface-sensitive techniques for analyzing the chemical states of elements at the electrode–electrolyte interface, offering detailed insights into the formation of the SEI/CEI. By examining the components and chemical states of species at the interface, XPS helps uncover the mechanisms that enhance battery performance. As such, it is an essential tool for optimizing interface stability and ionic conductivity in metal-sulfur batteries, ultimately guiding the design of more efficient and durable electrolyte systems.

Furthermore, TOF-SIMS is another crucial technique for investigating the elemental and molecular distribution at the electrode–electrolyte interface. Unlike conventional mass

spectrometry, TOF-SIMS utilizes a focused ion beam to sputter the surface of a material, releasing secondary ions that are analyzed based on their mass-to-charge ratio. This technique enables the identification of trace elements and molecular species at the near-surface regions of electrodes, making it especially valuable for studying interfacial layers in metal-sulfur batteries. Additionally, it allows researchers to monitor the dissolution, migration, and re-deposition of polysulfides during charge–discharge cycles, providing insights into the mechanisms driving polysulfide instability. As a result, TOF-SIMS serves as a critical tool for analyzing chemical and molecular interactions at the electrode–electrolyte interface, deepening our understanding of performance degradation and offering essential data for developing more stable and efficient electrolyte systems for metal-sulfur batteries.

In situ Raman Spectroscopy has emerged as a powerful tool for monitoring the dynamic behavior of electrolyte and electrode materials in real-time during the cycling of metal-sulfur batteries. Raman spectroscopy works by detecting the vibrational modes of molecules and ions, providing detailed information about the molecular structure and bonding within both the electrolyte and electrode materials. This makes it particularly valuable for studying the solvation structures in the electrolyte, which are critical to the overall performance of metal-sulfur batteries. Unlike ex situ techniques, in situ Raman spectroscopy allows continuous tracking of chemical structure and composition changes during charge and discharge cycles, offering insights into the mechanisms that govern battery performance. Consequently, in situ Raman spectroscopy provides real-time data on the chemical and structural dynamics within metal-sulfur batteries, particularly at the electrode–electrolyte interface. By monitoring solvation/desolvation processes, polysulfide behavior, and electrode evolution, this technique is essential for understanding the complex interactions in these batteries, optimizing electrolyte formulations, improving battery efficiency, and enhancing cycle stability.

In addition to these techniques, cryo-electron microscopy (cryo-EM) is gaining attention as an advanced tool for visualizing the microstructural changes within electrolyte and electrode materials. Cryo-EM enables imaging at extremely high resolution under cryogenic conditions, preserving the native structure of the materials. This method allows for the observation of the nanoscale morphology of electrode materials, the monitoring of dendrite formation or SEI development, and the analysis of phase distribution within the electrolyte and electrode components. The ability to directly visualize these structures provides invaluable insights for optimizing the interface stability and enhancing the overall performance of metal-sulfur batteries.

Together, these advanced characterization techniques offer a comprehensive view of electrolyte and electrode behavior under operating conditions. By combining real-time monitoring with high-resolution imaging and chemical analysis, these methods enable the precise optimization of electrolyte formulations, the design of improved solid-electrolyte interfaces, and the identification of critical issues, such as electrolyte degradation, dendrite formation, and shuttle effects. These insights are crucial for enhancing the performance, stability, and safety of metal-sulfur batteries, ultimately contributing to more efficient and durable energy storage solutions.

5.3. Solvation Structure-Function Relationship

The solvation structure of an electrolyte plays a crucial role in determining its performance, especially in metal-sulfur batteries. The relationship between the solvation structure and electrolyte functionality, such as specifically ionic conductivity, stability, and suppression of polysulfide shuttle, is fundamental to optimizing battery performance.

In general, the solvation of alkali-metal cations (Li^+, Na^+, K^+) influences the ionic conductivity of the electrolyte and the solvation behavior of active species, such as polysulfides (LiPS, NaPS, KPS). Solvents with strong solvation properties, such as DME and dimethyl sulfoxide (DMSO), tend to form highly stable complexes with alkali-metal cations, which can improve ionic conductivity and ensure sufficient conversion reaction kinetics. However, strong solvation systems may enhance polysulfide dissolution, which aggravates the polysulfide shuttle effect and ultimately results in capacity degradation and poor cycling stability. On the other hand, weakly solvating solvents offer lower solvation energy to alkali-metal cations, resulting in higher ion-pairing and thus a decrease in ionic conductivity. However, weak solvation environments are advantageous as they not only suppress polysulfide dissolution, but also promote the formation of an inorganic-rich interphase, thereby mitigating the shuttle effect. By restricting polysulfide mobility, the electrolytes with weak solvation structure significantly enhance the long-term cycling stability and overall electrochemical of metal-sulfur batteries. The challenge is that while weak solvation suppresses the shuttle effect, it can limit the ionic conductivity, thus affecting the overall efficiency of charge/discharge processes. Therefore, a balance between solvation strength and ionic conductivity is crucial for achieving optimal electrolyte performance. This delicate balance plays a key role in enhancing the energy density and cycle life of metal-sulfur batteries, as it governs both the kinetic and thermodynamic behaviors of polysulfides and the overall charge/discharge kinetics.

To sum up, the relationship between solvation structure and electrochemical function involves a delicate balance among ionic conductivity, suppression of polysulfide dissolution, and interfacial stability. Achieving an optimal solvation environment that minimizes polysulfide solubility, while ensuring sufficient ionic mobility, is essential for improving the performance and durability of metal-sulfur batteries. Looking ahead, development of advanced electrolyte systems will require the precise engineering of solvent combinations to harmonize solvation strength, ion transport, and chemical stability, particularly in managing the trade-offs between conductivity and parasitic side reactions.

5.4. Machine Learning in Electrolyte Optimization

The application of machine learning (ML) to electrolyte design holds great promise for accelerating the discovery of new components and optimization of electrolyte formulations. ML algorithms can be trained using large datasets generated from both experimental and computational studies to predict key electrolyte properties, such as ionic conductivity, viscosity, and stability. By analyzing these properties, ML models can uncover optimal solvent and salt combinations, refine electrolyte concentrations, and

Table 7. Comparison of organic liquid, aqueous, and all-solid-state electrolytes in alkali metal–sulfur batteries.

Property/Feature	Organic liquid electrolytes	Aqueous electrolytes	All-Solid-State electrolyte
Ionic conductivity	High ($\approx 10^{-2}$ S·cm^{-1})	Very high ($>10^{-2}$ S·cm^{-1})	Moderate to low (10^{-4}–10^{-6} S·cm^{-1})
Polysulfide solubility	High (causes shuttle effect)	Moderate to high	Suppressed (solid-state environment)
Shuttle effect	Severe	Moderate	Largely mitigated
Compatibility with alkali metals	Poor (high reactivity, dendrite growth)	Very poor (alkali metal reacts violently with water)	Challenging (interfacial instability, dendrites)
Interfacial resistance	Increases with cycling	Unstable due to corrosion	High (solid–solid interphase)
Safety	Flammable, leakage risk	Safer, but narrow voltage window	High safety, non-flammable
Processing complexity	Simple (organic solution)	Simple (aqueous solution)	Complex (high pressure, controlled assembly)
Cycle life	Moderate (limited by shuttle effect and unstable SEI)	Limited by side reactions and narrow voltage	Potentially long
Current research status	Mature, widely studied	Emerging, especially in hybrid systems	Rapidly growing interest, especially for solid-state devices

forecast long-term performance and degradation behaviors of electrolytes under cycling conditions, thereby accelerating the development of next-generation metal-sulfur battery systems. This data-driven strategy markedly reduces the time and resources needed for electrolyte development, expediting progress in the field of metal-sulfur batteries.

5.5. Tailored Electrolyte Design Strategies for future Li-S, Na-S, and K-S Systems

Looking forward, the rational design of electrolytes for alkali metal–sulfur batteries necessitates a nuanced consideration of the distinct physicochemical characteristics inherent to lithium, sodium, and potassium systems. Although these battery chemistries encounter shared challenges, such as polysulfide dissolution and metal dendrite formation, their interfacial chemistries, redox potentials, and ion transport dynamics diverge considerably, thereby demanding tailored electrolyte engineering strategies.

First of all, mitigating the shuttle effect and fortifying the lithium–electrolyte interface is required for Li-S system. Advanced type electrolytes, including HCEs and LHCEs, along with dual-salt systems present promising pathways to suppress parasitic side reactions and achieve elevated Coulombic efficiencies. As for Na-S systems, electrolyte optimization should prioritize solvents or additives that attenuate Na^+ solvation structures and restrict polysulfide mobility due to the greater solubility and reactivity of intermediate polysulfide species. Notably, the incorporation of ionic liquids or weakly coordinating ether-based solvents has demonstrated potential in enhancing both electrochemical stability and sodium compatibility for Na-S system. Also, K-S batteries remained unexplored compared to others, the sluggish reaction kinetics and a highly reductive anode surface are the occupied challenges for K-S system. As a result, electrolyte development for K-S batteries must prioritize achieving high K^+ transference numbers, broadening electrochemical stability windows, and promoting the formation of a robust SEI to ensure interfacial stability and long-term performance.

To accelerate advances in metal-sulfur batteries, we propose a technology roadmap that outlines priority research directions suitable for each system. These directions include electrolyte structural optimization focusing on parameters such as concentration, solvent polarity, and ionic coordination, as well as additive screening guided by theoretical modeling to harness the synergistic benefits of both electrolyte phases. By implementing targeted strategies customized for each alkali-metal system, it becomes possible to fully unlock the potential of solid and liquid electrolytes and thereby enable the development of high-performance sulfur batteries.

5.6. Emerging Electrolyte Systems: Aqueous and Solid-State Electrolytes

Beyond conventional organic liquid electrolytes, aqueous electrolytes and all-solid-state electrolytes (SSEs) have emerged as promising alternatives for sulfur electrochemistry due to their inherent safety and thermal stability.[206–209] However, their integration with alkali metal–sulfur (Li/Na/K–S) battery systems presents both opportunities and substantial limitations.

Aqueous electrolytes are attractive for their low cost, high ionic conductivity, and environmental benignity.[209] Nonetheless, their electrochemical window is intrinsically limited to $\approx$1.23 V, which renders them incompatible with metallic Li, Na, or K anodes due to parasitic hydrogen evolution and anode corrosion.[208] To address this, most aqueous S battery systems utilize intercalation-type anodes (e.g., Zn-based) configurations, sacrificing energy density for enhanced safety.[210] Additionally, the limited solubility of sulfur species in aqueous media and the instability of polysulfides in water encounter further challenges to efficient sulfur redox chemistry in these systems.

SSEs, including sulfide-, oxide-, and polymer-based systems, enable high safety and eliminate leakage and flammability concerns.[206,207] They also hold promise for suppressing dendritic growth and stabilizing the metal–electrolyte interface. However, SSEs face severe interfacial contact issues and sluggish ion transport at room temperature, especially in the Na-S and K-S systems, where the larger ionic radii of Na^+ and K^+ exacerbate transport resistance.[211] Furthermore, managing the formation

and confinement of solid or gaseous polysulfide intermediates within solid-state environments remains a nontrivial challenge. Advances in composite solid electrolytes, interface engineering, and novel sulfur host structures are critical to unlocking the full potential of SSE-based alkali metal–sulfur batteries. A comparative summary of organic liquid, aqueous, and all-solid-state electrolytes in alkali metal-sulfur batteries is presented in **Table 7**, highlighting their respective electrochemical properties, safety profiles, and interfacial behaviors.

In summary, while aqueous and solid-state systems offer appealing safety and stability advantages, their practical implementation in Li/Na/K–S batteries requires further innovation in electrolyte chemistry, electrode interface design, and cell architecture. For now, liquid organic electrolytes remain the most versatile and well-developed option for high-energy-density sulfur batteries involving metallic alkali anodes.

5.7. Future Directions and Conclusion

In conclusion, significant progress has been made in the development of electrolytes for metal-sulfur batteries, but several challenges remain. Innovations in electrolyte chemistry, including the development of high-concentration electrolytes, functional additives, and novel solvent systems, are essential to improving the performance and stability of these batteries. Advanced characterization techniques will be required to provide crucial insights into electrolyte behavior under practical conditions, enabling more precise optimization of formulations. Machine learning and data-driven approaches will further accelerate the discovery of new materials and electrolytes, reducing development time and costs.

The ongoing research and advancements in electrolyte systems, combined with innovative approaches in materials science and computational modeling, will ultimately pave the way for the next generation of metal-sulfur batteries. These batteries have the potential to become a leading technology for high-performance, long-life energy storage solutions.

Acknowledgements

This work was supported by the U.S. Department of Energy, Office of Basic Energy Sciences, Division of Materials Science and Engineering under award number DE-SC0005397.

Conflict of Interest

The authors declare no conflict of interest.

Keywords

alkali metal-anode, electrode-electrolyte interface, electrolyte additive, liquid electrolyte, metal-sulfur batteries

Received: May 17, 2025
Revised: June 16, 2025
Published online: July 1, 2025

[1] A. Manthiram, *Nat. Commun.* **2020**, *11*, 1550.
[2] W. Li, B. Song, A. Manthiram, *Chem. Soc. Rev.* **2017**, *46*, 3006.
[3] Z. Cui, C. Liu, A. Manthiram, *Adv. Mater.* **2025**, 2420463.
[4] C. Liu, A. Dolocan, Z. Cui, A. Manthiram, *J. Am. Chem. Soc.* **2025**, *147*, 6023.
[5] Z. Cui, C. Liu, A. Manthiram, *Adv. Mater.* **2024**, *36*, 2409272.
[6] R. Zhang, C. Wang, P. Zou, R. Lin, L. Ma, T. Li, I.-h. Hwang, W. Xu, C. Sun, S. Trask, H. L. Xin, *Nat. Energy* **2023**, *8*, 695.
[7] T. Liu, L. Yu, J. Liu, J. Lu, X. Bi, A. Dai, M. Li, M. Li, Z. Hu, L. Ma, D. Luo, J. Zheng, T. Wu, Y. Ren, J. Wen, F. Pan, K. Amine, *Nat. Energy* **2021**, *6*, 277.
[8] A. Manthiram, Y. Fu, S. H. Chung, C. Zu, Y. S. Su, *Chem. Rev.* **2014**, *114*, 11751.
[9] S. Bai, X. Liu, K. Zhu, S. Wu, H. Zhou, *Nat. Energy* **2016**, *1*, 16094.
[10] R. Liu, Z. Wei, L. Peng, L. Zhang, A. Zohar, R. Schoeppner, P. Wang, C. Wan, D. Zhu, H. Liu, Z. Wang, S. H. Tolbert, B. Dunn, Y. Huang, P. Sautet, X. Duan, *Nature* **2024**, *626*, 98.
[11] G. Zhou, H. Chen, Y. Cui, *Nat. Energy* **2022**, *7*, 312.
[12] P. G. Bruce, S. A. Freunberger, L. J. Hardwick, J. M. Tarascon, *Nat. Mater.* **2011**, *11*, 19.
[13] D. Cao, X. Shen, A. Wang, F. Yu, Y. Wu, S. Shi, S. A. Freunberger, Y. Chen, *Nat. Catal.* **2022**, *5*, 193.
[14] Y.-W. Song, L. Shen, X.-Y. Li, C.-X. Zhao, J. Zhou, B.-Q. Li, J.-Q. Huang, Q. Zhang, *Nat. Chem. Eng.* **2024**, *1*, 588.
[15] X. Y. Li, M. Zhao, Y. W. Song, C. X. Bi, Z. Li, Z. X. Chen, X. Q. Zhang, B. Q. Li, J. Q. Huang, *Chem. Soc. Rev.* **2025**, *54*, 4822.
[16] X. Y. Li, B. Q. Li, S. Feng, Z. Li, L. Shen, S. Y. Sun, Z. X. Chen, T. Jin, X. Chen, M. Zhao, X. Q. Zhang, J. Q. Huang, Q. Zhang, *J. Am. Chem. Soc.* **2025**, *147*, 15435.
[17] C. X. Bi, N. Yao, X. Y. Li, Q. K. Zhang, X. Chen, X. Q. Zhang, B. Q. Li, J. Q. Huang, *Adv. Mater.* **2024**, *36*, 2411197.
[18] X. Y. Li, S. Feng, M. Zhao, C. X. Zhao, X. Chen, B. Q. Li, J. Q. Huang, Q. Zhang, *Angew. Chem., Int. Ed.* **2022**, *61*, 202114671.
[19] J.-N. Zhang, Q. Li, C. Ouyang, X. Yu, M. Ge, X. Huang, E. Hu, C. Ma, S. Li, R. Xiao, W. Yang, Y. Chu, Y. Liu, H. Yu, X.-Q. Yang, X. Huang, L. Chen, H. Li, *Nat. Energy* **2019**, *4*, 594.
[20] H. Park, H. Park, K. Song, S. H. Song, S. Kang, K. H. Ko, D. Eum, Y. Jeon, J. Kim, W. M. Seong, H. Kim, J. Park, K. Kang, *Nat. Chem.* **2022**, *14*, 614.
[21] C. Wang, X. Wang, R. Zhang, T. Lei, K. Kisslinger, H. L. Xin, *Nat. Mater.* **2023**, *22*, 235.
[22] H. J. Peng, J. Q. Huang, Q. Zhang, *Chem. Soc. Rev.* **2017**, *46*, 5237.
[23] M. Zhao, B. Q. Li, X. Q. Zhang, J. Q. Huang, Q. Zhang, *ACS Cent. Sci.* **2020**, *6*, 1095.
[24] L. Zeng, J. Zhu, P. K. Chu, L. Huang, J. Wang, G. Zhou, X. F. Yu, *Adv. Mater.* **2022**, *34*, 2204636.
[25] Y. T. Liu, S. Liu, G. R. Li, X. P. Gao, *Adv. Mater.* **2021**, *33*, 2003955.
[26] Z. X. Chen, M. Zhao, L. P. Hou, X. Q. Zhang, B. Q. Li, J. Q. Huang, *Adv. Mater.* **2022**, *34*, 2201555.
[27] H. Yuan, J. Q. Huang, H. J. Peng, M. M. Titirici, R. Xiang, R. Chen, Q. Liu, Q. Zhang, *Adv. Energy Mater.* **2018**, *8*, 1802107.
[28] G. Li, S. Wang, Y. Zhang, M. Li, Z. Chen, J. Lu, *Adv. Mater.* **2018**, *30*, 1705590.
[29] Y. Chen, T. Wang, H. Tian, D. Su, Q. Zhang, G. Wang, *Adv. Mater.* **2021**, *33*, 2003666.
[30] L. Zhou, D. L. Danilov, F. Qiao, J. Wang, H. Li, R. A. Eichel, P. H. L. Notten, *Adv. Energy Mater.* **2022**, *12*, 2202094.
[31] A. Manthiram, S. H. Chung, C. Zu, *Adv. Mater.* **2015**, *27*, 1980.
[32] W. Yao, K. Liao, T. Lai, H. Sul, A. Manthiram, *Chem. Rev.* **2024**, *124*, 4935.
[33] B. Jin, T. Lai, A. Manthiram, *ACS Energy Lett.* **2023**, *8*, 3767.
[34] B. Jin, L. Yang, J. Zhang, Y. Cai, J. Zhu, J. Lu, Y. Hou, Q. He, H. Xing, X. Zhan, F. Chen, Q. Zhang, *Adv. Energy Mater.* **2019**, *9*, 1902938.

[35] J. Ding, H. Zhang, W. Fan, C. Zhong, W. Hu, D. Mitlin, *Adv. Mater.* **2020**, *32*, 1908007.
[36] X. Xu, D. Zhou, X. Qin, K. Lin, F. Kang, B. Li, D. Shanmukaraj, T. Rojo, M. Armand, G. Wang, *Nat. Commun.* **2018**, *9*, 3870.
[37] Y. X. Wang, B. Zhang, W. Lai, Y. Xu, S. L. Chou, H. K. Liu, S. X. Dou, *Adv. Energy Mater.* **2017**, *7*, 1602829.
[38] H. Yang, B. Zhang, Y. X. Wang, K. Konstantinov, H. K. Liu, S. X. Dou, *Adv. Energy Mater.* **2020**, *10*, 2001764.
[39] L. Ma, Y. Lv, J. Wu, Y. Chen, Z. Jin, *Adv. Energy Mater.* **2021**, *11*, 2100770.
[40] A. Y. S. Eng, V. Kumar, Y. Zhang, J. Luo, W. Wang, Y. Sun, W. Li, Z. W. Seh, *Adv. Energy Mater.* **2021**, *11*, 2003493.
[41] X. Yu, A. Manthiram, *Adv. Funct. Mater.* **2020**, *30*, 2004084.
[42] Z. W. Seh, Y. Sun, Q. Zhang, Y. Cui, *Chem. Soc. Rev.* **2016**, *45*, 5605.
[43] Y. X. Wang, W. H. Lai, S. L. Chou, H. K. Liu, S. X. Dou, *Adv. Mater.* **2020**, *32*, 1903952.
[44] H. Hao, T. Hutter, B. L. Boyce, J. Watt, P. Liu, D. Mitlin, *Chem. Rev.* **2022**, *122*, 8053.
[45] W. Yao, J. Xu, L. Ma, X. Lu, D. Luo, J. Qian, L. Zhan, I. Manke, C. Yang, P. Adelhelm, R. Chen, *Adv. Mater.* **2023**, *35*, 2212116.
[46] L. Zhao, Y. Tao, Y. Zhang, Y. Lei, W. H. Lai, S. Chou, H. K. Liu, S. X. Dou, Y. X. Wang, *Adv. Mater.* **2024**, *36*, 2402337.
[47] H. Liu, W. H. Lai, Y. Lei, H. Yang, N. Wang, S. Chou, H. K. Liu, S. X. Dou, Y. X. Wang, *Adv. Energy Mater.* **2022**, *12*, 2103304.
[48] T. Tao, S. Lu, Y. Fan, W. Lei, S. Huang, Y. Chen, *Adv. Mater.* **2017**, *29*, 1700542.
[49] X. Zhou, Z. Yu, Y. Yao, Y. Jiang, X. Rui, J. Liu, Y. Yu, *Adv. Mater.* **2022**, *34*, 2200479.
[50] Y. Li, K. Sun, Y. Fu, S. Wang, C. Zhuge, X. Yin, Z. Yang, Z. Li, D. Liu, X. Wang, D. He, *Adv. Mater.* **2024**, *36*, 2406343.
[51] C. Dong, C. Ma, C. Zhou, Y. Yu, J. Wang, K. Yu, C. Shen, J. Gu, K. Yan, A. Zheng, M. Gong, X. Xu, L. Mai, *Adv. Mater.* **2024**, *36*, 2407070.
[52] L. Chen, Y. Sun, X. Wei, L. Song, G. Tao, X. Cao, D. Wang, G. Zhou, Y. Song, *Adv. Mater.* **2023**, *35*, 2300771.
[53] P. Wang, F. Sun, S. Xiong, Z. Zhang, B. Duan, C. Zhang, J. Feng, B. Xi, *Angew. Chem., Int. Ed.* **2022**, *61*, 202116048.
[54] Y. Zhao, Y. Ye, F. Wu, Y. Li, L. Li, R. Chen, *Adv. Mater.* **2019**, *31*, 1806532.
[55] Y. X. Yin, S. Xin, Y. G. Guo, L. J. Wan, *Angew. Chem., Int. Ed.* **2013**, *52*, 13186.
[56] J. Qin, R. Wang, P. Xiao, D. Wang, *Adv. Energy Mater.* **2023**, *13*, 2300611.
[57] Z. W. Zhang, H. J. Peng, M. Zhao, J. Q. Huang, *Adv. Funct. Mater.* **2018**, *28*, 1707536.
[58] Y. Wang, X. L. Huang, H. Liu, W. Qiu, C. Feng, C. Li, S. Zhang, H. K. Liu, S. X. Dou, Z. M. Wang, *ACS Nano* **2022**, *16*, 5103.
[59] Q. Zhao, Q. Zhu, Y. Liu, B. Xu, *Adv. Funct. Mater.* **2021**, *31*, 2100457.
[60] H. J. Peng, J. Q. Huang, X. B. Cheng, Q. Zhang, *Adv. Energy Mater.* **2017**, *7*, 1700260.
[61] W. Yao, W. Zheng, J. Xu, C. Tian, K. Han, W. Sun, S. Xiao, *ACS Nano* **2021**, *15*, 7114.
[62] W. Yao, J. Xu, Y. Cao, Y. Meng, Z. Wu, L. Zhan, Y. Wang, Y. Zhang, I. Manke, N. Chen, C. Yang, R. Chen, *ACS Nano* **2022**, *16*, 10783.
[63] W. Yao, C. Tian, C. Yang, J. Xu, Y. Meng, I. Manke, N. Chen, Z. Wu, L. Zhan, Y. Wang, R. Chen, *Adv. Mater.* **2022**, *34*, 2106370.
[64] S. Zhang, Y. Yao, X. Jiao, M. Ma, H. Huang, X. Zhou, L. Wang, J. Bai, Y. Yu, *Adv. Mater.* **2021**, *33*, 2103846.
[65] Z. Li, I. Sami, J. Yang, J. Li, R. V. Kumar, M. Chhowalla, *Nat. Energy* **2023**, *8*, 84.
[66] H. Li, M. Chuai, X. Xiao, Y. Jia, B. Chen, C. Li, Z. Piao, Z. Lao, M. Zhang, R. Gao, B. Zhang, Z. Han, J. Yang, G. Zhou, *J. Am. Chem. Soc.* **2023**, *145*, 22516.
[67] C. Y. Zhang, X. Lu, X. Han, J. Yu, C. Zhang, C. Huang, L. Balcells, A. G. Manjon, J. Jacas Biendicho, J. Li, J. Arbiol, G. Sun, J. Y. Zhou, A. Cabot, *J. Am. Chem. Soc.* **2023**, *145*, 18992.
[68] Y. Zhang, C. Kang, W. Zhao, Y. Song, J. Zhu, H. Huo, Y. Ma, C. Du, P. Zuo, S. Lou, G. Yin, *J. Am. Chem. Soc.* **2023**, *145*, 1728.
[69] Z. Shen, X. Jin, J. Tian, M. Li, Y. Yuan, S. Zhang, S. Fang, X. Fan, W. Xu, H. Lu, J. Lu, H. Zhang, *Nat. Catal.* **2022**, *5*, 555.
[70] L. Peng, Z. Wei, C. Wan, J. Li, Z. Chen, D. Zhu, D. Baumann, H. Liu, C. S. Allen, X. Xu, A. I. Kirkland, I. Shakir, Z. Almutairi, S. Tolbert, B. Dunn, Y. Huang, P. Sautet, X. Duan, *Nat. Catal.* **2020**, *3*, 762.
[71] W. Hua, T. Shang, H. Li, Y. Sun, Y. Guo, J. Xia, C. Geng, Z. Hu, L. Peng, Z. Han, C. Zhang, W. Lv, Y. Wan, *Nat. Catal.* **2023**, *6*, 174.
[72] H. Li, R. Meng, C. Ye, A. Tadich, W. Hua, Q. Gu, B. Johannessen, X. Chen, K. Davey, S. Z. Qiao, *Nat. Nanotechnol.* **2024**, *19*, 792.
[73] S. Zhou, J. Shi, S. Liu, G. Li, F. Pei, Y. Chen, J. Deng, Q. Zheng, J. Li, C. Zhao, I. Hwang, C. J. Sun, Y. Liu, Y. Deng, L. Huang, Y. Qiao, G. L. Xu, J. F. Chen, K. Amine, S. G. Sun, H. G. Liao, *Nature* **2023**, *621*, 75.
[74] E. Cha, M. D. Patel, J. Park, J. Hwang, V. Prasad, K. Cho, W. Choi, *Nat. Nanotechnol.* **2018**, *13*, 337.
[75] X. Ji, K. T. Lee, L. F. Nazar, *Nat. Mater.* **2009**, *8*, 500.
[76] C. Zhao, G. L. Xu, Z. Yu, L. Zhang, I. Hwang, Y. X. Mo, Y. Ren, L. Cheng, C. J. Sun, Y. Ren, X. Zuo, J. T. Li, S. G. Sun, K. Amine, T. Zhao, *Nat. Nanotechnol.* **2021**, *16*, 166.
[77] Y. Tian, G. Li, Y. Zhang, D. Luo, X. Wang, Y. Zhao, H. Liu, P. Ji, X. Du, J. Li, Z. Chen, *Adv. Mater.* **2019**, *32*, 1904876.
[78] Z. Han, S. Zhao, J. Xiao, X. Zhong, J. Sheng, W. Lv, Q. Zhang, G. Zhou, H. M. Cheng, *Adv. Mater.* **2021**, *33*, 2170351.
[79] C. Ye, H. Jin, J. Shan, Y. Jiao, H. Li, Q. Gu, K. Davey, H. Wang, S. Z. Qiao, *Nat. Commun.* **2021**, *12*, 7195.
[80] X. Sun, Y. Qiu, B. Jiang, Z. Chen, C. Zhao, H. Zhou, L. Yang, L. Fan, Y. Zhang, N. Zhang, *Nat. Commun.* **2023**, *14*, 291.
[81] C. Ye, H. Li, Y. Chen, J. Hao, J. Liu, J. Shan, S. Z. Qiao, *Nat. Commun.* **2024**, *15*, 4797.
[82] H. Zhang, M. Zhang, R. Liu, T. He, L. Xiang, X. Wu, Z. Piao, Y. Jia, C. Zhang, H. Li, F. Xu, G. Zhou, Y. Mai, *Nat. Commun.* **2024**, *15*, 5451.
[83] Z. Du, X. Chen, W. Hu, C. Chuang, S. Xie, A. Hu, W. Yan, X. Kong, X. Wu, H. Ji, L. J. Wan, *J. Am. Chem. Soc.* **2019**, *141*, 3977.
[84] H. Lin, L. Yang, X. Jiang, G. Li, T. Zhang, Q. Yao, G. W. Zheng, J. Y. Lee, *Energy Environ. Sci.* **2017**, *10*, 1476.
[85] M. Xu, Q. Zhu, Y. Li, Y. Gao, N. Sun, B. Xu, *Energy Environ. Sci.* **2024**, *17*, 7735.
[86] C. Zhao, B. Jiang, Y. Huang, X. Sun, M. Wang, Y. Zhang, N. Zhang, *Energy Environ. Sci.* **2023**, *16*, 5490.
[87] X. Wang, D. Luo, J. Wang, Z. Sun, G. Cui, Y. Chen, T. Wang, L. Zheng, Y. Zhao, L. Shui, G. Zhou, K. Kempa, Y. Zhang, Z. Chen, *Angew. Chem., Int. Ed.* **2021**, *60*, 2371.
[88] X. Wang, X. Zhang, Y. Zhao, D. Luo, L. Shui, Y. Li, G. Ma, Y. Zhu, Y. Zhang, G. Zhou, A. Yu, Z. Chen, *Angew. Chem., Int. Ed.* **2023**, *62*, 202306901.
[89] H. Zhang, B. Song, W. Zhang, B. An, L. Fu, S. Lu, Y. Cheng, Q. Chen, K. Lu, *Angew. Chem., Int. Ed.* **2023**, *62*, 202217009.
[90] M. Li, R. P. Hicks, Z. Chen, C. Luo, J. Guo, C. Wang, Y. Xu, *Chem. Rev.* **2023**, *123*, 1712.
[91] D. Hubble, D. E. Brown, Y. Zhao, C. Fang, J. Lau, B. D. McCloskey, G. Liu, *Energy Environ. Sci.* **2022**, *15*, 550.
[92] A. M. Li, P. Y. Zavalij, F. Omenya, X. Li, C. Wang, *Nat. Nanotechnol.* **2025**, *20*, 388.
[93] J. He, A. Bhargav, L. Su, J. Lamb, J. Okasinski, W. Shin, A. Manthiram, *Nat. Energy* **2024**, *9*, 446.

[94] Y. Jin, P. M. L. Le, P. Gao, Y. Xu, B. Xiao, M. H. Engelhard, X. Cao, T. D. Vo, J. Hu, L. Zhong, B. E. Matthews, R. Yi, C. Wang, X. Li, J. Liu, J.-G. Zhang, *Nat. Energy* **2022**, *7*, 718.
[95] J. Jang, C. Wang, G. Kang, C. Han, J. Han, J.-S. Shin, S. Ko, G. Kim, J. Baek, H.-T. Kim, H. Lee, C. B. Park, D.-H. Seo, Y. Li, J. Kang, *Nat. Energy* **2025**, *10*, 502.
[96] I. R. Choi, Y. Chen, A. Shah, J. Florian, C. Serrao, J. Holoubek, H. Lyu, E. Zhang, J. H. Lee, Y. Lin, S. C. Kim, H. Park, P. Zhang, J. Lee, J. Qin, Y. Cui, Z. Bao, *Nat. Energy* **2025**, *10*, 365.
[97] S. Zhang, R. Li, T. Deng, Q. Ma, X. Hong, H. Zhang, R. Zhang, S. Ding, Y. Wu, H. Zhu, M. Li, H. Zhang, D. Lu, B. Ma, L. Lv, Y. Li, L. Chen, Y. Shen, R. Guo, X. Fan, *Nat. Energy* **2024**, *9*, 1285.
[98] Z. Yu, H. Wang, X. Kong, W. Huang, Y. Tsao, D. G. Mackanic, K. Wang, X. Wang, W. Huang, S. Choudhury, Y. Zheng, C. V. Amanchukwu, S. T. Hung, Y. Ma, E. G. Lomeli, J. Qin, Y. Cui, Z. Bao, *Nat. Energy* **2020**, *5*, 526.
[99] D. Lu, R. Li, M. M. Rahman, P. Yu, L. Lv, S. Yang, Y. Huang, C. Sun, S. Zhang, H. Zhang, J. Zhang, X. Xiao, T. Deng, L. Fan, L. Chen, J. Wang, E. Hu, C. Wang, X. Fan, *Nature* **2024**, *627*, 101.
[100] Q. Xu, T. Li, Z. Ju, G. Chen, D. Ye, G. I. N. Waterhouse, Y. Lu, X. Lai, G. Zhou, L. Guo, K. Yan, X. Tao, H. Li, Y. Qiu, *Nature* **2025**, *637*, 339.
[101] A. M. Li, O. Borodin, T. P. Pollard, W. Zhang, N. Zhang, S. Tan, F. Chen, C. Jayawardana, B. L. Lucht, E. Hu, X. Q. Yang, C. Wang, *Nat. Chem.* **2024**, *16*, 922.
[102] J. Xu, J. Zhang, T. P. Pollard, Q. Li, S. Tan, S. Hou, H. Wan, F. Chen, H. He, E. Hu, K. Xu, X. Q. Yang, O. Borodin, C. Wang, *Nature* **2023**, *614*, 694.
[103] J. Huang, K. Wu, G. Xu, M. Wu, S. Dou, C. Wu, *Chem. Soc. Rev.* **2023**, *52*, 4933.
[104] H. Yang, C. Guo, J. Chen, A. Naveed, J. Yang, Y. Nuli, J. Wang, *Angew. Chem., Int. Ed.* **2019**, *58*, 791.
[105] J. Y. Wei, X. Q. Zhang, L. P. Hou, P. Shi, B. Q. Li, Y. Xiao, C. Yan, H. Yuan, J. Q. Huang, *Adv. Mater.* **2020**, *32*, 2003012.
[106] J. Holoubek, H. Liu, Z. Wu, Y. Yin, X. Xing, G. Cai, S. Yu, H. Zhou, T. A. Pascal, Z. Chen, P. Liu, *Nat. Energy* **2021**, *2021*, 303.
[107] L.-P. Hou, X.-Q. Zhang, N. Yao, X. Chen, B.-Q. Li, P. Shi, C.-B. Jin, J.-Q. Huang, Q. Zhang, *Chem* **2022**, *8*, 1083.
[108] Y. Liu, L. Xu, Y. Yu, M. He, H. Zhang, Y. Tang, F. Xiong, S. Gao, A. Li, J. Wang, S. Xu, D. Aurbach, R. Zou, Q. Pang, *Joule* **2023**, *7*, 2074.
[109] C. Zhao, H. Jeong, I. Hwang, T. Li, Y. Wang, J. Bai, L. Li, S. Zhou, C. C. Su, W. Xu, Z. Yang, M. Almazrouei, C.-J. Sun, L. Cheng, G.-L. Xu, K. Amine, *Joule* **2024**, *8*, 3397.
[110] Y. Liu, Y. An, C. Fang, Y. Ye, Y. An, M. He, Y. Jia, X. Hong, Y. Liu, S. Gao, Y. Hao, J. Chen, J. Zheng, Y. Lu, R. Zou, Q. Pang, *Nat. Chem.* **2025**, *17*, 614.
[111] J. Wu, J. Liu, Z. Lu, K. Lin, Y.-Q. Lyu, B. Li, F. Ciucci, J.-K. Kim, *Energy Storage Mater.* **2019**, *23*, 8.
[112] J. He, A. Bhargav, W. Shin, A. Manthiram, *J. Am. Chem. Soc.* **2021**, *143*, 20241.
[113] J. Wu, Y. Tian, Y. Gao, Z. Gao, Y. Meng, Y. Wang, X. Wang, D. Zhou, F. Kang, B. Li, G. Wang, *Angew. Chem., Int. Ed.* **2022**, *61*, 202205416.
[114] D. Guo, J. Wang, T. Lai, G. Henkelman, A. Manthiram, *Adv. Mater.* **2023**, *35*, 2300841.
[115] M. H. Pai, T. Lai, A. Manthiram, *Adv. Funct. Mater.* **2024**, *34*, 2407450.
[116] W. Yao, M. H. Pai, A. Manthiram, *J. Am. Chem. Soc.* **2025**, *147*, 12061.
[117] L. Wang, J. Bao, Q. Liu, C.-F. Sun, *Energy Storage Mater.* **2019**, *18*, 470.
[118] S. Lee, H. Park, J. Rizell, U. H. Kim, Y. Liu, X. Xu, S. Xiong, A. Matic, A. T. Zikri, H. Kang, Y. K. Sun, J. Kim, J. Y. Hwang, *Adv. Funct. Mater.* **2022**, *32*, 2209145.
[119] S. Ye, N. Yao, X. Chen, M. Ma, L. Wang, Z. Chen, Y. Yao, Q. Zhang, Y. Yu, *Angew. Chem., Int. Ed.* **2023**, *62*, 202307728.
[120] H. Liang, P. Kumar, Z. Ma, F. Zhao, H. Cheng, H. Xie, Z. Cao, L. Cavallo, Q. Li, J. Ming, *ACS Energy Lett.* **2024**, *9*, 3536.
[121] Y. Huang, L. Lin, C. Zhang, L. Liu, Y. Li, Z. Qiao, J. Lin, Q. Wei, L. Wang, Q. Xie, D. L. Peng, *Adv. Sci.* **2022**, *9*, 2106004.
[122] M. Wang, Z. Sun, H. Ci, Z. Shi, L. Shen, C. Wei, Y. Ding, X. Yang, J. Sun, *Angew. Chem., Int. Ed.* **2021**, *60*, 24558.
[123] Z. Shi, M. Li, J. Sun, Z. Chen, *Adv. Energy Mater.* **2021**, *11*, 2100332.
[124] Z. Yan, L. Zhao, Y. Wang, Z. Zhu, S. L. Chou, *Adv. Funct. Mater.* **2022**, *32*, 2205622.
[125] M. S. Syali, D. Kumar, K. Mishra, D. K. Kanchan, *Energy Storage Mater.* **2020**, *31*, 352.
[126] X. Zhao, Y. Lu, Z. Qian, R. Wang, Z. Guo, *EcoMat* **2020**, *2*, 12038.
[127] Y. J. Lei, H. L. Yang, Y. Liang, H. W. Liu, B. Zhang, L. Wang, W. H. Lai, Y. X. Wang, H. K. Liu, S. X. Dou, *Adv. Energy Mater.* **2022**, *12*, 2202523.
[128] A. K. Haridas, C. Huang, *Mater. Today Energy* **2023**, *32*, 101228.
[129] M. Zhao, B. Q. Li, H. J. Peng, H. Yuan, J. Y. Wei, J. Q. Huang, *Angew. Chem., Int. Ed.* **2020**, *59*, 12636.
[130] J. Wu, T. Ye, Y. Wang, P. Yang, Q. Wang, W. Kuang, X. Chen, G. Duan, L. Yu, Z. Jin, J. Qin, Y. Lei, *ACS Nano* **2022**, *16*, 15734.
[131] R. Yan, T. Ma, M. Cheng, X. Tao, Z. Yang, F. Ran, S. Li, B. Yin, C. Cheng, W. Yang, *Adv. Mater.* **2021**, *33*, 2008784.
[132] P. Wang, B. Xi, M. Huang, W. Chen, J. Feng, S. Xiong, *Adv. Energy Mater.* **2021**, *11*, 2002893.
[133] J. Xu, Y. Qiu, J. Yang, H. Li, P. Han, Y. Jin, H. Liu, B. Sun, G. Wang, *Adv. Funct. Mater.* **2023**, *34*, 2306206.
[134] W. Liu, P. Liu, D. Mitlin, *Adv. Energy Mater.* **2020**, *10*, 2002297.
[135] S. C. Kim, J. Wang, R. Xu, P. Zhang, Y. Chen, Z. Huang, Y. Yang, Z. Yu, S. T. Oyakhire, W. Zhang, L. C. Greenburg, M. S. Kim, D. T. Boyle, P. Sayavong, Y. Ye, J. Qin, Z. Bao, Y. Cui, *Nat. Energy* **2023**, *8*, 814.
[136] X. Fan, L. Chen, O. Borodin, X. Ji, J. Chen, S. Hou, T. Deng, J. Zheng, C. Yang, S.-C. Liou, K. Amine, K. Xu, C. Wang, *Nat. Nanotechnol.* **2018**, *13*, 715.
[137] S. Chen, J. Zheng, L. Yu, X. Ren, M. H. Engelhard, C. Niu, H. Lee, W. Xu, J. Xiao, J. Liu, J.-G. Zhang, *Joule* **2018**, *2*, 1548.
[138] Y. Wang, X. Yang, Y. Meng, Z. Wen, R. Han, X. Hu, B. Sun, F. Kang, B. Li, D. Zhou, C. Wang, G. Wang, *Chem. Rev.* **2024**, *124*, 3494.
[139] Y. Wang, Z. Li, Y. Hou, Z. Hao, Q. Zhang, Y. Ni, Y. Lu, Z. Yan, K. Zhang, Q. Zhao, F. Li, J. Chen, *Chem. Soc. Rev.* **2023**, *52*, 2713.
[140] Y. X. Yao, X. Chen, C. Yan, X. Q. Zhang, W. L. Cai, J. Q. Huang, Q. Zhang, *Angew. Chem., Int. Ed.* **2021**, *60*, 4090.
[141] L. Huang, T. Lu, G. Xu, X. Zhang, Z. Jiang, Z. Zhang, Y. Wang, P. Han, G. Cui, L. Chen, *Joule* **2022**, *6*, 906.
[142] R. He, K. Deng, D. Mo, X. Guan, Y. Hu, K. Yang, Z. Yan, H. Xie, *Angew. Chem., Int. Ed.* **2024**, *63*, 202317176.
[143] D. Guo, S. Thomas, J. K. El-Demellawi, Z. Shi, Z. Zhao, C. G. Canlas, Y. Lei, J. Yin, Y. Zhang, M. N. Hedhili, M. Arsalan, Y. Zhu, O. M. Bakr, O. F. Mohammed, H. N. Alshareef, *Energy Environ. Sci.* **2024**, *17*, 8151.
[144] T. Ma, Y. Ni, D. Li, Z. Zha, S. Jin, W. Zhang, L. Jia, Q. Sun, W. Xie, Z. Tao, J. Chen, *Angew. Chem., Int. Ed.* **2023**, *62*, 202310761.
[145] L. L. Su, N. Yao, Z. Li, C. X. Bi, Z. X. Chen, X. Chen, B. Q. Li, X. Q. Zhang, J. Q. Huang, *Angew. Chem., Int. Ed.* **2024**, *63*, 202318785.
[146] Y. Jie, S. Wang, S. Weng, Y. Liu, M. Yang, C. Tang, X. Li, Z. Zhang, Y. Zhang, Y. Chen, F. Huang, Y. Xu, W. Li, Y. Guo, Z. He, X. Ren, Y. Lu, K. Yang, S. Cao, H. Lin, R. Cao, P. Yan, T. Cheng, X. Wang, S. Jiao, D. Xu, *Nat. Energy* **2024**, *9*, 987.
[147] Q. Pang, A. Shyamsunder, B. Narayanan, C. Y. Kwok, L. A. Curtiss, L. F. Nazar, *Nat. Energy* **2018**, *3*, 783.
[148] M. He, X. Li, X. Yang, C. Wang, M. L. Zheng, R. Li, P. Zuo, G. Yin, X. Sun, *Adv. Energy Mater.* **2021**, *11*, 2101004.
[149] Y. He, P. Zou, S.-M. Bak, C. Wang, R. Zhang, L. Yao, Y. Du, E. Hu, R. Lin, H. L. Xin, *ACS Energy Lett.* **2022**, *7*, 2866.

[150] X. Gao, Z. Yu, J. Wang, X. Zheng, Y. Ye, H. Gong, X. Xiao, Y. Yang, Y. Chen, S. E. Bone, L. C. Greenburg, P. Zhang, H. Su, J. Affeld, Z. Bao, Y. Cui, *Proc. Natl. Acad. Sci. USA* **2023**, *120*, 2301260120.
[151] T. Lai, A. Bhargav, A. Manthiram, *Adv. Funct. Mater.* **2023**, *33*, 2304568.
[152] R. Meng, X. He, S. J. H. Ong, C. Cui, S. Song, P. Paoprasert, Q. Pang, Z. J. Xu, X. Liang, *Angew. Chem., Int. Ed.* **2023**, *62*, 202309046.
[153] T. Deng, J. Wang, H. Zhao, Z. Jin, L. Jin, X. Men, J. Wang, Y. Liu, W. Tang, A. M. Abdelkader, R. V. Kumar, S. Ding, Y. Fu, K. Xi, *Adv. Energy Mater.* **2024**, *14*, 2402319.
[154] I. Kim, S. Kim, H. Cho, J. Jung, H. Kwon, D. Kim, Y. Shin, H. T. Kim, *Adv. Energy Mater.* **2024**, *15*, 2403828.
[155] K. Liao, M. H. Pai, A. Manthiram, *Adv. Energy Mater.* **2025**, *15*, 2403733.
[156] X. Liu, S. Wu, Z. Hao, L. Shang, M. Guo, J. Hou, S. Shao, H. Li, Y. Li, Y. Lu, K. Zhang, Z. Yan, J. Chen, *Angew. Chem., Int. Ed.* **2025**, *64*, 202416731.
[157] M. He, L. Zhu, Y. Liu, Y. Jia, Y. Hao, G. Ye, X. Hong, Z. Xiao, Y. Ma, J. Chen, M. B. Shafqat, Q. Pang, *Angew. Chem., Int. Ed.* **2025**, *64*, 202415053.
[158] C. Geng, W. Qu, Z. Han, L. Wang, W. Lv, Q. H. Yang, *Adv. Energy Mater.* **2023**, *13*, 2204036.
[159] Z. Yu, X. Huang, M. Zheng, S. Q. Zhang, Y. Yang, J. Lu, *Adv. Mater.* **2023**, *35*, 2300861.
[160] Y. Ren, A. Manthiram, *Adv. Energy Mater.* **2022**, *12*, 2202566.
[161] L. P. Hou, N. Yao, J. Xie, P. Shi, S. Y. Sun, C. B. Jin, C. M. Chen, Q. B. Liu, B. Q. Li, X. Q. Zhang, Q. Zhang, *Angew. Chem., Int. Ed.* **2022**, *61*, 202201406.
[162] Y. Ren, A. Bhargav, W. Shin, H. Sul, A. Manthiram, *Angew. Chem., Int. Ed.* **2022**, *61*, 202207907.
[163] X. Y. Li, S. Feng, C. X. Zhao, Q. Cheng, Z. X. Chen, S. Y. Sun, X. Chen, X. Q. Zhang, B. Q. Li, J. Q. Huang, Q. Zhang, *J. Am. Chem. Soc.* **2022**, *144*, 14638.
[164] J. Lian, W. Guo, Y. Fu, *J. Am. Chem. Soc.* **2021**, *143*, 11063.
[165] M. Zhao, X. Chen, X. Y. Li, B. Q. Li, J. Q. Huang, *Adv. Mater.* **2021**, *33*, 2007298.
[166] K. Chen, R. Fang, Z. Lian, X. Zhang, P. Tang, B. Li, K. He, D.-w. Wang, H.-M. Cheng, Z. Sun, F. Li, *Energy Storage Mater.* **2021**, *37*, 224.
[167] Z. Wang, J. Liu, B. Zhang, L. Sun, L. Cong, L. Lu, A. Mauger, C. M. Julien, H. Xie, H. Sun, *Energy Storage Mater.* **2020**, *24*, 373.
[168] A. Gupta, A. Bhargav, A. Manthiram, *ACS Energy Lett.* **2021**, *6*, 224.
[169] J. Xie, Y. W. Song, B. Q. Li, H. J. Peng, J. Q. Huang, Q. Zhang, *Angew. Chem., Int. Ed.* **2020**, *59*, 22150.
[170] Y. Fu, Z. Wu, Y. Yuan, P. Chen, L. Yu, L. Yuan, Q. Han, Y. Lan, W. Bai, E. Kan, C. Huang, X. Ouyang, X. Wang, J. Zhu, J. Lu, *Nat. Commun.* **2020**, *11*, 845.
[171] M. Zhao, B.-Q. Li, X. Chen, J. Xie, H. Yuan, J.-Q. Huang, *Chem* **2020**, *6*, 3297.
[172] C. Luo, X. Liang, Y. Sun, W. Lv, Y. Sun, Z. Lu, W. Hua, H. Yang, R. Wang, C. Yan, J. Li, Y. Wan, Q.-H. Yang, *Energy Storage Mater.* **2020**, *33*, 290.
[173] M. Kohl, F. Borrmann, H. Althues, S. Kaskel, *Adv. Energy Mater.* **2016**, *6*, 1502185.
[174] Y. Ren, N. Hortance, J. McBride, K. B. Hatzell, *ACS Energy Lett.* **2020**, *6*, 345.
[175] D. Wang, J. Hwang, C. y. Chen, K. Kubota, K. Matsumoto, R. Hagiwara, *Adv. Funct. Mater.* **2021**, *31*, 2105524.
[176] S. Murugan, S. V. Klostermann, P. Schützendübe, G. Richter, J. Kästner, M. R. Buchmeiser, *Adv. Funct. Mater.* **2022**, *32*, 2201191.
[177] S. Weng, Y. Liu, S. Lu, J. Xu, J. Xue, H. Tu, Z. Wang, L. Liu, Y. Gao, G. Sun, H. Li, X. Wu, *Angew. Chem., Int. Ed.* **2024**, *64*, 202421602.
[178] Y. Liu, S. Lu, S. Weng, J. Xu, H. Tu, Z. Wang, J. Xue, L. Liu, F. Zhang, G. Sun, Y. Gao, C. Qian, Z. Liu, H. Li, X. Wu, *Adv. Energy Mater.* **2024**, *35*, 2404890.
[179] D. Guo, J. Wang, Z. Cui, Z. Shi, G. Henkelman, H. N. Alshareef, A. Manthiram, *Adv. Funct. Mater.* **2024**, *34*, 2409494.
[180] W. Yao, M. H. Pai, A. Manthiram, *Angew. Chem., Int. Ed.* **2025**, *137*, 202424547.
[181] M. H. Pai, A. Manthiram, *Adv. Energy Mater.* **2025**, https://doi.org/10.1002/aenm.202500026.
[182] X. Yu, A. Manthiram, *Energy Storage Mater.* **2018**, *15*, 368.
[183] J.-Y. Hwang, H. M. Kim, Y.-K. Sun, *J. Mater. Chem. A* **2018**, *6*, 14587.
[184] N.-C. Lai, G. Cong, Y.-C. Lu, *J. Mater. Chem. A* **2019**, *7*, 20584.
[185] R. Ma, L. Fan, J. Wang, B. Lu, *Electrochim. Acta* **2019**, *293*, 191.
[186] P. Xiong, X. Han, X. Zhao, P. Bai, Y. Liu, J. Sun, Y. Xu, *ACS Nano* **2019**, *13*, 2536.
[187] X. Yuan, B. Zhu, J. Feng, C. Wang, X. Cai, R. Qin, *J. Power Sources* **2020**, *480*, 228874.
[188] K. Yang, S. Kim, X. Yang, M. Cho, Y. Lee, *Small Methods* **2022**, *6*, 2100899.
[189] X. Chen, Y. Meng, D. Xiao, L. Qin, *ACS Appl. Mater. Interfaces* **2024**, *16*, 24464.
[190] K. Xu, *Chem. Rev.* **2014**, *114*, 11503.
[191] X. Li, M. Banis, A. Lushington, X. Yang, Q. Sun, Y. Zhao, C. Liu, Q. Li, B. Wang, W. Xiao, C. Wang, M. Li, J. Liang, R. Li, Y. Hu, L. Goncharova, H. Zhang, T. K. Sham, X. Sun, *Nat. Commun.* **2018**, *9*, 4509.
[192] Z. Shen, W. Zhang, S. Mao, S. Li, X. Wang, Y. Lu, *ACS Energy Lett.* **2021**, *6*, 2673.
[193] S. Xin, Y. X. Yin, Y. G. Guo, L. J. Wan, *Adv. Mater.* **2014**, *26*, 1261.
[194] Y. Liu, X. Li, Y. Sun, R. Yang, Y. Lee, J.-H. Ahn, *J. Alloys Compd.* **2021**, *853*, 157316.
[195] X. Y. Li, S. Feng, Y. W. Song, C. X. Zhao, Z. Li, Z. X. Chen, Q. Cheng, X. Chen, X. Q. Zhang, B. Q. Li, J. Q. Huang, Q. Zhang, *J. Am. Chem. Soc.* **2024**, *146*, 14754.
[196] Z. Li, L. P. Hou, N. Yao, X. Y. Li, Z. X. Chen, X. Chen, X. Q. Zhang, B. Q. Li, Q. Zhang, *Angew. Chem., Int. Ed.* **2023**, *62*, 202309968.
[197] L. P. Hou, Z. Li, N. Yao, C. X. Bi, B. Q. Li, X. Chen, X. Q. Zhang, Q. Zhang, *Adv. Mater.* **2022**, *34*, 2205284.
[198] X. Q. Zhang, Q. Jin, Y. L. Nan, L. P. Hou, B. Q. Li, X. Chen, Z. H. Jin, X. T. Zhang, J. Q. Huang, Q. Zhang, *Angew. Chem., Int. Ed.* **2021**, *60*, 15503.
[199] H. Liu, W. H. Lai, Q. Yang, Y. Lei, C. Wu, N. Wang, Y. X. Wang, S. L. Chou, H. K. Liu, S. X. Dou, *Nanomicro Lett.* **2021**, *13*, 121.
[200] S. Gu, N. Xiao, F. Wu, Y. Bai, C. Wu, Y. Wu, *ACS Energy Lett.* **2018**, *3*, 2858.
[201] G. R. Pastel, T. P. Pollard, O. Borodin, M. A. Schroeder, *Chem. Rev.* **2025**, *125*, 3059.
[202] A. L. Phan, B. Nan, P. M. L. Le, Q. Miao, Z. Wu, K. Le, F. Chen, M. Engelhard, T. Dan Nguyen, K. S. Han, J. Heo, W. Zhang, M. Baek, J. Xu, X. Zhang, P. Liu, L. Ma, C. Wang, *Adv. Mater.* **2024**, *36*, 2406594.
[203] S. C. Kim, X. Gao, S. L. Liao, H. Su, Y. Chen, W. Zhang, L. C. Greenburg, J. A. Pan, X. Zheng, Y. Ye, M. S. Kim, P. Sayavong, A. Brest, J. Qin, Z. Bao, Y. Cui, *Nat. Commun.* **2024**, *15*, 1268.
[204] Y. Ren, T. Lai, A. Manthiram, *ACS Energy Lett.* **2023**, *8*, 2746.
[205] L. Wang, N. Ren, W. Jiang, H. Yang, S. Ye, Y. Jiang, G. Ali, L. Song, X. Wu, X. Rui, Y. Yao, Y. Yu, *Angew. Chem., Int. Ed.* **2024**, *63*, 202320060.
[206] J. Zhou, M. L. Holekevi Chandrappa, S. Tan, S. Wang, C. Wu, H. Nguyen, C. Wang, H. Liu, S. Yu, Q. R. S. Miller, G. Hyun, J. Holoubek, J. Hong, Y. Xiao, C. Soulen, Z. Fan, E. E. Fullerton, C. J. Brooks, C.

Wang, R. J. Clement, Y. Yao, E. Hu, S. P. Ong, P. Liu, *Nature* **2024**, *627*, 301.
[207] H. Song, K. Munch, X. Liu, K. Shen, R. Zhang, T. Weintraut, Y. Yusim, D. Jiang, X. Hong, J. Meng, Y. Liu, M. He, Y. Li, P. Henkel, T. Brezesinski, J. Janek, Q. Pang, *Nature* **2025**, *637*, 846.
[208] Y. Feng, X. Yu, B. Wang, T. Zhang, W. Zhou, Y. Wang, X. Li, J. Zhao, J. Zhao, W. Li, C. Ma, D. Zhao, D. Chao, *Angew. Chem., Int. Ed.* **2025**, *64*, 202420514.
[209] Y. Feng, B. Wang, W. Zhou, H. Jin, X. Yu, T. Zhang, J. Zhao, H. Li, J. Zhao, W. Li, C. Ma, D. Chao, D. Zhao, *J. Am. Chem. Soc.* **2024**, *146*, 25343.
[210] Z. Chen, Z. Huang, J. Zhu, D. Li, A. Chen, Z. Wei, Y. Wang, N. Li, C. Zhi, *Adv. Mater.* **2024**, *36*, 2402898.
[211] X. Chi, Y. Zhang, F. Hao, S. Kmiec, H. Dong, R. Xu, K. Zhao, Q. Ai, T. Terlier, L. Wang, L. Zhao, L. Guo, J. Lou, H. L. Xin, S. W. Martin, Y. Yao, *Nat. Commun.* **2022**, *13*, 2854.

Min-Hao Pai is currently a Ph.D. candidate in the Materials Science and Engineering Graduate Program at the University of Texas at Austin, under the supervision of Professor Arumugam Manthiram. He received his B.S. degree in chemistry from Shanghai Jiao Tong University in 2018 and his M.S. degree from National Taiwan University in 2021. His research centers on advancing high-energy-density metal-sulfur batteries through the development of novel cathode materials and the design of next-generation electrolytes.

Arumugam Manthiram holds the George T. and Gladys H. Abell Endowed Chair of Engineering at the University of Texas at Austin. His research focuses on the development of electrodes and electrolytes for a wide range of rechargeable battery systems, including lithium-ion, sodium-ion, lithium-sulfur, sodium-sulfur, and all-solid-state batteries. His broader interests extend to new materials design, scalable synthesis, advanced characterization techniques, and the elucidation of structure–property–performance relationships. Dr. Manthiram has authored more than 1000 journal articles with 133 000 citations and an h-index of 176.